ТЕХНІКА ТА ЕНЕРГЕТИКА

Засновник:
Національний університет біоресурсів і природокористування України

Рік заснування: 2010

Рекомендовано до друку та поширення
через мережу Інтернет Вченою радою
Національного університету біоресурсів і природокористування України
(протокол № 1 від 11 серпня 2023 р.)

Свідоцтво про державну реєстрацію
друкованого засобу масової інформації
серії КВ № 25126-15066 ПР від 17 лютого 2022

Журнал входить до переліку наукових фахових видань України
Категорія «Б». Галузь наук – Технічні.
Спеціальність: 131 – «Прикладна механіка», 133 – «Галузеве машинобудування»,
141 – «Електроенергетика, електротехніка та електромеханіка»,
151 – «Автоматизація та комп'ютерно-інтегровані технології»
(Наказ Міністерства освіти і науки України від 17 березня 2020 року № 409)

Журнал представлено у міжнародних наукометричних базах даних, репозитаріях та пошукових системах: Index Copernicus International,
Google Scholar, Фахові видання України,
Національна бібліотека України імені В. І. Вернадського,
BASE, Academic Resource Index ResearchBib, DOAJ, J-Gate

Адреса редакції:
Національний університет біоресурсів і природокористування України
03041, вул. Героїв Оборони, 15, м. Київ, Україна
E-mail: info@technicalscience.com.ua
www: https://technicalscience.com.ua/uk

MACHINERY & ENERGETICS

Founders:
National University of Life and Environmental Sciences of Ukraine

Year of foundation: 2010

Recommended for printing and distribution
via the Internet by the Academic Council
of National University of Life and Environmental Sciences of Ukraine
(Minutes 1 of August 11, 2023)

Certificate of state registration
of the print media
Series KV No. 25126-15066 PR of February 17, 2022

The journal is included in the list of Professional Scientific Publications of Ukraine
Category "B". Branch of sciences – Technical.
Specialty: 131 – "Applied Mechanics", 133 – "Branch Mechanical Engineering",
141 – "Electric Power Industry, Electrical Engineering and Electromechanics",
151 – "Automation and Computer-Integrated Technologies"
(Order of the Ministry of Education and Science of Ukraine of March 17, 2020, No. 409)

The journal is presented international scientometric databases, repositories and scientific systems: Index Copernicus International,
Google Scholar, Professional publications of Ukraine,
Vernadsky National Library of Ukraine, BASE,
Academic Resource Index ResearchBib, DOAJ, J-Gate

Editors office address:
National University of Life and Environmental Sciences of Ukraine
03041, 15 Heroiv Oborony, Kyiv, Ukraine
E-mail: info@technicalscience.com.ua
www: https://technicalscience.com.ua/en

Редакційна колегія

Міжнародні члени редколегії:

Editorial Board

ЗМІСТ

CONTENTS

Machinery & Energetics
Vol. 14, No. 3. 2023

Journal homepage:
https://technicalscience.com.ua/en

UDC 631.37
DOI: 10.31548/machinery/3.2023.09

Ivan Beloev*
PhD in Technical Sciences, Associate Professor
"Angel Kanchev" University of Ruse
7017, 8 Studentska Str., Ruse, Bulgaria
https://orcid.org/0000-0003-2014-1970

Volodymyr Kuvachov
Doctor of Technical Sciences, Professor
Dmytro Motornyi Tavria State Agrotechnological University
72310, 18 B. Khmelnytsky Ave., Melitopol, Ukraine
https://orcid.org/0000-0002-5762-256X

Valerii Adamchuk
Doctor of Technical Sciences, Professor
Institute of Mechanics and Automatics of Agroindustrial Production
of the National Academy of Agrarian Sciences of Ukraine
08631, 11 Vokzalna Str., Glevakha, Kyiv region, Ukraine
https://orcid.org/0000-0003-0358-7946

Zinoviy Ruzhylo
PhD in Technical Sciences, Associate Professor
National University of Life and Environmental Sciences of Ukraine
03041, 15 Heroiv Oborony Str., Kyiv, Ukraine
https://orcid.org/0000-0003-3582-8687

Analytical study of the turns of bridge machines

Abstract. The research is devoted to the topical problem of the efficiency of turning wide-span bridge machines in the track farming system. The research aims to study the curvilinear movement along the soil traces of a constant technological track of an arbitrary multi-supported bridge machine, considering its design and method of turning, parameters, modes of movement and loading. Experimental studies were conducted, involving the use of a modern strain track and specially designed equipment for electrical measurements of non-electrical quantities. The processing of research data was carried out on a personal computer. A methodology for compiling private models of turning off the bridge vehicle moving along the soil trace of the constant technological track was developed. As a result of the joint solution problem of the bridge machine turning, it is possible to determine all output parameters of curvilinear motion: trajectory, tractive forces, turning radius, slipping, and actual speeds. The force interaction of the bridge machine's undercarriage with the soil trace of a constant track is presented based on flat sliding with a variable anisotropic friction coefficient of adhesion φ_{yd}, depending on the properties of the track. As the radius of the wheel, the width of its tire and the air pressure in it, as well as the vertical load that acts on it, the coefficient of traction of the bridge machine φ_{yd} increases, which may cause higher slippage. The adequacy of the model of stationary turning of the overhead machine is confirmed by experimental estimation of the resistance coefficient of the power onboard turning. The convergence of the theoretical and experimental values of this

Article's History: Received: 05.04.2023; Revised: 12.07.2023; Accepted: 11.08.2023.

Suggested Citation:
Beloev, I., Kuvachov, V., Adamchuk, V., & Ruzhylo, Z. (2023). Analytical study of the turns of bridge machines. *Machinery & Energetics,* 14(3), 9-20. doi: 10.31548/machinery/3.2023.09.

*Corresponding author

coefficient is within the confidence interval ± σ in the whole investigated weight range of the bridge machine prototype. This allows us to assess the influence of design parameters and schemes on the turning characteristics as early as the design stage of a new bridge machine, thus optimizing the design process. The results of the research can be applied to the organization of the process of turning the existing models of bridge machines

Keywords: controlled traffic farming, gantry systems, curvilinear motion, coefficient of traction, coefficient of adhesion, front steered wheels

INTRODUCTION

The movement of bridge machines along the tracks of a permanent technological track creates somewhat different conditions and requirements for the operation of its pneumatic tire than for a traditional tractor moving along the agricultural background. As such, one of the requirements for the parameters of the technological track is their sufficient compaction, which improves the traction, coupling, and operational properties of bridge agricultural vehicles moving along them (Lou *et al*., 2021; Tamirat *et al*., 2022; Kørup *et al*., 2022). According to M.N. Thomsen *et al*. (2018), the restrictions on the permissible norms of the impact of undercarriage systems on the soil in the area of the tramline can be neglected. On the other hand, it has been established that the width of the bridge wheel should be as small as possible. This reduces the loss of field area under the technological zone.

Wide-span tractor (vehicles) for controlled traffic farming, like any vehicle, is a rather complex control object that can be adapted to manual or automatic control and is built according to the kinematic or power principle of turning. D.L. Antille *et al.* (2019) pointed out that kinematic rotation is implemented by turning the steered wheels (front, rear, or both front and rear) relative to the car frame. Wide-span tractors (vehicles) with steerable wheels are the most widely used.

S.Z.S. Al-khayyt (2018) presented studies aimed at optimizing the trajectory of curvilinear motion (PSO) by replacing the LSPB (linear segment with parabolic blend) trajectory when building an array of points on the trajectory. The PSO parameters were thus obtained to ensure that the LSPB trajectories accurately display the given waypoints. Interaction of the optimal trajectory of LSPB with PSO was demonstrated using mathematical modelling. The aforementioned method for the operational planning of the curvilinear turn of the bridge machine is quite simple and is used to solve such problems. However, the influence of the mass-geometric and structural-technological parameters of the wheeled vehicle on the process of its curvilinear movement is not considered.

M. Melnik *et al.* (2017) obtained parametric equations for the trajectory of the unsteady movement of a wheeled vehicle with front-steered wheels as a function of the angle of rotation of its body, which allows describing the processes of entering a left or right turn and exiting it. Using the models presented by the authors, it is possible to investigate the process of turning a wheeled vehicle as a function of time.

As such, many studies are devoted to the curvilinear movement of traditional wheeled and tracked vehicles, although, concerning bridge vehicles, this process has not been studied enough. The rotation of aggregates during fieldwork is also actively studied by scholars. A. Startsev *et al.* (2023) presented a mathematical model built to assess the rectilinear stability of the tractor unit in the uncontrolled turn mode. M. Song *et al*. (2013) attempted to optimize the point trajectory and simulate the creation of a given path for mowers as they turn. The authors proposed an algorithm based on experimental path-planning operation models for an autonomous mower. The results of production tests showed a certain convergence of the turning points.

Numerous global studies also aimed to study the movement of mobile units on a wheeled caterpillar mover. For example, M. Fashutdinov *et al*. (2020) considered the theoretical prerequisites for modelling the dynamics of the rotation of agricultural units with a wheel-caterpillar mover. The authors obtained mathematical models for determining the indicators of the turning of agricultural units. However, during modelling the process of curvilinear motion of a traditional tractor unit, the main assumption underlying the force interaction of the mover with the soil is the independence of the resulting force and friction moment. This limits the scope of models in this direction to large and medium turning radii and movement without loads.

The studies aimed to develop a model for turning a bridge machine moving along a compacted soil track of a constant tramline based on the theory of flat slip with a variable anisotropic coefficient of friction, which makes it possible to substantiate all the output parameters of its curvilinear movement.

MATERIALS AND METHODS

Experimental studies were carried out throughout 2020-2021 in a specially created laboratory for testing a bridge machine at Dmytro Motornyi Tavria State Agrotechnological University (Ukraine).

To conduct experimental studies, a four-wheeled overhead vehicle prototype was used (Fig. 1). Wheel track width was 3.5 m, base length was 2.3 m, and 9.5R32 tires were used.

Experimental studies were conducted in a specially equipped laboratory for testing with a test section length of 50 m.

Figure 1. Experimental bridge machine

Source: V. Bulgakov *et al*. (2021)

When conducting experimental studies, modern methods of strain measurement were used with a tense-resistive torque sensor. Transmission and fixation of strain gauge signals through transducers were transferred to a personal computer (PC). The results of strain measurement data were processed by statistical methods using a PC. The torque on the wheels of the axle machine was measured with a TW-2T-60K-S sensor, production – China, the characteristics of which are as follows:

Max Torque Capacity – 81 kN·m; Nonlinearity (% of Full-Scale Output) – 1%; Configuration – Heavy Duty Single or Dual Wheel.

The signal received from the torque sensor through an analogue digital converter was received and processed by a PC in the Excel software environment, discussed in detail by D. Zhuravel *et al*. (2020) and V. Borysov *et al*. (2020).

Modern methods of mathematical modelling of the behaviour of complex dynamic systems, agricultural machines and machine units were used. These methods involve modelling the movement of these objects by developing their equivalent circuits for both the entire machine-tractor unit and its element (wheel), as well as compiling differential equations of motion based on them. The resulting analytical dependencies were solved using well-known application programs on a PC. The results obtained are presented in the form of graphical dependencies.

RESULTS AND DISCUSSION

The operation of any wheeled vehicle occurs under many outside factors (forces and their moments), which change its position in space and deviate the movement from a given trajectory. The quality of processing one or another dynamic system of input variables depends on its characteristics. Relatively wide-span tractors (vehicles) such is its scheme, as well as design and other parameters. Therefore, the correct choice of the latter, from the standpoint of the necessary controllability and stability of its movement, provides it with the optimal transformation of the control and perturbing effects acting on it.

In the design of complex and expensive bridge machines (Fig. 2), the simulation process is becoming increasingly common, allowing to reduction, and sometimes eliminating, various types of in-situ testing (Pedersen *et al*., 2016). In the operational cycle of any bridge machine a curvilinear motion (turning), the characteristics of which are often decisive in the design of new or evaluation of existing models of equipment, must be considered.

a) ASA-Lift WS 9600 WS

b) ETC CTBE

Figure 2. Agricultural bridge machines

Currently, there are many steering models, most of which have been developed for fast-wheeled and tracked machines (Hac *et al*., 2009; Shahgoli *et al*., 2010; Nastasoiu & Ispas, 2014). The steering of such machines is adapted to manual steering and is built according to the kinematic or force principle of rotation. However, the application of these models to bridge wide-span machines is not always justified, due to the peculiarities of their technological cycle. Furthermore, some scientists recommend using exactly the power (onboard) rotation of the axle machine, which is implemented by rotating the wheels of the different sides of the machine at different speeds. Alternatively, combined

kinematic-force diagrams are proposed for use, improving the controllability of overhead machines.

The specific features of the bridge machine sometimes pose additional problems in the study of curvilinear motion, not all of which have been solved until today. The idea of the scientific approach is to consider the bridge machine as a controlled object, the curvilinear motion of which is determined by the links imposed on it, provided by the design and control system, and interacting with the soil track of a constant technological track.

Traditional turning of wheeled machines is performed on a certain area, the size of which depends on the minimum radius of the turn, and includes several phases: entering the turn, the turn itself and exiting from the turn (Nadykto *et al*., 2015). Due to the presence of elasticities in the "wheel–supporting surface" system, the trajectory of the mobile machine when turning does not depend unambiguously on the turn of the steering wheel. All this makes it difficult to automate the process of turning (Nastasoiu & Ispas, 2014). The most widespread methods for turning mobile machines are those that involve rotating the steered wheels (front, rear or both front and rear) relative to the body or by changing the position of one part of the mobile machine relative to the other in the horizontal plane (articulated frame). In this case, if the machine has all the steering wheels, they can turn simultaneously on the front and rear axles in different directions (full-return mode or "path in the track") or to one side (crab mode). Considering the general structure of its chassis and steering drive, a purely on-board (power) turn in the horizontal plane, which is carried out by different rotation speeds of the wheels of the right and left side, is considered a promising way to turn the overhead machine. In this case, a four-wheeled axle machine with a sideways turn is turned around the absolute centre of turn of the intersection of the extension of the front and rear axles. The lateral displacement of the machine relative to the trajectory line is possible only as a result of uncontrolled sideways drift.

There are two main theoretical methods for wheeled machine rotation in terms of describing the force interaction between the propulsor and the supporting surface.

First – for machines with steerable wheels and articulated frames, the lateral departure method is widely used (Pascuzzi, 2015). The description of force interaction is based on the Rocard hypothesis of linear dependence of lateral force on the angle of wheel departure, explained by the elastic properties of the tire and applicable in the absence of sliding (Wang *et al*., 2016). Attempts to account for wheel slip of a machine within the theory of lateral guidance run counter to the underlying assumptions, and sometimes violate the laws of mechanics. Models of this type have proven themselves well in describing the rotation of fast cars on a solid base with large turning radii, where there is virtually no slip of the wheels and, the transverse force can be easily explained by the action of the normal acceleration. However, the movement of a bridge vehicle with wheels that do not have large hooks, due to their lack of use when driving on the constant hard track, will inevitably slip when turning. Therefore, models based on lateral guidance cannot be applied to describe the curvilinear motion of a bridge machine.

Another type of mobile machine with non-swivelling wheels and power sideways rotation, where the interaction of the propulsor with the ground is characterized by increased slip (Wang *et al*., 2008). The elastic properties of the tire are neglected in these models. Following those, the basic forces in contact are reduced to a single equilibrium force applied at the centre of pressure, which corresponds to progressive sliding, incompatible with curvilinear motion. Adding a friction torque to the result traction limit will exceed the traction limit of the machine. When a machine turns, with the friction torque present, the value of the resultant force must be less than its traction limit. The larger the torque, the smaller the final force, which makes it unpredictable and does not allow the ground reaction to be explicitly noted.

Different methodological approaches in describing the interaction of wheeled and tracked movers with the soil complicate their application to a bridge vehicle, especially with a combined mover. In the theory of turning of wheeled and tracked machines, models of passive turning, which takes place in the technological cycle of many bridge machines, are insufficiently studied.

At the beginning of the study, the assumption that the turning of the bridge machine, regardless of the type of its mover, is accompanied by sliding within the soil trace of a constant track was considered. The elementary tangential friction (adhesion) forces caused by the contact of the propulsor with the bearing surface of the soil track of a constant technological track are determined by the direction of relative motion and the anisotropy of the interaction between the propulsor and the soil. In this case, in the process of turning the bridge machine, its propulsor performs a flat motion (Fig. 3).

At each point of contact of the axle-motor with the constant track (Fig. 3), a basic friction force $dT = \varphi \cdot q \cdot dF$ (where φ – adhesion coefficient, q – the normal pressure at the elementary site dF of the bearing surface) is present, directed in the opposite direction to the linear velocity V, which in turn is perpendicular to the radius r, connecting the point with the instantaneous centre of the sliding (adhesion) velocities.

Combining all basic forces (Fig. 3) to the instantaneous centre of velocities (point C), and adding them over the contact area, expressions for the projections of the resultant force (in the longitudinal T_y and transverse T_x directions) and the moment M are obtained:

$$\left.\begin{aligned} T_x &= -\int_\eta \int_\xi q\varphi_x \frac{y-\eta}{\sqrt{(x-\xi)^2+(y-\eta)^2}} d\xi\, d\eta, \\ T_y &= \int_\eta \int_\xi q\varphi_y \frac{x-\xi}{\sqrt{(x-\xi)^2+(y-\eta)^2}} d\xi\, d\eta, \\ M &= \int_\eta \int_\xi q\left(\frac{\varphi_x(y-\eta)^2+\varphi_y(x-\xi)^2}{\sqrt{(x-\xi)^2+(y-\eta)^2}}\right) d\xi\, d\eta, \end{aligned}\right\} \quad (1)$$

where q – the normal pressure at the contact point with coordinates ξ, η; φ_x, φ_y – transverse and longitudinal coefficients of adhesion at the point with coordinates ξ, η.

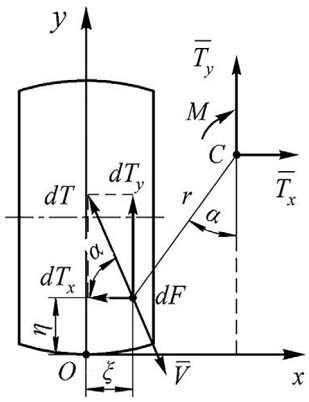

Figure 3. Formation of forces in the contact of the wheel of a bridge machine with the constant track
Note: dT – basic friction force; **φ** – friction coefficient; q – normal pressure; dF – elementary area of the support surface; V – linear velocity; r – radius connecting the point with the instantaneous centre of sliding (adhesion) velocities; C – instantaneous centre of velocities; T_x, T_y – projections of the resulting force in the transverse and longitudinal directions; M – moment; **α** – angle of inclination of the elementary friction force in the longitudinal direction
Source: developed by the authors

Dependence (1) considers the relationship between the force and the friction (adhesion) moment, as well as the anisotropy of the interaction through different adhesion coefficients φ_x, φ_y. The force factors in it are formed in the contact of each propulsor support with the soil. The integration limits can be used for any shape and size of the contact surface. However, in describing the rotation of a bridge vehicle, dependence (1) does not consider the deformation of the soil in the traces of the constant technological track and the elastic properties of pneumatic tires.

Elastic properties of the soil trace of a constant track will be considered by variable coefficients φ_x, φ_y. To determine them, the maximum tangential traction force, which is developed by the wheel of a bridge machine, is assumed to be:

$$P_{kmax} = \varphi_{yd} \cdot N_{ek}, \tag{2}$$

where φ_{yd} – longitudinal coefficient of traction at full slip, N_{ek} – vertical operating load, which acts on the wheel of the bridge machine. From tractor theory, it is known that the maximum tangential traction force that a tractor wheel develops can be determined from the expression (Nadykto *et al.*, 2020):

$$P_{kmax} = \delta_{max} \cdot S_k \cdot k_0 \cdot L, \tag{3}$$

where δ_{max} – slip ratio (maximum) of the axle machine wheels, S_k – sum of the vertical projections of the bearing surfaces of the wheel sprocket submerged in the soil, k_0 – sum of the vertical projections of the bearing surfaces of the wheel sprocket submerged in the soil, L – is the length of the arc of traction of the wheel hitches with the bearing surface (the trace of the permanent tramline), the value of which find from the expression (Nadykto *et al.*, 2020):

$$L = r_k \cdot \left(\arctan \frac{f_k \cdot (1 - f_k^2)^{\frac{1}{2}}}{0.5 - f_k^2} + 2 \cdot f_k^2 \right), \tag{4}$$

where r_k – wheel radius, f_k – wheel rolling resistance coefficient.

The rolling radius r_k of the wheel of a bridge machine can be determined by its static radius r_0 and normal tire deflection h_z:

$$r_k = r_0 + h_z. \tag{5}$$

The normal tire deflection of a mobile machine or tractor wheel can be determined from the expression (Mitkov *et al.*, 2021):

$$h_z = \frac{N_{ek}}{\pi \cdot \rho_w \cdot \sqrt{2 \cdot r_0 \cdot b_0}}, \tag{6}$$

where ρ_w – tire pressure, r_0, b_0 – static radius and wheel diameter of the bridge machine.

The sum of the vertical projections S_k of the bearing surfaces of the wheel axles of the bridge machine, buried in the soil, determined from the expression (Mitkov *et al.*, 2021):

$$S_k = \pi \cdot h_z \cdot [(2 \cdot r_0 - h_z) \cdot (b_0 - h_z)]^{\frac{1}{2}}. \tag{7}$$

By substituting the values of S_k, L, r_k (4-7) into (3) and equating the expressions (2) have:

$$\delta_{max} \cdot \pi \cdot h_z \cdot [(2 \cdot r_0 - h_z) \cdot (b_0 - h_z)]^{\frac{1}{2}} \cdot (r_0 + h_z) \left(\arctan \frac{f_k \cdot (1 - f_k^2)^{\frac{1}{2}}}{0.5 - f_k^2} + 2 \cdot f_k^2 \right) = \varphi_{yd} \cdot N_{ek}. \tag{8}$$

From the analysis of the obtained equation (8) it follows that with the increase of the coefficient of adhesion φ_{yd} of the bridge machine under the contact of its wheels with the bearing surface of the constant track, the maximum slip coefficient δ_{max} increases. With the increase of the wheel radius r_0, the width of the tires b_0 and air pressure ρ_w, as well as the vertical load N_{ek}, exerted, the wheel grip φ_{yd} with the bearing surface of the permanent technological track increases as well. Hence the conclusion is that the greater the traction of the wheel of the bridge machine with the bearing surface of the constant technological track, the more slipping can be achieved. The nature of this

relationship is determined by the parameters of the bridge machine, the mode of its movement and the properties of the bearing surface of the traces of a constant track.

Results of studies of the maximum slip coefficient estimation δ_{max} of the wheel of a bridge machine from the value of its friction coefficient φ_{yd} are shown in Figure 4.

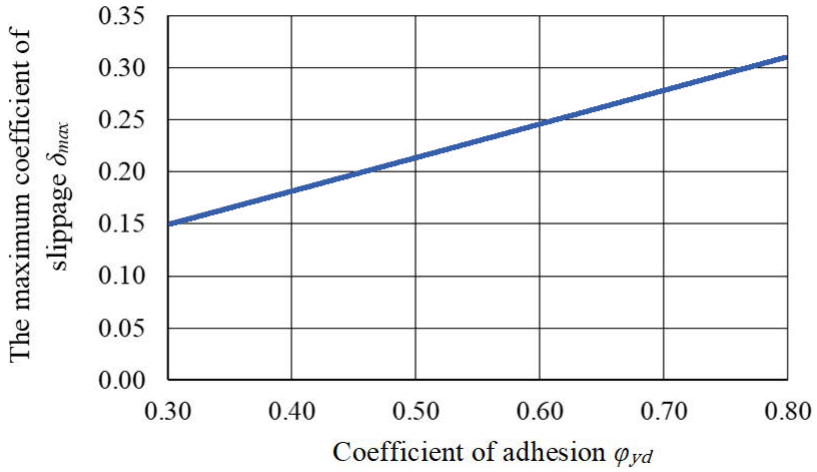

Figure 4. Dependence of the maximum slipping ratio of the bridge machine δ_{max} from the coupling coefficient φ_{yd} with the bearing surface of the soil trace of the permanent technological track
Note: δ_{max} – slip coefficient; φ_{yd} – adhesion coefficient
Source: developed by the authors

The result obtained in Figure 4 can be explained as follows. The phenomenon of slipping of the bridge machine wheels is caused by the displacement of the support surface of the trace of the constant track by the tires until the necessary amount of tangential stress is formed in it. The higher the strength of the bearing surface on which the wheel of the bridge machine moves, the less the slippage affects the connection between the soil particles. As a result, the depth of the wheels sinking into the soil is reduced and, accordingly, the energy consumption for the formation of a groove by the star-shaped hooks is reduced. Therefore, the degree of wheel slip is determined by the amount of horizontal deformation (shearing) of the soil, which is carried out by the star gears. The specified horizontal deformation of the soil depends on the specific pressure on the bearing surface of the permanent trace of the technological track and on its ability to resist deformation.

The force factors T_x, T_y, M in the contact of the wheel of the bridge machine with the bearing surface of the constant trace of the technological track depend on the unknown coordinates of the instantaneous velocity centre, which reduces the force problem to the kinematics of its motion. Next, it was investigated the kinematics of the curvilinear motion of the constant track system – mover–bridge machine, and describe the connections arising in the process of its rotation. It was introduced a stationary coordinate system (xOy), the machine's motion system ($x_1O_1y_1$) and local frames of reference (x_{ij} y_{ij}), associated with each of the thrusters of the bridge machine (Fig. 5).

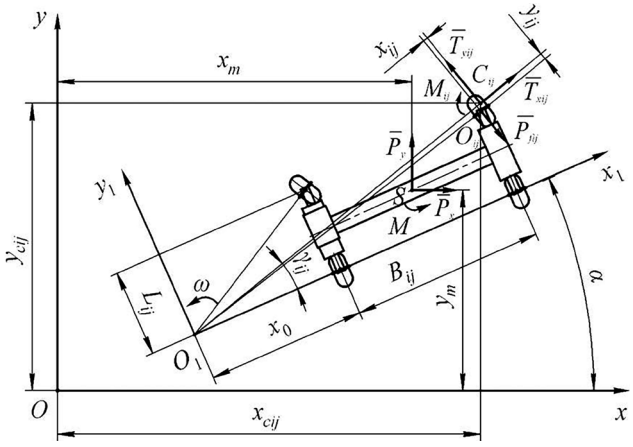

Figure 5. Diagram of unsteady rotation of an arbitrary multi-support bridge machine
Note: xOy – system of fixed coordinates; $x_1O_1y_1$ – system of moving coordinates coinciding with the centre of rotation of the machine; x_m, y_m, α – current coordinates of the centre of mass and the angle of rotation of the machine body in the fixed coordinate system; P_{fij} – resistance to movement ij of the supporting wheel; m, J – mass and moment of inertia of the machine relative to the vertical axis passing through its centre of mass; P_x, P_y, M – external forces and external moment, reduced to the centre of mass of the machine; T_{xij}, T_{yij}, M_{ij} – force factors in contact ij of the support wheel with the trace of the constant technological track; γ_{ij} – angle of rotation ij of the support relative to the vertical axis in the machine system
Source: developed by the authors

To describe the unsteady motion of an arbitrary multi-support bridge machine with n axes (i = 1, ..., n) and m supports on each axis (j = 1, ..., m) a generalized model of its controlled rotation should be formulated:

$$\left.\begin{aligned} m\cdot\ddot{x}_m &= \sum_{i=1}^{n}\sum_{j=1}^{m}\left[T_{xij}\cdot\cos(\gamma_{ij}+\alpha) - T_{yij}\cdot\sin(\gamma_{ij}+\alpha) + f_{ij}\cdot G_{ij}\cdot\sin(\gamma_{ij}+\alpha)\right] + P_x,\\ m\cdot\ddot{y}_m &= \sum_{i=1}^{n}\sum_{j=1}^{m}\left[T_{xij}\cdot\sin(\gamma_{ij}+\alpha) + T_{yij}\cdot\cos(\gamma_{ij}+\alpha) - f_{ij}\cdot G_{ij}\cdot\cos(\gamma_{ij}+\alpha)\right] + P_y,\\ J\cdot\ddot{\alpha} &= \sum_{i=1}^{n}\sum_{j=1}^{m}\left[T_{yij}\cdot\sin\gamma_{ij} - T_{xij}\cdot\cos\gamma_{ij}\cdot(L_{ij} - y_m + x_{ij}\cdot\sin\gamma_{ij} + y_{ij}\cdot\cos\gamma_{ij}) - \right.\\ &\quad -f_{ij}\cdot G_{ij}\cdot\cos\gamma_{ij}\cdot(B_{ij} - x_m) - f_{ij}\cdot G_{ij}\cdot\sin\gamma_{ij}\cdot(L_{ij} - x_m) - M_{ij} +\\ &\quad \left.+(T_{yij}\cdot\cos\gamma_{ij} + T_{xij}\cdot\sin\gamma_{ij})\cdot(B_{ij} - x_m + x_{ij}\cdot\cos\gamma_{ij} - y_{ij}\cdot\sin\gamma_{ij})\right] + M, \end{aligned}\right\} \quad (9)$$

where x_m, y_m, α – the current coordinates of the centre of mass and the angle of rotation of the machine body in a fixed Cartesian system, $f_{ij}\cdot G_{ij} = P_{fij}$ – resistance of support wheel movement ij, m, J – mass and moment of inertia of the machine relative to the vertical axis passing through its centre of mass, P_x, P_y, M – external forces and external momentum applied to the centre of mass of the machine, T_{xij}, T_{yij}, M_{ij} – force factors in the contact of the support wheel ij with a constant technological track. The initial conditions of motion of the bridge machine (coordinates of the instantaneous velocity centre) are taken from the solution of the moving-away problem. Next, it was written down the coupling reactions of the bridge machine for the considered diagram (Fig. 5). In the case of the power (onboard) rotation of the bridge machine, when the supports of its thrusters are unguided, it is sufficient to consider its stationary rotation, according to which the beginning of the moving system $x_1O_1y_1$ coincides with the turning centre of the turning machine. In this case, the kinematics of the unguided randomly positioned support wheel of the bridge machine is shown in Figure 6. Based on Figure 6, the actual speed V_{Dij} of the contact patch points (point A_{ij}) of each arbitrarily positioned support wheel ij of a bridge machine is the sum of the theoretical speed V_{Tij} and sliding speeds V_{CKij}.

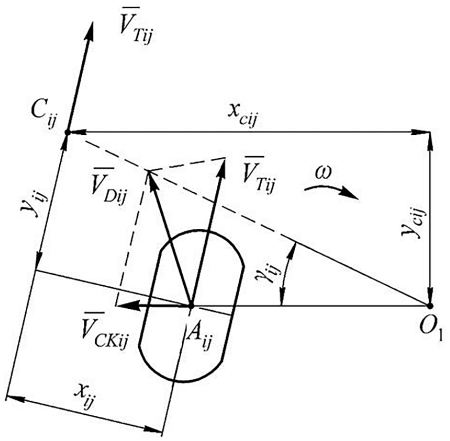

Figure 6. Kinematics of an unguided randomly positioned support wheel of a bridge machine

Note: C_{ij} – point of the wheel body located above it; V_{Tij} – theoretical speed of movement directed along the rolling plane ij of the support wheel; A_{ij} – point of the contact spot of any ij arbitrarily located support wheel of the bridge machine; V_{Dij} – actual speed of the contact spot point; V_{Tij} – theoretical speed; V_{CKij} – sliding speed; x_{cij}, y_{cij} – coordinates of the instantaneous centre of speeds of the propeller support in the machine system; V_{Tij} – theoretical speed of the axis ij of the support; O_1C_{ij} – distance from the centre of rotation of the machine to the instantaneous centre of speeds ij of the support; γ_{ij} – angle of rotation ij of the support relative to vertical axis in the machine system

Source: developed by the authors

The only point in Figure 6 without slip is the instantaneous velocity centre, therefore the wheel body point (C_{ij}), located above it has only theoretical velocity V_{Tij}, directed along the rolling plane of the support wheel ij. Using the orthogonality theorem for the unguided thruster support, according to which, when the machine rotates, the instantaneous centre of velocities of the support area of an arbitrarily located thruster support lies on the perpendicular dropped from the centre of rotation of the machine to the plane of its rolling, write the bond equations for each support wheel in the form:

$$x_{cij}\cdot\sin_{\gamma ij} - ycij\cdot\cos\gamma_{ij} = 0, \quad (10)$$

and

$$V_{Tij} = \omega\cdot(O_1C_{ij}), \quad (11)$$

where x_{cij}, y_{cij} – coordinates of the instantaneous velocity centre of the thruster support in the machine system, V_{Tij} – theoretical speed of the ij axis of the support, O_1C_{ij} – distance from the centre of rotation of the machine to the instantaneous centre of velocities ij of the support, γ_{ij} – rotation angle ij of the support relative to the vertical axis in the machine system.

The geometric relation equation (10) reflects the design scheme and parameters of the bridge machine (base, track, number of supports and their mutual positioning) since the transformation of coordinates of the instantaneous centre of speeds (x_{cij}, y_{cij}) for any design of the support and running system (with steerable or nonrotating support wheels) is performed by consecutive shifting and turning.

The kinematic relationship equation (11) is determined by the turn control scheme and reflects the mode of motion of each support (driven, leading, braking). In some cases, it is more convenient to write equation (11) through force factors, since the latter are functions of instantaneous velocity centre coordinates:

- driven wheel (flange) of a bridge machine:

$$T_{yij} = 0, \tag{12}$$

- brake wheel (side) of an overhead machine:

$$x_{cij} = 0, \tag{13}$$

- individually driven motor-wheel:

$$\omega = \frac{V_{Tij}}{\sqrt{x_{cij}^2 + y_{cij}^2}}, \tag{14}$$

- individually driven motor-wheel:

$$k = \frac{V_{mj+1}}{V_{mj}} = \frac{x_0 + B + x_{j+1}}{x_0 + x_j}. \tag{15}$$

A different combination of geometric (10) and kinematic equations (12-15) allows for a description of restrictions imposed by the design scheme of the bridge vehicle (number of propulsor supports, their mutual arrangement, steering scheme, base, and track) and control system on its curvilinear motion parameters. As a result of solving the system of equations (9) considering the unknowns x_m, y_m, α and the coordinates of the instantaneous velocity centre (x_{ij}, y_{ij}), all force and kinematic characteristics of curvilinear motion of the bridge machine were acquired, namely angular velocity, trajectory of motion, longitudinal and transverse components of the velocity of the centre of mass, actual turning radius, normal acceleration, traction forces and slipping on the leading supports, distribution of normal reactions on the supports, power losses and their change in time, depending on the control parameters.

Considering that when turning, the bridge machine moves within the boundaries of the trace of a constant track, its curvilinear movement must occur with a constant radius. Therefore, the generalized model of controlled curvilinear motion requires a transformation to build partial models of the system solution (9). For this, it is enough to consider the stationary and statistical stationary modes of the turning of the bridge machine. A stationary turn is characterized by a constant radius and acceleration of the bridge machine and is realized with constant control parameters:

$$\ddot{\gamma}_{ij} = 0, \ddot{\alpha} = 0. \tag{16}$$

The model of the stationary rotation is made in the natural coordinates of the moving trihedron ($\alpha = 0$). The unknowns are the coordinates of the centre of rotation in the machine system of its angle speed y_0, its angle speed ω and the coordinates of the instantaneous velocity centre x_{ij}, y_{ij}. The stationary rotation model is a system of $2nm$ coupling equations (10-15) and three equations of motion:

$$\left.\begin{aligned} -m\cdot\omega^2\cdot y_0 &= \sum_{i=1}^{n}\sum_{j=1}^{m}\left(T_{xij}\cdot\cos\gamma_{ij} - T_{yij}\cdot\sin\gamma_{ij} + f_{ij}\cdot G_{ij}\cdot\sin\gamma_{ij}\right) + P_x,\\ -m\cdot\omega^2\cdot x_0 &= \sum_{i=1}^{n}\sum_{j=1}^{m}\left(T_{xij}\cdot\sin\gamma_{ij} + T_{yij}\cdot\cos\gamma_{ij} + f_{ij}\cdot G_{ij}\cdot\cos\gamma_{ij}\right) + P_y,\\ 0 &= \sum_{i=1}^{n}\sum_{j=1}^{m}\left[-M_{ij} + T_{yij}\cdot\sqrt{x_{cij}^2 + y_{cij}^2} - f_{ij}\cdot G_{ij}\cdot\left(\sqrt{x_{cij}^2 + y_{cij}^2} - x_{ij}\right)\right] + M. \end{aligned}\right\} \tag{17}$$

Static stationary rotation is characterized by low operating speeds ($\omega = 0$) of the bridge machine, with the centrifugal forces being so small that they can be neglected. This reduces by one the number of unknowns and converts equations of motion (17) to equilibrium equations (the left parts are zero). The number of geometric coupling equations (10) is equal to the number of bridge machine propulsor supports, and the number of kinematic coupling equations (11) is reduced by one due to the exclusion of angular rotation speed ω:

$$\omega = \frac{V_{ij}}{R_{ij}}. \tag{18}$$

The adequacy of partial models (17) was tested using the force and kinematic parameters of the bridge machine prototype movement (Fig. 2). Experimental verification of the main theoretical provisions was performed on the example of a stationary force (on-board) rotation of the prototype of a bridge vehicle, which allowed to exclude the influence of various random factors. The experiment consisted of 6 trials with different weights of the bridge machine with three times the number of repetitions of each trial. A simulation of the bridge machine loading was carried out by placing additional mass on it (Ostanin, 2022). During the experiment, the driving radius and torques on driving wheels were measured, with their subsequent recalculation to the moment of resistance to turning:

$$M_c = 0.5\mathrm{B}\cdot(T_{y2} - T_{y1}). \tag{19}$$

The power diagram of the on-board turning prototype of the bridge machine is shown in Figure 7.

Following Figure 7, the turning model of a bridge vehicle consists of:

- three equations of motion (17):

$$\left.\begin{aligned} 0 &= \sum_{i=1}^{n}\sum_{j=1}^{m}\left(T_{xij}\cdot\cos\gamma_{ij} - T_{yij}\cdot\sin\gamma_{ij} + f_{ij}\cdot G_{ij}\cdot\sin\gamma_{ij}\right) + P_x,\\ 0 &= \sum_{i=1}^{n}\sum_{j=1}^{m}\left(T_{xij}\cdot\sin\gamma_{ij} + T_{yij}\cdot\cos\gamma_{ij} + f_{ij}\cdot G_{ij}\cdot\cos\gamma_{ij}\right) + P_y,\\ 0 &= \sum_{i=1}^{n}\sum_{j=1}^{m}\left[M_{ij} + T_{yij}\cdot\sqrt{x_{cij}^2 + y_{cij}^2} - f_{ij}\cdot G_{ij}\cdot\left(\sqrt{x_{cij}^2 + y_{cij}^2}\right)\right] - M, \end{aligned}\right\} \tag{20}$$

- two equations of geometric relations (10):

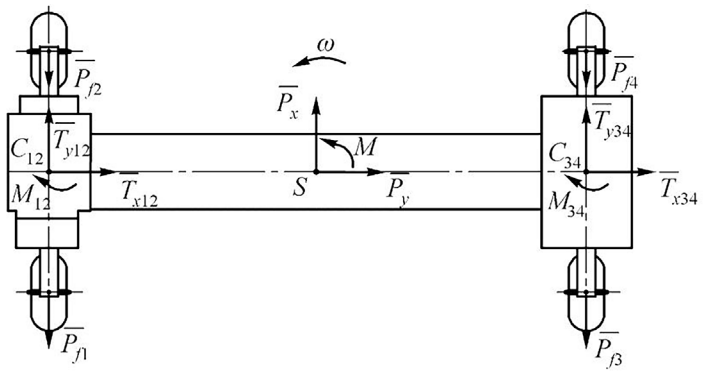

Figure 7. Diagram of forces acting on the bridge machine, when it performs a force (onboard) turn
Note: T_{xij}, T_{yij}, M_{ij} – force factors reduced to the centre of mass of the left and right sides of the bridge machine in contact *ij* of the support wheels with traces of a constant tramline; P_x, P_y, M – external forces and external moment reduced to the centre of mass of the machine; P_{fij} – resistance movement *ij* of the supporting wheel; ω – angular speed of rotation
Source: developed by the authors

$$\left.\begin{array}{l} y_0 + y_1 = 0, \\ y_1 = y_2, \end{array}\right\}, \quad (21)$$

one equation of kinematic connections with one of the sides of the bridge machine disconnected:

$$T_{y1} = 0. \quad (22)$$

The adequacy of the model was evaluated by the force parameter – the coefficient of resistance to rotation:

$$\mu = \frac{4 \cdot M_c}{G \cdot L}. \quad (23)$$

The analysis of the convergence of theoretical and experimental values showed that the theoretical dependence $\mu(G)$ lies within the confidence interval $\pm\sigma$ throughout the investigated weight range G of the prototype bridge machine (Fig. 8) (Aghbalyan & Simonyan, 2022).

The obtained research results allow to assess the impact of design parameters and schemes on the characteristics of turning at the design stage of a new bridge machine, thereby optimizing its design. Issues related to the study of the traction qualities of wheeled vehicles are considered by A. Panchenko *et al*. (2019), and V. Bulgakov *et al*. (2021). They noted that for the machine as a whole, traction and dynamic properties are usually estimated by the traction efficiency and dynamic factor. However, each of the wheels of the bridge machine operates under certain conditions in terms of vertical load, input torque, and driving conditions. Therefore, the traction properties of the wheel of the bridge machine depend on a large number of parameters. These include its design parameters, on the one hand, and the physical and mechanical properties of the surface of permanent tramline tracks, on the other.

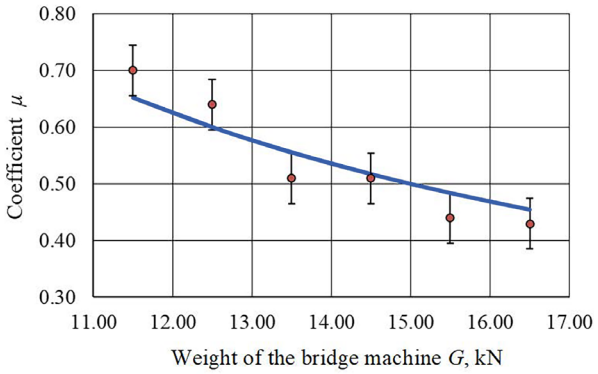

Figure 8. Theoretical dependence and experimental values of the coefficient μ from the weight G of the bridge machine
Note: μ – turning resistance coefficient; G – weight of the bridge machine
Source: developed by the authors

The obtained research results significantly supplement the known knowledge about the turning of wheeled vehicles, for example, presented by V. Nadykto *et al*. (2015) and S.P. Pozhidaev *et al*. (2016), who used the theory of active controlled movement (under the action of an operator) as a research basis. The obtained mathematical models consider the passive rotation of bridge machines in the process of their curvilinear movement without a control action from the operator. In particular, the uneven traction resistance that the bridge machine experiences along the width of its

span; uneven vertical load on the support wheels from the left and right sides of the machine; the presence of support wheels for agricultural implements located in the area of the width of the span of the bridge machine and another, which redistributes its traction and coupling properties unevenly from its left and right sides. S.P. Pozhidaev *et al.* (2016) studied the kinematics and force interaction of the wheel or caterpillar of a traditional tractor with the soil at the moment of turning in detail. However, the issues of the curvilinear motion of a wide-gauge wheeled vehicle with a power (on-board) method of its control were not considered in this study, which makes it impossible to use the obtained theoretical and experimental studies to simulate the curvilinear motion of a bridge vehicle.

At the same time, the movement of the bridge machine along the soil tracks of a permanent tramline creates such conditions under which the modelling of forces in the contact of the mover with the surface of the tramline leads to the disappearance of the boundary between the wheeled and caterpillar mover and suggests the possibility of a unified approach to describing their force interaction with the support surface. Therefore, following M. Fashutdinov *et al.* (2020), greatly simplifies the process of studying the turning property of a bridge machine, even with a wheeled-caterpillar mover, as was considered, where the machine turn models are based on various methodological approaches when describing the interaction of the mover with the soil.

The obtained mathematical models of the curvilinear motion of bridge machines consider the variety of their design schemes and control systems, which impose certain restrictions on the characteristics of the curvilinear motion, manifested in the form of superimposed kinematic and geometric relationships. This significantly distinguishes the well-known theories of unsteady motion of a wheeled vehicle with front steered wheels, presented, for example, by V. Melnik *et al.* (2017).

T. Szakács (2010), I. Demšar *et al*. (2012), and M.Z. Song *et al*. (2014) researched large external loads acting on the bridge machine and the use of propulsion devices with small lugs on it was considered the presented studies to characterise their significant slip when turning within the boundaries of the permanent tramline track on the headland. Such an approach to describing the interaction of the propeller of a wide-span machine with the soil is absent when describing the movement of traditional mobile machines when they perform a turn.

Thus, the results of the study and its analysis showed that with an increase in the weight of the bridge machine due, for example, to an increase in its size or the use of heavier technological equipment on it, when moving along the soil track of a constant tramline, the resistance coefficient μ of its rotation tends to decrease. The obtained research results allow to address the problem of power rotation of a wide-span bridge machine, considering the slight deformation of the soil in the traces of a permanent tramline.

CONCLUSIONS

As a result of this research, a methodology for compiling private models of turning the bridge vehicle moving along the soil trace of the constant technological track was created. As a result of the joint solution problem of the bridge machine turning, it is possible to determine all output parameters of curvilinear motion: trajectory, tractive forces, turning radius, slipping, and actual speeds.

The force interaction of the bridge machine's undercarriage with the soil trace of a constant track is presented based on flat sliding with a variable anisotropic friction coefficient of adhesion φ_{yd}, depending on the properties of the track. As with the radius of the wheel, the width of its tire and the air pressure in it, as well as the vertical load that acts on it, the coefficient of traction of the bridge machine φ_{yd} increases, and more slippages can be achieved in doing so.

The adequacy of the model of stationary turning of the overhead machine is confirmed by experimental estimation of the resistance coefficient of the power on board turning. The convergence of the theoretical and experimental values of this coefficient is within the confidence interval $\pm\sigma$ in the whole investigated weight range of the prototype of the bridge machine. This allows to assess the influence of design parameters and schemes on the turning characteristics as early as the design stage of a new bridge machine, thus optimizing the design process.

The prospect for further research is the development of static and dynamic models of the turn of the bridge machine and, on their basis, to substantiate the parameters of the influence of structural and technological parameters on the dynamics of its turn, as well as the wear processes of its wheel tires.

ACKNOWLEDGEMENTS

None.

CONFLICT OF INTEREST

None.

REFERENCES

[1] Aghbalyan, S., & Simonyan, V. (2022). Study of hardening and structure of maraging powder steel grade PS-H18K9M5TR (18%Ni+9%Co+5%Mo+1%Ti+1%Re+66%Fe). *Scientific Herald of Uzhhorod University. Series "Physics"*, 52, 46-55. doi: 10.54919/2415-8038.2022.52.46-55.

[2] Al-khayyt, S.Z.S. (2018). Creating through points in linear function with parabolic blends path by optimization method. *Al-Khwarizmi Engineering Journal*, 14(1), 77-89. doi: 10.22153/kej.2018.10.005.

[3] Antille, D.L., Peets, S., Galambošová, J., Botta, G.F., Rataj, V., Macak, M., Tullberg, J.N., Chamen, W.C.T., White, D.R., Misiewicz, P.A., Hargreaves, P.R., Bienvenido, J.F., & Godwin, R.J. (2019). Review: Soil compaction and controlled traffic farming in arable and grass cropping systems. *Agronomy Research*, 17(3), 653-682. doi: 10.15159/AR.19.133.

[4] Borysov, V., Hevko, I., Torubara, O., Borysova, S., Milko, D., Zhuravel, D., Tsymbal, B., Bratishko, V., Samoichuk, K., & Postol, Y. (2020). Revealing new patterns in resource-saving processing of chromium-containing ore raw materials by solidphase reduction. *Eastern-European Journal of Enterprise Technologies*, 103, 24-29. doi: 10.15587/1729-4061.2020.196653.
[5] Bulgakov, V., Pascuzzi, S., Nadykto, V., Ivanovs, S., & Adamchuk, V. (2021). Experimental study of the implement-and-tractor aggregate used for laying tracks of permanent traffic lanes inside controlled traffic farming systems. *Soil and Tillage Research*, 208, article number 104895. doi: 10.1016/j.still.2020.104895.
[6] Demšar, I., Bernik, R., & Duhovnik, J. (2012). A mathematical model and numerical simulation of the static stability of a tractor. *Agriculturae Conspectus Scientificus*, 77(3), 143-150.
[7] Fashutdinov, M., Khafizov, K., Galiev, I., Gabdrafikov, F., & Khaliullin, F. (2020). Research of dynamics of turning of machine-tractor aggregate with tractor on wheeled-crawler mover. *BIO Web of Conferences*, 17, article number 00056. doi: 10.1051/bioconf/20201700056.
[8] Hac, A., Fulk, D., & Chen, H. (2009). Stability and control considerations of vehicle-trailer combination. *SAE International Journal of Passenger Cars – Mechanical Systems*, 1(1), 925-937. doi: 10.4271/2008-01-1228.
[9] Kørup, K., Bruun, S., Pedersen, H.H., Nielsen, J.A., Gómez-Muñoz, B., Boldsen, S.K., Rasmussen, A., & Olesen, J.E. (2022). Experiences from conservation agriculture approaches on conventional and organic arable farms. *SSRN Electronic Journal*. doi: 10.2139/ssrn.4292663.
[10] Lou, S., He, J., Li H., Wang, Q., Lu, C., Liu, W., Liu, P., & Zhang, Z. (2021). Current knowledge and future directions for improving subsoiling quality and reducing energy consumption in conservation fields. *Agriculture*, 11(7), article number 575. doi: 10.3390/agriculture11070575.
[11] Melnik, V., Dovzhyk, M., Tatyanchenko, B., Solarov, O., & Sirenko Yu. (2017). Analytical method of examining the curvilinear motion of a four-wheeled vehicle. *Easterm-Euroean Journal of Enterprise Technologies*, 3(7(87)), 59-65. doi: 10.15587/1729-4061.2017.101335.
[12] Mitkov, V., Kiurchev, S., Nurek, T., Chorna, T., Ihnatiev, Y., Kuvachov, V., Głowacki, S., Hutsol, T., Yermakov, S., & Terenov, D. (2021). *Scientific bases of the combined units aggregation based on arable and row-crop tractor*. Warszawa: Libra-Print. doi 10.22630/SGGW.IIM.9788382370072.
[13] Nadykto, V., Arak, M., & Olt, J. (2015). Theoretical research into the frictional slipping of wheel-type undercarriage taking into account the limitation of their impact on the soil. *Agronomy Research*, 13(1), 148-157.
[14] Nadykto, V., Kyurchev, V., Bulgakov, V., Findura, P. & Karaiev, O. (2020). Influence of the plough with tekrone moldboards and landsides on ploughing parameters. *Acta Technologica Agriculturae*, 23(1), 40-45.
[15] Nastasoiu, M., & Ispas, N. (2014). Study on the dynamic interaction between agricultural tractor and trailer during braking using Lagrange equation. *Applied Mechanic and Materials*, 659, 515-520. doi: 10.4028/www.scientific.net/AMM.659.515.
[16] Ostanin, V. (2022). Effects of repulsion and attraction between rotating cylinders in fluids. *Scientific Herald of Uzhhorod University. Series "Physics"*, 51, 39-47. doi: 10.54919/2415-8038.2022.51.39-47.
[17] Panchenko, A., Voloshina, A., Milaeva, I. & Luzan, P. (2019). Operating conditions' influence on the change of functional characteristics for mechatronic systems with orbital hydraulic motors. In V. Nadykto (Ed.), *Modern development paths of agricultural production: Trends and innovations* (pp. 169-176). Berlin: Springer. doi: 10.1007/978-3-030-14918-5_18.
[18] Pascuzzi, S. (2015). A multibody approach applied to the study of driver injuries due to a narrow-track wheeled tractor rollover. *Journal of Agricultural Engineering*, 46(3), 105-114. doi: 10.4081/jae.2015.466.
[19] Pedersen, H.H., Oudshoorn, F.W., & McPhee, J.E. (2016). Wide span – re-mechanising vegetable production. *Acta Horticulturae*, 1130, 551-557. doi: 10.17660/ActaHortic.2016.1130.83.
[20] Pozhidaev, S.P., Troyanovskaya, I.P., & Shkarovskii, G.V. (2016). *Some questions in the theory of movement of self-propelled machines and units*. Kyiv: Agrarian Media Group.
[21] Shahgoli, G., Fielke, J., Desbiolles, J. & Saunders, C. (2010). Optimising oscillation frequency in oscillatory tillage. *Soil and Tillage Research*, 106(2), 202-210. doi: 10.1016/j.still.2009.10.005.
[22] Song, M.Z., Kang, S.W., Chung, S.O., Kim, K.D., Chae, Y.S., Lee, D.H., Kim, Y.J., Yu, S.H. & Lee, K.H. (2013). Path planning algorithm for an autonomous mower tractor. *Korean Journal of Agricultural Science*, 42(1), 63-71. doi: 10.7744/cnujas.2015.42.1.063.
[23] Song, P., Zong, C.-F., & Tomizuka, M. (2014). A terminal sliding mode based torque distribution control for an individual-wheel-drive vehicle. *Journal of Zhejiang University: Science A*, 15(9), 681-693. doi: 10.1631/jzus.A1400101.
[24] Startsev, A., Romanov, S., & Storozhev, I. (2023). Motion stability of tractor transport unit in uncontrolled rotation mode. In *Proceedings of the 8th International Conference on Industrial Engineering* (pp. 300-308). Berlin: Springer. doi: 10.1007/978-3-031-14125-6_30.
[25] Szakács, T. (2010). Developing stability control theories for agricultural transport systems. *Acta Polytechnica Hungarica*, 7(2), 25-37.
[26] Tamirat, T.W., Pedersen, S.M., Robert Farquharson, J., de Bruin, S., Forristal, P.D., Sørensen, C.G., Nuyttens, D., & Pedersen, H.H. (2022). Controlled traffic farming and field traffic management: Perceptions of farmers groups from Northern and Western European countries. *Soil and Tillage Research*, 217, article number 105288. doi: 10.1016/j.still.2021.105288.
[27] Thomsen, M.N., Tamirat, W.T., Pedersen, S.M., Lind, K.M., Pedersen, H.H., de Bruin, S., Nuyttens, D., Vangeyte, J., Forristal, P.D. & Sørensen C.G. (2018). *Farmers perception of Controlled Traffic Farming (CTF) and associated technologies. IFRO working paper*. Copenhagen: University of Copenhagen.

[28] Wang, Q., Zhao, H., & He, J. (2016). Design and experiment of blades–combined no and minimum–till wheat planter under controlled traffic farming system. *Transactions of the Chinese Society of Agricultural Engineering*, 32(17), 12-17. doi: 10.11975/j.issn.1002-6819.2016.17.002.
[29] Wang, X., Gao, H., Tullberg, J., Li, H., Kuhn, N., McHugh, A., & Li, Y. (2008). Traffic and tillage effects on runoff and soil loss on the Loess Plateau of Northern China. *Australian Journal of Soil Research*, 46, 667-675. doi: 10.1071/SR08063.
[30] Zhuravel, D., Samoichuk, K., Petrychenko, S., Bondar, A., Hutsol, T., Kuboń, M, Niemiec, M, Mykhailova, L., Gródek-Szostak, Z., & Sorokin, D. (2020). Modeling of diesel engine fuel systems reliability when operating on biofuels. *Energies*, 15(5), article number 1795.

Іван Белоєв
Кандидат технічних наук, доцент
Русенський Університет «Ангел Кинчев»
7017, вул. Студентська, 5, м. Русе, Болгарія
https://orcid.org/0000-0003-2014-1970

Володимир Петрович Кувачов
Доктор технічних наук, професор
Таврійський державний агротехнологічний університет ім. Дмитра Моторного
72310, просп. Б. Хмельницького, 18, м. Мелітополь, Запорізька обл., Україна
https://orcid.org/0000-0002-5762-256X

Валерій Васильович Адамчук
Доктор технічних наук, професор
Інститут механіки та автоматики агропромислового виробництва
Національної академії аграрних наук України
08631, вул. Вокзальна, 11, смт. Глеваха, Київська обл., Україна
https://orcid.org/0000-0003-0358-7946

Зіновій Володимирович Ружило
Кандидат технічних наук, доцент
Національний університет біоресурсів і природокористування України
03041, вул. Героїв Оборони, 15, м. Київ, Україна
https://orcid.org/0000-0003-3582-8687

Аналітичне дослідження поворотів мостових машин

Анотація. Робота присвячена вирішенню актуальної проблеми ефективності повороту мостових машин у колійній системі землеробства. Метою роботи є дослідження криволінійного руху по слідах ґрунту постійної технологічної колії мостової машини з урахуванням її конструктивної схеми та способу повороту, параметрів, режимів руху та навантаження. Експериментальні дослідження проводились з використанням сучасної тензометричної доріжки та спеціально розробленого обладнання для електричних вимірювань неелектричних величин. Обробку даних дослідження проводили на персональному комп'ютері. В результаті проведених досліджень розроблено методику складання математичних моделей повороту мостової машини, яка рухається по ґрунтовому сліду постійної технологічної колії. Після спільного розв'язання моделей повороту мостової машини можна визначити всі вихідні параметри її криволінійного руху: траєкторію, сили тяги, радіус повороту, ковзання, фактичні швидкості. Представлено силову взаємодію ходової частини мостової машини з ґрунтовим слідом постійної колії на основі плоского ковзання зі змінним коефіцієнтом анізотропного тертя зчеплення φ_{yd} залежно від властивостей колії. Зі збільшенням радіуса колеса, ширини шини та тиску повітря в ньому, а також вертикального навантаження, що діє на нього, збільшується коефіцієнт зчеплення мостової машини φ_{yd}, при цьому можна досягти більшого пробуксовування. Адекватність моделі стаціонарного повороту підвісної машини підтверджено експериментальною оцінкою коефіцієнта опору силового бортового повороту. Збіжність теоретичних та експериментальних значень цього коефіцієнта знаходиться в межах довірчого інтервалу $\pm\sigma$ у всьому досліджуваному ваговому діапазоні прототипу мостової машини. Це дозволяє оцінити вплив конструктивних параметрів і схем на поворотні характеристики ще на етапі проектування нової мостової машини, таким чином оптимізуючи процес проектування. Результати досліджень можна застосувати до організації процесу повороту діючих моделей мостових машин

Ключові слова: кероване землеробство; портальні системи; криволінійний рух; коефіцієнт зчеплення; коефіцієнт адгезії

Machinery & Energetics
Vol. 14, No. 3. 2023

Journal homepage:
https://technicalscience.com.ua/en

UDC 658.562.2:635.11:633.63
DOI: 10.31548/machinery/3.2023.21

Myroslav Budzanivskyi*
Postgraduate Student
Institute of Mechanics and Automatics of Agroindustrial Production
National Academy of Agrarian Sciences of Ukraine
08631, 11/1 Vokzalna Str., Glevakha, Kyiv region, Ukraine
https://orcid.org/0000-0002-0508-3816

Experimental studies of the quality of root crop heads residue cleaning using a new cleaner

Abstract. Given the high technical requirements for cleaning root crop heads from residues, the development of new, more advanced cleaners is an important and urgent issue. The research aims to improve the quality of the cleaning process by determining the optimal kinematic, structural, and operational parameters of a new root crop head cleaner from root residues. A new design of the root crop head cleaner was created, which allowed the use of cleaning elements with different mechanical properties and sizes, and changing its kinematic parameters depending on the crop it processes. A new experimental setup was also made to install this cleaner and change its operational parameters. A new mathematical model of a multifactorial experiment was developed for the study. Based on the results of the field experimental study, correlation analysis, and statistical numerical calculations using a computer, the optimal design, kinematic, and operational parameters of the improved cleaner were determined, at which the highest quality of cleaning (the lowest amount of stover residues per linear metre) is observed. Based on the results of the correlation analysis, the following optimal parameters of the improved root crop head cleaner were obtained: the location of the ends of the rubber cleaning blades relative to the soil surface, i.e., the parameter h should not exceed 1.5 cm. The angular velocity ω of the counter-rotating movements of the cleaning shafts should correspond to the following range of values – 36.4...76.6 rpm. The translational speed V of the cleaner should not exceed 2.0 m·s^{-1}. The obtained structural, kinematic, and operational parameters can be successfully used in design bureaus when designing advanced machines for harvesting various root crops, and in research institutions and universities when conducting modern research in the field of agricultural engineering

Keywords: stubble; residues; plan matrix; optimal parameters; rubber blades

INTRODUCTION

For harvesting commercially grown root crops, which include sugar beet, fodder and table beet, carrots, etc., the most common technology is separate harvesting, i.e., when a separate unit harvests the tops on the root and then uses a root harvester to dig the roots out of the soil. Previously, the technology for harvesting the tops of the heads involved preliminary continuous cutting at an elevated height and then mechanical cutting of the upper parts of the heads together with the residues. In this case, the cut parts of the heads were not collected, but rather scattered over the surface of the field, and later ploughed into the soil as fertiliser. V. Bulgakov *et al.* (2021a) thoroughly investigated and found that the useful parts of root crops are irretrievably lost along with the cut-off parts of the heads. This is especially noticeable when harvesting sugar beet when up to 14% of sugar can be lost along with the cut-off root heads. In addition, mechanical cutting of root crop heads almost immediately causes the loss of juice from their bodies, and the cut part becomes a place through which microbes and viruses begin to penetrate the body, causing further decay and loss. In general, it is impossible to store such root crops, even for a short period, and they must be processed immediately. In this case, short-term storage results in an intensive loss of their presentation.

Article's History: Received: 20.03.2023; Revised: 28.06.2023; Accepted: 11.08.2023.

Suggested Citation:
Budzanivskyi, M. (2023). Experimental studies of the quality of root crop heads residue cleaning using a new cleaner. *Machinery & Energetics,* 14(3), 21-33. doi: 10.31548/machinery/3.2023.21.

*Corresponding author

Modern foreign-made topsy-turvy harvesting machines are designed not only to cut but also to grind the entire array of cut green topsy-turvy and spread it over the field as a plant fertiliser.

As such, the technology of harvesting the tops was further improved and included a preliminary continuous cut of the green mass of tops, and then a separate operation was performed to clean the heads of root crops from the remains of tops on the root without damage and to knock the bodies of root crops out of the soil. Almost everywhere, root crop tops are now collected, removed from the fields, and used effectively for biogas production. Sugar beetroots themselves, even with uncut heads, are widely used in many countries for bioethanol production.

L. Pogorely (1983), L. Pogorely & M. Tatyanko (2004) not only present different types of peelers (sickle, chain, impact, etc.) but also investigate the principles of operation used in machines for cutting tops and peeling root heads from residues by the world's leading manufacturers. However, in most designs, cleaning forces are applied to the heads of root crops from one side, which, given the current trend towards increasing the speed of translational movement, does not always lead to high-quality cleaning. The creation of theoretical foundations for mechanical combing and crushing of the residual tops from sugar beet root heads on the root were thoroughly studied by V. Martynenko (1997), V. Martynenko & B. Kucher (2002) and V. Bulgakov *et al.* (2021b). They developed the fundamental scientific basis for removing top residues from root crop heads utilizing milling, shaft cutting, impact on the residues, as well as the use of a cleaner with blades mounted on a vertical drive shaft (such as a daisy). However, even in this case, the cleaning forces are applied to the residues on the root heads from one side only, and during the forward movement of the cleaner, the front and rear parts of the heads may not be processed at all. If the speed of the forward movement of the peeler is increased, the quality of work of such peelers is significantly reduced. The development of various designs of root crop head cleaners for removing tops from the root and the theoretical and experimental substantiation of their parameters are reflected in numerous works. In particular, A. Borys (2011) studied a combined copying and cancelling cleaner. M. Khelemendyk (2001) examined in detail the combination of shaped bar drums that slide onto each head. B. Shabelnyk (1998) investigated a head cleaner for fodder beetroots; M. Borys (2013) reviewed a combined paddle cleaner. O. Gurchenko (2007) investigated a combined paddle cleaner equipped with a passive head trimmer; I. Storozhuk & V. Pankiv (2015) – a combined cleaner with a rotary shaft and a passive head trimmer; Ye. Ihnatiev (2017) – a flanged cleaner with separate cleaning heads; O. Syplyvets (2001) – conducted a study of a combined cleaner and a separate aftercut. The creation of new cleaners has been the subject of design developments in recent years (Patent of Ukraine No. 115404..., 2017; Berezhenko, 2020).

However, despite this design diversity and the theoretical and experimental studies of them, the results obtained indicate that they are unfortunately not able to achieve high-quality cleaning since almost all cleaners provide cleaning forces to root crop heads, albeit in different planes, but at high forward speeds they cannot clean all parts of the heads.

Thus, the search for the most effective design solutions for root crop head cleaners from root residues is relevant and should consider their kinematic, structural and operational characteristics, which should ensure the high-quality performance of this technological process.

The research aims to determine the optimal parameters of a new root crop head cleaner for removing root residues that can significantly improve the quality of the cleaning process.

MATERIALS AND METHODS

Experimental studies were carried out in 2022 in the field, using a new experimental setup manufactured at the National University of Life and Environmental Sciences of Ukraine at the Department of Mechanics, Faculty of Construction and Design. A new root crop head cleaner was developed at the Institute of Mechanics and Automatics of Agroindustrial Production of the National Academy of Agrarian Sciences of Ukraine under the direction of Prof. V. Bulgakov, which consists of two cleaning shafts with pivotal cleaning elements in the form of pairs of rubber blades mounted on hubs. The design of the two-shaft root crop head cleaner and the experimental setup for its study are new, and experimental studies using pairs of cleaning blades on each of the cleaning drive shafts were carried out for the first time. The cleaning shafts in this design cover each row of root crops on both sides and, due to counter-rotating movements, simultaneously strike the heads of root crops from both sides with the ends of their working cleaning elements, combing off the remains of the tops. The ends of the pairs of rubber blades on each of the two drive shafts are staggered, forming a cleaning channel with mutual overlap on the symmetry axis of the cleaner, which covers a row of root crops on both sides. The bulk of the green tops from the heads of root crops had to be cut off by a top harvester beforehand. But after that, they were left with residues in the form of uncut green tips, as well as dry and dead thin stems of considerable length, which lie on the soil surface. The root crops themselves are in the soil and firmly connected to it. After cleaning the heads of root crops from the remains of the tops on the roots, the next step is to dig the root crops out of the soil.

To simulate the functioning of this cleaner in real field conditions and, accordingly, to study the quality of its operation under different parameters and modes, a new design of a field experimental installation was developed and manufactured, which can be used only for the study of a two-shaft cleaner with pairs of cleaning rubber blades mounted pivotally on several hubs of each shaft, having counter-rotational motion, inside which it is installed. The

experimental setup has the following features: it provides for the study of the quality of cleaning the heads of root crops from one row of crops, is aggregated by a wheeled row crop tractor of class 1.4, which sets the cleaner, different speeds of translational movement along the row of root crops, and different angular speeds of rotational movements, provides conditions for the counter-rotational direction of its cleaning shafts, and also makes it possible to change and fix different angles of inclination of the cleaning shafts in the horizontal and vertical planes. It is also possible to set different heights of the ends of the pairs of flexible cleaning blades relative to the soil surface.

Figure 1 shows a diagram of the experimental setup for studying the quality of cleaning root crop heads from the remains of tops on the root. The experimental setup is a root crop head cleaner mounted on frame 3, which is single row. The frame 3 is mounted behind the wheeled aggregating tractor 1 with the help of the hitch 2. At the same time, frame 3 in its front part rests on two supports and copies wheels 5 with mechanisms for changing the distance of frame 3 to the soil surface. In the rear part of frame 3, there is a cleaner consisting of two horizontal cleaning shafts 6. The shaft 6 is driven in counter-rotating movements by drive elements 4 from the rear PTO of the tractor 1. The cleaning shafts 6 are mounted horizontally in the transverse plane, and their longitudinal axes in this plane are located at an angle α. At the same time, five hubs 8 are mounted on each cleaning shaft 6 with a corresponding pitch using a keyed connection 9. Each hub 8 contains on its outer surfaces, mounted utilizing leashes pivotally on the axes, pairs of rubber blades 7, of which it contains four (located at the ends of mutually perpendicular axes). In this case, the ends of the rubber blades of one cleaning shaft are located in the gaps between the blades of the second cleaning shaft. The angle at which the cleaning shafts are installed ensures an appropriate root crop capture zone in the front part of the cleaner and is of little importance. The directions of translational movement of the experimental setup and the rotational movements of its components are shown in the diagram by arrows.

Figure 2 shows a non-exhaustive view from the end of the cleaning shaft 6 with pairs of rubber cleaning blades 7 mounted on hubs 8.

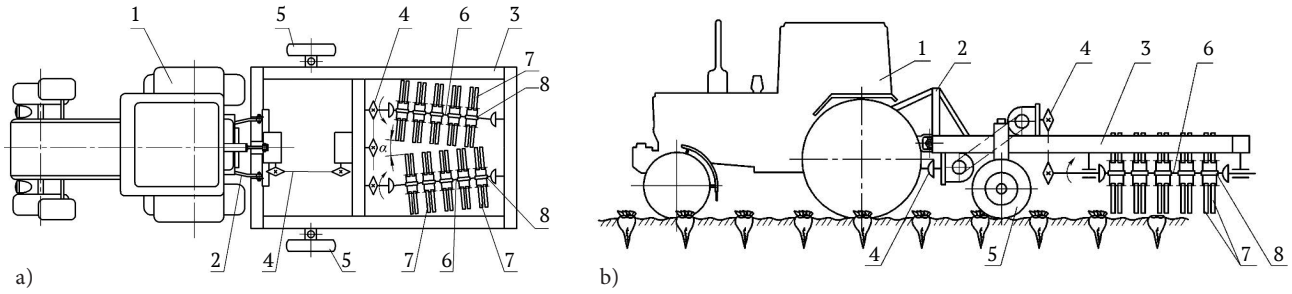

Figure 1. Diagram of a field experimental setup for studying the quality of cleaning root crop heads from the remains of tops on the root

Note: a) side view; b) top view, 1 – aggregating tractor; 2 – hitch; 3 – frame; 4 – elements of driving the cleaning shafts in counter–rotating motion; 5 – support and copy wheels; 6 – driving cleaning shafts; 7 – pairs of rubber cleaning blades; 8 – hubs with hinged cleaning blades

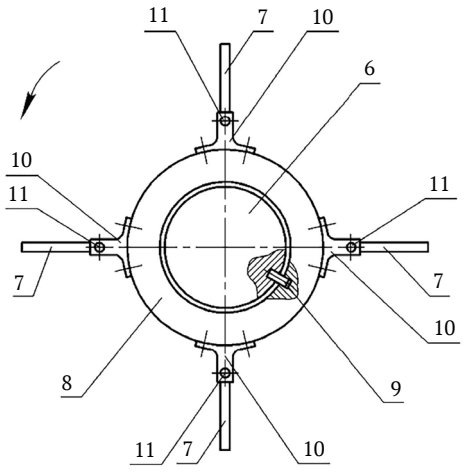

Figure 2. Installation of rubber blade pairs on the drive cleaning shaft

Note: 6 – cleaning shaft; 7 – rubber blade; 8 – hub; 9 – keyed connection of the shaft and hub; 10 – leash; 11 – hinge axis

Figure 3 shows a general view of one element of the cleaning working body, which consists of a pair of side-by-side rubber blades 1 mounted pivotally on axis 2 on the hub of the cleaning blade with two leads 3.

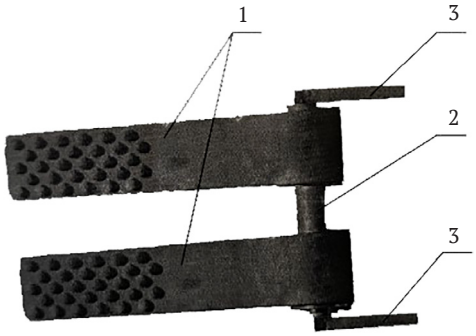

Figure 3. General view of the cleaning element
Note: 1 – rubber blades; 2 – hinge axle; 3 – hub leads

This cleaner uses conventional rubber blades used on the OGD-6A type cleaner (Root head cleaner, double-shaft, capable of cleaning 6 rows of root crops, "A" – modernised, can be separately aggregated with a tractor of class 1.4 or 2.0; Manufacturer: Ternopil Harvester Plant, Ukraine), which have standard dimensions: length 25...33 cm; width 6...8 cm, thickness 1.5...2.0 cm. At the outer ends of each blade, along their entire width, there were staggered rubber protrusions, 0.3...0.5 cm high and hemispherical in shape. The hinge point of each blade was reinforced with a thin metal – tin. All blades are made of solid moulded rubber.

Figure 4 shows a general view of the experimental set-up attached to a wheeled aggregating tractor during the field experimental studies.

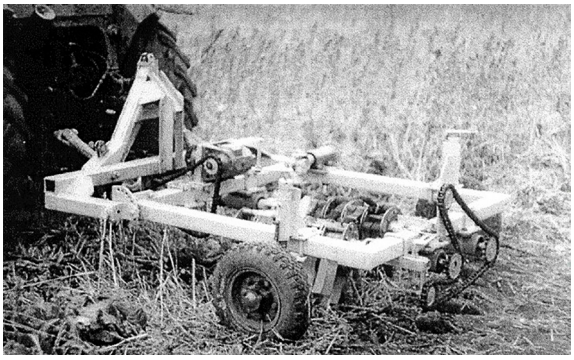

Figure 4. Experimental setup during field experimental research

Figure 5 shows a view of a field of root crops prepared for the head cleaner, in which a linear metre is highlighted, from which the main bulk of the tops has already been cut with a standard top harvester, but the tops remain. This field area is bordered by a wooden frame, which is the size of a running metre with a width equal to the sum of half the standard row spacing from the crop row axis. All residues were collected from the area bounded by the frame after passing through the stubble harvester. However, before passing the cleaner, the frame was removed from the scoring area, but its boundaries were fixed with wooden stakes that were driven into the soil.

Figure 5. The field area prepared for the cleaner

The methodology for conducting field experimental studies to determine the quality of cleaning root crop heads from the remains of tops on the root was in line with modern requirements in some respects (V. Nadykto, 2017; H. Beloev, 2021).

From the beginning, a field area with root crops was carefully prepared (the area with sugar beet crops was the most suitable for this purpose), which was (in terms of timing and agrophysical crop assessment) suitable for harvesting. The physical and mechanical properties of the soil with the crops, as well as the biological condition of the root crops themselves, were measured and comprehensively analysed. Then, the operation of cutting the tops from the heads of root crops was performed using a conventional tops harvester, type BM-6A (a tops harvester capable of

harvesting tops from 6 rows of root crops, manufactured by the Ternopil Harvester Plant, Ukraine). At the same time, the harvester itself did not have a head cleaner, which was previously disconnected from it. After the passage of the six-row pumpkin top harvester, the plantation was assessed based on the results of the first main continuous cut of the green mass of the pumpkin top. Here, the main indicator in assessing the performance of the top harvester was the quality of the cut of the heads (the presence of highly cut root bodies, chips, cracks, and root bodies being knocked out of the soil) and the presence of those residues of tops that the tops harvester was unable to cut and collect properly. Such a thorough assessment of the quality of the top harvester gave every reason to further compare and reliably assess the quality of cleaning the heads of root crops from residues on the root with the improved cleaner itself, i.e., to actually "separate" the quality of cleaning during the first and second cleaning.

Subsequently, the process of cleaning the heads of root crops with this cleaner took place, while two adjacent rows were immediately selected, and similar conditions were determined using a frame with the contours of one running metre. Next, all residues were manually cut off both after passing through the stubble harvester alone and after simultaneous passage through the stubble harvester and the cleaner. In both cases, all residues were carefully collected and weighed on an electronic balance with an accuracy of ± 0.1 g. The obtained weighing results in both cases, i.e., before and after the passage of the cleaner, made it possible to assess the quality of cleaning the heads of root crops from residues.

The degree of cleaning of root crop heads from residues on the root was then calculated using the following formula:

$$\delta = \frac{M - M_{cl}}{M} \times 100, \quad (1)$$

where δ – root crop heads cleaning degree, %; M – weight of residual tops before the cleaner passage, g; M_{cl} – weight of residual tops after the cleaner operation, g.

The conditions for conducting field experimental studies of the improved cleaner were as follows: soil type and name by mechanical composition – black soil, low-humus, medium loamy; average soil hardness – 2.0...2.8 MPa; average soil moisture – 12.1...14.5%; surface relief – flat; root crop yield – 53.4 t·ha^{-1}; tops yield – 13.3 t·ha^{-1}; plant density – 82.9 thousand pcs.t·ha^{-1}; average distance between root crops – 8.8 cm; type of tops by shape: "rosette" – 21.1%, "semi-rosette" – 50.8%, "cone" – 28.1%; location of root heads relative to the soil surface level: from 0 to 20 mm – 36.4%.

The following instruments and equipment were used in the field experimental studies: the angular velocity of rotational movements of the drive cleaning shafts was measured and recorded using a strain gauge (Fig. 6), the translational speed of the experimental unit was measured using a measuring wheel (Fig. 7).

Figure 6. Load cell for measuring the angular speed of rotation of cleaning shafts

Figure 7. The track wheel mounted on the cleaner

The strain gauge was mounted on the rear PTO shaft of the aggregating tractor, which made it possible to immediately record and measure the angular velocity of its shank using the developed program and connected to a PC using an electronic converter. Next, the angular velocity of the cleaner's drive shafts was converted to the angular velocity of the cleaner, and the required variable angular velocities of the rotational movements of the cleaner shafts themselves were set using interchangeable sprockets in the drive. The design of the drive of the cleaning shafts in the experimental setup was made using cardan shafts, a gearbox and chain gears, which ensured their counter rotation in the direction of the axis of the row of root crops. The measuring wheel, which was connected to the cleaner frame, also provided accurate values of the translational movement of the cleaner during field experimental studies in different modes of its operation using the developed program and connection to a personal computer (PC) through a converter. The exact location of the ends of the rubber blades relative to the field surface was determined each time using a metal ruler, which allowed the screw mechanisms of the cleaner frame copy wheels to accurately set different values of the height of the location. These measurements were made with an accuracy of 1 mm.

To determine the influence of independent factors on the quality indicators of the investigated root crop head

cleaner from the residues of tops on the root, a comparative multifactorial experiment was planned and conducted, or a full-factorial experiment (FFE) of the FFE type P^k, where P – the number of levels of variation of the factor; k – the number of factors present in the experiment (Dushynsky, 2000). An indicator that characterises the quality of the cleaner's operation is the residue of stubble per linear metre ($g \cdot m^{-1}$) that occurs after it passes through the scoring section of the row. This parameter in the model of the multifactorial experiment was chosen as an optimisation function, i.e. a dependent variable that can be taken as a functional: $Y = f(x_1; x_2; x_3)$, where Y – residues of stubble from the first to the i-th case; $x_1, x_2, \ldots, x_i$ – natural independent variable factors.

These natural independent factors were selected following the relevant conditional plan of the multivariate experiment, which was implemented in the following sequence. To determine the amount of stubble residue Y on each running metre, the following independent variables were taken as the independent variables:

- is the speed of translational movement V, which was encoded by the index X_1;
- is the angular speed of rotation of the cleaning shafts ω, which was coded by an index X_2;
- the height of the rubber blade ends relative to the horizontal soil surface h, which was coded by the index X_3.

When coding the factors, the factor space is linearly transformed – the origin is moved to the centre of the experiment, and the scale on the axes is chosen in units of factor variation. The factors were coded using the following relationship:

$$X_i = \frac{2 \cdot (x_i - x_{i0})}{x_{\max} - x_{\min}}, \quad (2)$$

where X_i – the coded value of the factor (dimensionless value); x_i – the value of the factor in named (natural) units; x_{i0} – the natural value of the factor at the zero level; $x_{\max}$, $x_{\min}$ – the maximum and minimum values of the factor, respectively.

When constructing the planning matrix of the full-factorial experiment, coded designations of the upper, lower and zero levels of variation by each factor were introduced, which were respectively designated as (+1), (–1), (0). The factors that determine the quality of the technological process under consideration were selected and coded, and the levels of their variation were established simultaneously in natural and coded forms (Table 1).

Table 1. Results of coding factors and their levels of variation FFE 3^3

Factors	Markings		Variation levels, natural / coded		
	Coded	Natural			
Translational speed V, $m \cdot s^{-1}$	X_1	x_1	0.9/–1	1.6/0	2.1/+1
Angular velocity of rotational movements of the cleaning shafts ω, $rad \cdot s^{-1}$	X_2	x_2	36.6/–1	56.5/0	76.6/+1
Height of the blade ends relative to the soil surface h, cm	X_3	x_3	0/–1	2/0	4/+1

Source: compiled by the author

The natural variables were then coded based on the data in Table 1 and their values were set as follows:

$$\begin{aligned} X_1 &= 1.67 \cdot V - 2.67, \\ X_2 &= 0.05 \cdot \omega - 2.81, \\ X_3 &= 0.5 \cdot h - 1. \end{aligned} \quad (3)$$

After coding the factors, a planning matrix of the corresponding multivariate experiment of the FFE 3^3 type was compiled for the total number of experiments $N = 3^3$.

To reliably assess the quality of the root crop head cleaner's operation from the residues of tops on the root during field experimental studies, the required number of measurements of the controlled parameters (repetition of experiments) was determined according to the methodology outlined in (Hailys, 1992). In this case, the experiments were conducted in six replications.

When implementing the compiled plan matrices, to eliminate the influence of uncontrolled and unregulated factors on the results obtained, the plan matrix was randomised by the random balance method, which was implemented by randomly drawing the serial numbers of experiments, i.e., randomly.

The randomized design matrix of the multivariate experiment FFE 3^3 is shown in Table 2.

Table 2. Randomised design of a FFE-type experiment 3^3

No. experiment	Factor levels				Factor interrelation				Optimisation factor Repetitions						Average values
	x_0	x_1	x_2	x_3	$x_1 \times x_2$	$x_1 \times x_3$	$x_2 \times x_3$	$x_1 \cdot x_2 \times -x_3$	1	2	3	4	5	6	T, $g \cdot m^{-1}$
1	+1	–1	–1	–1	+1	+1	+1	–1	14.6	12.8	14.5	26.6	28.8	24.6	20.3167
2	+1	+1	–1	–1	–1	–1	+1	+1	12.2	13.9	12.8	9.8	16.2	15.5	13.40
3	+1	0	–1	–1	0	0	+1	0	31.6	37.2	38.4	28.4	37.3	36.8	34.95
4	+1	–1	+1	–1	–1	+1	–1	+1	2.8	2.7	6.1	5.8	5.1	2.7	4.20
5	+1	+1	+1	–1	+1	–1	–1	–1	4.1	9.3	9.2	10.4	8.9	11.1	8.8333
6	+1	0	+1	–1	0	0	–1	0	4.7	6.2	5.8	8.1	8.7	9.7	7.20
7	+1	–1	0	–1	0	+1	0	0	5.9	10.3	12.6	13.5	8.2	11.4	10.3167

Continued Table 2.

No. experiment	Factor levels				Factor interrelation				Optimisation factor Repetitions						Average values
8	+1	+1	0	−1	0	−1	0	0	8.9	13.7	10.8	10.7	14.5	12.8	11.90
9	+1	0	0	−1	0	0	0	0	9.7	17.3	16.8	21.7	31.6	30.4	21.25
10	+1	−1	−1	+1	+1	−1	−1	+1	124.8	156.1	156.2	111.4	120.3	120.8	131.60
11	+1	+1	−1	+1	−1	+1	−1	−1	167.8	156.3	154.1	110.7	106.9	121.4	136.20
12	+1	0	−1	+1	0	0	−1	0	68.4	72.3	70.9	70.5	90.1	84.3	76.0833
13	+1	−1	+1	+1	−1	−1	+1	−1	6.2	6.0	8.8	7.9	9.9	10.1	8.15
14	+1	+1	+1	+1	+1	+1	+1	+1	90.1	87.0	64.7	54.7	58.7	58.4	68.9333
15	+1	0	+1	+1	0	0	+1	0	34.1	43.5	43.1	53.6	34.1	44.3	42.1167
16	+1	−1	0	+1	0	−1	0	0	15.8	18.2	21.7	22.4	21.6	22.3	20.3333
17	+1	+1	0	+1	0	+1	0	0	99.0	110.8	125.3	130.1	128.6	131.5	120.8833
18	+1	0	0	+1	0	0	0	0	60.1	71.0	80.8	82.7	88.6	91.4	79.10
19	+1	−1	−1	0	+1	0	0	0	88.1	106.7	100.7	85.3	132.5	89.1	100.40
20	+1	+1	−1	0	−1	0	0	0	102.5	99.4	112.8	99.9	94.3	110.3	103.20
21	+1	0	−1	0	0	0	0	0	42.2	52.6	59.6	59.1	66.8	59.5	56.6333
22	+1	−1	+1	0	−1	0	0	0	4.1	4.2	9.1	7.6	7.2	8.8	6.83333
23	+1	+1	+1	0	+1	0	0	0	64.7	61.6	44.6	43.3	50.5	50.1	52.4667
24	+1	0	+1	0	0	0	0	0	10.9	12.3	11.2	13.9	13.1	12.3	12.2833
25	+1	−1	0	0	0	0	0	0	8.0	13.2	18.8	19.6	15.5	20.0	15.85
26	+1	+1	0	0	0	0	0	0	66.7	73.1	74.1	76.1	83.8	78.5	75.3833
27	+1	0	0	0	0	0	0	0	69.4	84.8	91.6	95.5	42.2	61.8	74.2167

Source: compiled by the author

Statistical processing of the results of experimental studies obtained after the implementation of the multifactorial experiment was carried out in the following sequence.

Thus, the response function (i.e., the optimisation parameter) was taken as an approximating mathematical model of a full square polynomial (Hailys, 1992), which describes the real experimental process:

$$Y = b_0 + b_1 \cdot x_1 + b_2 \cdot x_2 + b_3 \cdot x_3 + b_{12} \cdot x_1 \cdot x_2 + b_{13} \cdot x_1 \cdot x_3 + b_{23} \cdot x_2 \cdot x_3 + b_{123} \cdot x_1 \cdot x_2 \cdot x_3 + b_{11} \cdot x_1^2 + b_{22} \cdot x_2^2 + b_{33} \cdot x_{32}^2, \quad (4)$$

where Y – experimentally obtained values; b_0, b_1, b_2, b_3, b_{12}, b_{13}, b_{23}, b_{123}, b_{11}, b_{22} and b_{33} – regression coefficients of the corresponding values of the input factors x_i; x_1, x_2 and x_3 – initial coded factors.

The coefficients of the approximating polynomial, represented as a full quadratic equation, were determined by the corresponding general formulas (Hailys, 1992), subject to orthogonality and symmetry:

- free term b_0 and coefficients b_i i-th factor will be:

$$b_i = (\sum_{u=1}^{N} x_{iu} \cdot \bar{y}_u) \cdot (\sum_{u=1}^{N} x_{iu}^2)^{-1} = (\sum_{u=1}^{N} x_{iu} \cdot \bar{y}_u) \cdot (N)^{-1}, \quad (5)$$

- interrelation coefficient b_{ij} can have two such values under the influence of two and three variable factors:

$$b_{ij} = (\sum_{u=1}^{N} x_{iu} \cdot x_{ij} \cdot \bar{y}_u) \cdot (N)^{-1}, \quad b_{ijk} = (\sum_{u=1}^{N} x_{iu} \cdot x_{ij} \cdot x_{ku} \cdot \bar{y}_u) \cdot (N)^{-1}, \quad (6)$$

where x_{iu}, x_{ij} and x_{ku} – the value of the coded variable in the corresponding column of the experiment plan; $\bar{y}_u$ – average value of u-th experiment; u – serial number of the experiment; i – factor number; j, k – factor number other than i; N – number of conducted experiments.

The reproducibility of the obtained values of the experimental array with an identical number of repetitions for each experiment was checked by the Cochrane criteria, which was determined as follows:

$$G = (S_{v\max}) \cdot (\sum_{(u=1)}^{n} S_v)^{-1}, \quad (7)$$

where G – Cochrane's calculated value of the criterion; $S_{v\max}$ – numerical value of the maximum variance in u-th point; S_v – variance, which characterises the dispersion of research results of u-th experiment.

The variance of the reproducibility of the experiments was determined according to the following expression:

$$S^2(Y) = [\sum_{u=1}^{N} (Y_{ui} - \bar{Y}_u)^2] \cdot [N \cdot (m-1)]^{-1}, \quad (8)$$

where Y_{ui} – numerical values of i-th response of u-th experiment; $\bar{Y}_u$ – average response value of u-th experiment; m – repetition values of each u-th experiment.

The calculated value of the Cochrane criterion $G = 0.0702$. The calculated values of the Cochrane criterion were compared with the table values $G_T = 0.1327$ with a limit of $\alpha = 0.05$. Condition $G \leqslant G_T$ is true and variances are assumed to be homogeneous, which means that the process is reproducible.

Statistical significance of the coefficients of the regression equation b_i was tested by t-Student's test and was determined in the following sequence:

- is the variance of experimental errors in the lines of the FFE plan:

$$S^2(b) = \frac{1}{N \cdot m} \cdot S^2(Y); \quad (9)$$

- reproduction error:

$$S(b) = \sqrt{S^2(Y)}; \quad (10)$$

- condition of coefficients significance $b_{i(jk)}$:

$$b_{i(jk)} > t_T \cdot S(b), \quad (11)$$

where t_T – the table value of the Student's coefficient, which is selected from the table depending on the degree of freedom of correspondence f and significance level α, $t_T = 1.96$.

The degree of compliance freedom equals:

$$f=(m-1)\cdot N. \quad (12)$$

If the significance condition is not met, the following coefficient b_i of regression equation was assumed to be insignificant (equal to zero), and the corresponding term x_i of regression equation was excluded.

Thus, the following regression equation was obtained:

$$Y=48.6309+10.1185\cdot x_1-17.1025\cdot x_2+20.4086\cdot \\ \cdot x_3+4.0951\cdot x_1\cdot x_2-6.5278\cdot x\_2\cdot x_3+6.1716\cdot \\ \cdot x_1\cdot x_3+1.6531\cdot x_1\cdot x_2\cdot x_3-2.207\cdot x_3^2. \quad (13)$$

The adequacy of the chosen mathematical model to the experimental data, i.e., the correspondence of the mathematical model to the real process, was checked by the *F* Fisher's criteria by calculation:

- variance of adequacy:

$$S_{ag}^2=\frac{m}{N-\acute{g}}\cdot\sum_{u=1}^{N}(\bar{Y}_u-\tilde{y}_u)^2, \quad (14)$$

where $N-\acute{g}$ – number of degrees of freedom of the variance of adequacy; $\acute{g}$ – number of significant coefficients in the regression equation; $\bar{Y}_u$ – average response value in *u*-th experiment; $\tilde{y}_u$ – response value in *u*-th plane point, calculated by the regression equation;

- calculated Fisher's conformity criteria F_p:

$$F_p=\frac{S_{ag}^2}{S^2(Y)}, \quad (15)$$

where $S_2(Y)$ – experiment reproduction variance;

- tabulated value of the Fisher's criteria F_T per set variance levels α and two degrees of conformity were defined using the following expressions (Dushynsky, 2000):

$$f_{ag}=N-g, \quad (16)$$

and

$$f_y=N\cdot(n-1). \quad (17)$$

The condition for the adequacy of the chosen mathematical model was tested using the following inequality:

$$F_p<F_T. \quad (18)$$

The obtained value F_p was compared with the table value F_T. The calculated value of Fisher's criteria is equal to $F_p=1.48$, and, according to $F_T=1.88$ at the 5% level of significance. Thus, the condition of adequacy of the chosen mathematical model is met, i.e., the regression equation of the multivariate experiment is adequate to the experimental data. The multiple correlation coefficient *R* was then determined using the following expression:

$$R=\sqrt{1-\frac{\sum_{u=1}^{N}(\bar{Y}_u-\tilde{y}_u)^2}{\sum_{u=1}^{N}(\bar{Y}_u-\bar{Y})^2}}, \quad (19)$$

where $\bar{Y}$ is the average value of the function determined from the experimental data.

The calculations have established that the value of the multiple correlation coefficient is $R=0.85$. Accordingly, in natural coordinates, the regression equation after transformation and simplification of expressions will be as follows:

$$Y=63.498-4.9527\cdot V-0.8498\cdot\omega+19.5504\cdot h-0.2723\cdot\omega\cdot h+ \\ +1.2733\cdot V\cdot h+0.2026\cdot V\cdot\omega+0.0688\cdot V\cdot\omega\cdot h-0.5518\cdot h^2. \quad (20)$$

Thus, the obtained regression equation (20) describes the dependence of the residues *Y* of tops on the heads of root crops when they are cleaned by the improved design of the cleaner on its translational speed *V*, the angular speed of rotational movement ω of its two cleaning shafts when they move in the opposite direction, and the height *h* of the ends of the rubber blades relative to the soil surface, which separate the residues from the heads of root crops.

The use of the regression equation (20) allowed us to process and analyse the results of the experimental studies using the Statistica 13.0 software package for PC.

RESULTS AND DISCUSSION

Based on the results of statistical calculations, three-dimensional spatial dependences of the response surfaces of the top residues per linear metre during the operation of the root crop head cleaner and their two-dimensional cross-section were constructed to visualise the results of the experimental field studies.

The obtained regression dependencies of the residues of tops per linear metre during the operation of the root crop head cleaner in the form of a functional characterised the effects of single factors (speed of translational movement of the cleaner *V*, angular speed ω of rotation of the cleaning blades and height *h* of the blades relative to the soil surface) and their interaction on the optimisation parameter.

Figures 8-10 show the response surfaces of the residues of tops per linear metre during the operation of the root head cleaner and their two-dimensional cross-section as a function of two variable factors $x_{i(1,2)}$ with the constant unchanged corresponding third factor $x_{i(3)}$ = const, the value of which was at the zero level. The response surfaces of the residues of tops per linear metre were also constructed for the minimum and maximum levels of the third factor $x_{i(3)}$ = const and, respectively, the two variable factors $x_{i(1,2)}$.

According to the obtained graphical dependencies, the range in which the minimum values of tops residues *Y* are observed when cleaning root crop heads and the optimal values of the translational speed of the cleaner and the angular velocity *V* of rotational movements of its cleaning shafts is the zone where the angular velocity ω of rotations is almost maximum and should be within 65...80 rad·s^{-1}, and the translational speed of the cleaner should be within 1.0...1.8 m·s^{-1} (Fig. 8). Physically, this is explained by the fact that almost maximum values ω provide a greater number of blows to each head of the root crop. As for the speed *V*, it's not a high enough value, for example, 1.0 m·s^{-1} or even less, significantly increases the processing time of each head, which will naturally improve the quality of their cleaning from residues.

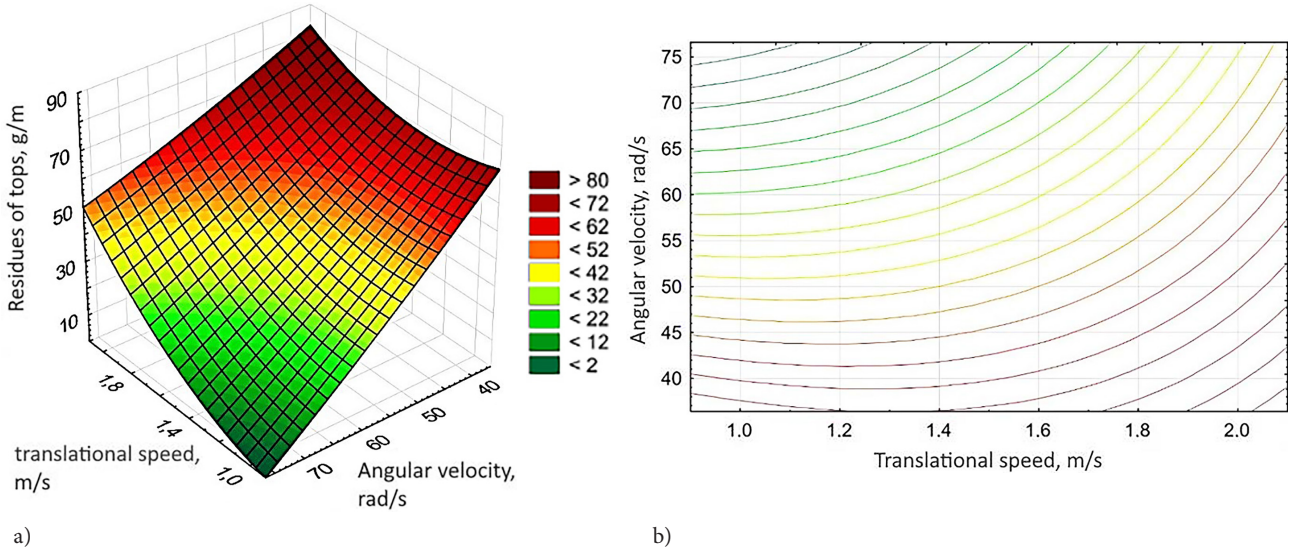

a) b)

Figure 8. Response surface (a) and its two-dimensional cross-section (b) of the leftover haulm on a running metre
Note: $Y = f(V; \omega)$, as velocity function V of translational motion and angular velocity ω and rotational movements of the cleaning shafts
Source: compiled by the author

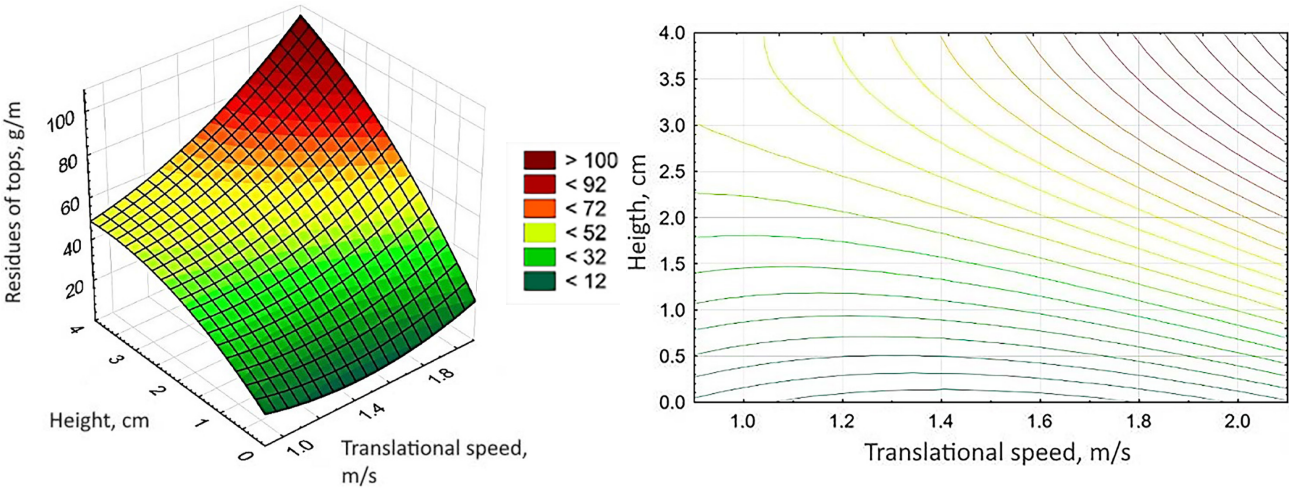

a) b)

Figure 9. Response surface (a) and its two-dimensional cross-section (b) of the leftover haulm on a running metre
Note: $Y = f(V; h)$, as velocity function V of translational movement and height h for setting the cleaning blades above the soil surface level
Source: compiled by the author

Similar results are observed from the graphical dependencies shown in Figure 9. Thus, the minimum residues Y on the heads of root crops are in the zone when the height h of the ends of the rubber blades above the soil surface should have minimum values and be in the range of 0.3...2.5 cm. In this case, the forward movement speed V of the cleaner can be in a wider range of values, namely 1.0...2.0 m·s^{-1}. However, it should be noted that the minimum heights of the ends of the rubber cleaning blades relative to the soil surface level are not very desirable. This results from the fact that these ends of the rubber blades should not touch the soil surface at all. Physically, this results in their initial impacts not on the root crop heads themselves, but on the soil. This significantly reduces the quality of cleaning of the root crop heads themselves. Furthermore, when the corresponding rotational movements are set to the cleaning shafts, the rubber blades are capable of stretching (i.e., their length increases under the influence of inertial forces), which can lead to their contact with the soil surface, the capture of its particles and, as a result, a decrease in cleaning performance and premature wear.

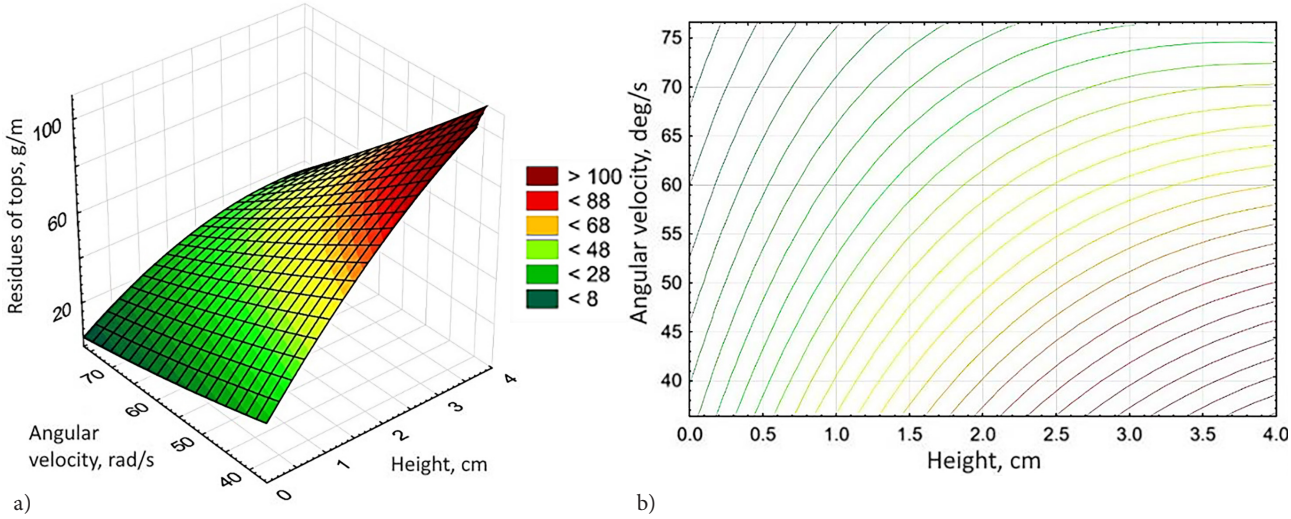

Figure 10. Response surface (a) and its two-dimensional cross-section (b) of the leftover haulm on a running metre
Note: $Y=f(h; \omega)$ as a function of the height h for the cleaning blades above the soil surface and the angular speed ω of the rotation of the cleaning shafts
Source: compiled by the author

The dependence of residues Y on the heads of root crops on the height h of the cleaning blades above the soil surface and the angular velocity ω of the rotational movements of the cleaning shafts indicates that the zone of optimal values of these parameters is at the maximum values ω and minimum values h, which is rather natural (Fig. 10).

In general, the analysis of the above regression equation and the graphical dependencies obtained show that the factors that increase the amount of stubble residue per linear metre are the height of the blades relative to the soil surface h and the speed V of forward movement. An increase in the angular velocity ω of the rotation of the cleaning shafts leads to a decrease in the amount of stubble residue.

Changing the forward speed of the cleaner V in the range of 0.9 to 2.1 m·s^{-1}, the amount of stubble residue increases by 1.55 times, when changing the angular speed of rotation of the cleaning shafts ω in the range of 36.4...76.6 rpm, the amount of stubble residue decreases by 2.09 times, and in the range of changes in the height of the blades relative to the soil surface h from 0 cm to 4 cm, the amount of stubble residue increases by 2.58 times.

It should be noted that during the field experimental studies to determine the quality of cleaning the heads of root crops from residues, the heads themselves were not damaged by rubber blades. After the run of the head harvester, which made a continuous cut of the green mass of the tops, there were cases of cutting off the upper parts of the heads, but only those that were high above the soil surface. No noticeable damage in the form of chips, cracks, or tearing of surfaces was observed after the cleaner passed through. There were also no cases of root crops being knocked out of the soil.

Comparing the results of the field experimental studies of the new cleaner with similar results of previous studies by other authors, certain difficulties arise. For example, no experimental studies have been conducted using a methodology that would allow evaluating the quality of head cleaning only by the cleaner itself, separating the indicators of continuous cutting by a stump harvester. Almost all known previous studies of recent years (Žitňák & Korenko, 2011; Berezhenko, 2020) concerned the assessment of the quality of head cleaning in general, i.e., the initial continuous cut (and root crop head cleaners, of whatever design, can clean the heads only after the main cut of the tops), then additional cleaning from residues and even mechanical cutting of the upper part of each head. In other words, the quality of the entire technological process of harvesting the tops was investigated and evaluated.

However, comparing the quality indicators of this root crop head cleaner with similar indicators of other types (albeit in terms of the general indicators of the entire process of simultaneous cutting and cleaning), there is reason to believe that the amount of residual tops is reduced by almost 1.8 to 2.2 times compared to the cleaners with horizontal rotation shafts and flexible cleaning blades mounted on them, which move across the rows of root crops (Pogorely, 1983; Martynenko, 1997; Martynenko & Kucher, 2002) and almost 1.25 to 1.28 times compared to the cleaners with vertical cleaning shafts with flexible elements moving along the rows of crops (Pogorely, 1983; Borys, 2012).

Comparing the results achieved in our field experiments, they are even better than in the cases when the blade root head cleaners are used in conjunction with the top head cutters. Thus, the results presented by I. Storozhuk & and V. Pankiv (2015) are almost similar to ours, and the results presented by E. Berezhenko (2020) show that in our case, the number of residual tops on the heads of root crops is reduced by about 5%.

It is possible to make a detailed and, to the extent feasible, comprehensive analysis of the high-quality indicators obtained by us and to make general comparisons with the results achieved by other authors. First of all, there is every reason to believe that this is since in our cleaner, the coverage of each root crop head during residue cleaning from both sides creates conditions under which the ends of the rubber cleaning vanes, acting simultaneously from both sides, can apply forces to the front of the heads and their rear, despite the straightforward forward movement. The ends of the rubber cleaning vanes achieve this due to their overlapping and the fact that they can enter the gaps between the root crops on both sides. In other words, the ends of the rubber blades of the two cleaning shafts, which are directed towards each other, first enter the space between the adjacent root crop heads, and then, in their forward movement, touch the front and rear parts of the heads located in the row.

Furthermore, in this particular case, since the ends of the rubber blades of one shaft are located between the ends of the blades of the second shaft, conditional zones of application of cleaning forces to each head are provided, which overlap. In other words, the cleaning rubber blade located on one side of the head first starts to interact with the side surface of the head located on the other side. This means that virtually all surfaces of the root crop heads, which have both spherical and flat external shapes, fall within the action zone of the ends of the rubber blades of both cleaning shafts. This not only ensures that the root bodies that are high above the surface level are not knocked out of the soil, but also covers all the surfaces of the heads.

It is the installation of four rubber cleaning blades on each hub that guarantees more intensive and consistent interaction of their ends with the surface of each root crop head. In addition, the presence of four hubs on each cleaning shaft carrying cleaning elements in the form of rubber blades significantly prolongs the time of their interaction (contact), which significantly affects the quality of cleaning.

Since two rubber cleaning vanes are mounted on each axis of the hinge, each hub, with two leads, the effect is that the first of the blades strikes the short green stalk of the chaff first and can capture it (if the stalk has not separated) and bend it, After that, the second rubber blade (after a very short period) immediately strikes again, but on the bent part of the green stalk, which guarantees its absolute separation. Gripping and bending are also facilitated by the fact that the outer (working) ends of each rubber blade have hemispherical rubber protrusions staggered along their entire width. Their position and shape facilitate the capture and bending of short and strong residues. In addition, the width of the ends of the rubber blades, their shape and the presence of protrusions contribute to the effective capture and detachment of dry and dead residues, which can be located both in the rows of crops and the gaps between the root crops themselves in the row. Moving in a bent position along the root crop head, the rubber cleaning vane can move along it with its narrow, end part. In this case, the sharp edges of the blade cut off the remaining tops. They effectively cut off both green, strong residues and dry, fallen stalks that are located on the spherical surfaces of the heads. Such design features of the advanced peeler contribute to a significant increase in the quality of cleaning of each root crop head, regardless of its shape and the presence of residues.

Even the small angle α at which the two cleaning shafts intersect in the horizontal plane creates favourable conditions so that at the end of the cleaning zone, i.e. at the very ends of the drive cleaning shafts, the cleaning rubber blades completely cover the entire upper part of each root head, which guarantees complete separation of the green and strong residues of the tops (green stem ends), which are also located here. It is in this part of the peeler that the cleaning force is significantly increased, as the blade ends strike the heads with direct, central blows from top to bottom. And, as this occurs while the cleaner is moving forward, the ends of the rubber blades are very effective in gripping and simultaneously dislodging the residue on the top of the heads.

Thus, the new design of the cleaner has a longitudinally located active cleaning channel, in which cleaning forces are applied to each root crop head from virtually all sides (from above, due to the counter-rotating movement of both cleaning shafts) and both sides. The provided adjustments allow to adjust the functioning of the cleaner for high-quality cleaning of any root crop. This not only significantly improves the quality of cleaning, but also ensures that root crops are not knocked out of the soil. No other known design that performs a similar technological process has such features and technical characteristics.

CONCLUSIONS

An improved design of a root crop head cleaner from root residues and a new mathematical model of a multifactorial experiment to assess the quality of its operation have been developed. According to the results of the field experimental study of the root crop head cleaner from root residues, equipped with pairs of rubber cleaning blades mounted on driven horizontal shafts with appropriate length pitches that cover the row on both sides, it was found that it is possible to significantly improve the quality of cleaning.

The regression analysis and numerical calculations using statistical methods with the help of a PC allowed us to establish the optimal design, kinematic and operational parameters of the improved cleaner, which ensure the highest quality of cleaning (the lowest amount of stubble residue per linear metre). For example, the position of the ends of the rubber cleaning blades relative to the soil surface, i.e. the parameter h should not exceed 1.5 cm. The angular speed ω of the counter-rotational movements of the cleaning shafts should be between 36.4 and 76.6 RPM. The translational speed V of the cleaner should not exceed 2.0 $m \cdot s^{-1}$.

The next stage of research is the experimental determination of the power and force characteristics of the developed design of the root crop head cleaner, depending on the external conditions of harvesting the tops and the

condition of the plantation where they are grown, as well as on the different geometric and physical and mechanical characteristics of its cleaning blades. In the future, it is also necessary to consider the issue of constructive changes to this cleaner. In particular, it provides its drive cleaning shafts with vibratory movements in different planes. The greatest ability to do this, which will not require a very complicated improvement, will be the creation of forced oscillatory movements of the drive cleaning shafts in the directions of their longitudinal axes. It should be assumed that these oscillations will further improve the quality of cleaning root crops from residues on the root in any condition of both the crop and the plantation on which they are grown.

ACKNOWLEDGEMENTS

None.

CONFLICT OF INTEREST

None.

REFERENCES

[1] Beloev, H., Adamchuk, V., Kaletnik, G., & Bulgakova, O. (2021). *The basis of scientific research in the field of agricultural engineering*. Ruse: Academic Publishing House Ruse University.
[2] Berezhenko, E. (2020). Analysis of methods for harvesting haulm root crops and designs of harvest modules. *Innovative Solutions in Modern Science,* 38(2), 46-54. doi: 10.26886/2414-634X.2(38)2020.4.
[3] Borys, A.M. (2011). Modeling of the technological process of the removal of the haulm by a combined method. *Bulletin of Agricultural Science*, 7, 66-68.
[4] Borys, A.M. (2012). Results of field experimental studies of a new copier-rotor sugar beet husk separator. *Collection of Scientific Works of the Vinnytsia National Agrarian University. Series: Technical Sciences*, 65(11), 94-97.
[5] Borys, M.M. (2013). Study of the dynamic interaction of the copier-rotor separator with the head of the root crop. *Bulletin of Agricultural Science*, 8, 76-78.
[6] Bulgakov, V., Ivanovs, S., Holovach, I., & Ihnatiev, Ye. (2021b). Mathematical model of interaction between share working body and beet root during vibrational digging. In *20th International Scientific Conference "Engineering for rural development"* (vol. 20, pp. 665-672). Jelgava: Latvia University of Life Sciences and Technologies. doi: 10.22616/ERDev.2021.20.TF140.
[7] Bulgakov, V.M., Golovach, I.V., Ruzhilo, Z.V., Ignatiev, E.I., Adamchuk, O.V., & Trokhanyak, O.M. (2021a). *Theory and technical means for harvesting sugar beet tops*. Kyiv: Agrarian Science.
[8] Dushynsky, V.V. (2000). *Basics of scientific research: Theory and practice with software*. Kyiv: NTUU "KPI".
[9] Gurchenko, O.P. (2007). Justification of the main parameters of the shovel cleaner of beet heads from the remains of the chaff. *Agricultural Machinery. Collection of Scientific Works*, 3, 30-37.
[10] Hailys, G.A. (1992). *Basics of the theory and calculation of agricultural machines*. Kyiv: USHA.
[11] Ihnatiev, Ye. (2017). Theoretical research and development of new design of beet tops harvesting machinery. In *V International Scientific Congress "Agricultural Machinery"* (pp. 19-21). Varna, Bulgaria.
[12] Khelemendyk, M.M. (2001). *Directions and methods of development of working bodies of agricultural machines*. Kyiv: Agrarian Science.
[13] Martynenko, V.Ya. (1997). *Tops harvesters machines*. Ternopil: "Polygraphist" LLC.
[14] Martynenko, V.Ya., & Kucher, B.T. (2002). Study of the cutting ability of the disc knives of the gorse-harvesting machines. *Bulletin of the Kharkiv State Technical University of Agriculture*, 4, 211-214.
[15] Nadykto, V.T. (2017). *Basics of the scientific research*. Kherson: Oldie Plus.
[16] Patent of Ukraine No. 115404. Cleanser of root heads. (2017, October). Retrieved from https://uapatents.com/5-115404-ochisnik-golovok-koreneplodiv.html
[17] Pogorely, L.V. (Ed.). (1983). *Beet harvesters: Design and calculation*. Kyiv: Tekhnika.
[18] Pogorely, L.V., & Tatyanko, N.V. (2004). *Beet harvesters: History, design, theory, forecast*. Kyiv: Phenix.
[19] Shabelnyk, B.P. (1998). *Conveyors-cleaners of root-harvesting machines (theory and calculation)*. Kyiv: Minosvita.
[20] Storozhuk, I.M., & Pankiv, V.R. (2015). Research results of harvesting haulm remnants of root crops. *INMATEH – Agricultural Engineering*, 46(2), 101-108.
[21] Syplyvets, O.O. (2001). Experimental studies of a new gorse-harvesting machine. *Agricultural Machinery. Collection of Scientific Articles*, 8, 223-233.
[22] Žitňák, M., & Korenko, M. (2011). Technical-economical indicators in the sugar beet transportation management. *Research in Agricultural Engineering*, 57, 63-71. doi: 10.17221/29/2010-RAE.

Мирослав Ігорович Будзанівський
Аспірант
Інститут механіки та автоматики агропромислового виробництва
Національної академії аграрних наук України
08631, вул. Вокзальна, 11/1, стм. Глеваха, Київська обл., Україна
https://orcid.org/0000-0002-0508-3816

Експериментальні дослідження якості очищення головок коренеплідних культур від решток на корені новим очисником

Анотація. У зв'язку з тим, що до очистки головок коренеплідних культур від решток висуваються високі технічні вимоги, розробка нових, більш вдосконалених очисників, є важливим і актуальним питанням. Метою даного дослідження було підвищення якості технологічного процесу очистки шляхом визначення оптимальних кінематичних, конструктивних та експлуатаційних параметрів нового очисника головок коренеплідних культур від решток на корені. Для цього була виготовлена нова конструкція очисника головок коренеплідних культур, яка дозволяла використовувати різні за механічними властивостями та розмірами очисні елементи, та змінювати його кінематичні параметри в залежності від тієї культури яку він обробляє. Також була виготовлена нова експериментальна установка, в якій було встановлено цей очисник і за допомогою якої змінювали його експлуатаційні параметри. Для проведення дослідження була розроблена нова математична модель багатофакторного експерименту. За результатами проведеного польового експериментального дослідження, кореляційного аналізу та статистичних числових розрахунків за допомогою ПК встановлені оптимальні конструктивні, кінематичні та експлуатаційні параметри вдосконаленого очисника, при яких спостерігається найвища якість очистки (найменша кількість залишків гички на погонному метрі). За результатами проведеного кореляційного аналізу були отримані такі оптимальні параметри вдосконаленого очисника головок коренеплідних культур від решток на корені: розташування кінців гумових очисних лопатей відносно поверхні ґрунту, тобто параметр h не повинен перевищувати 1.5 cm. Кутова швидкість ω зустрічно обертальних рухів очисних валів повинна відповідати такому інтервалу значень – 36.4…76.6 rpm. Швидкість V поступального руху очисника повинна бути не більшою ніж 2.0 $m \cdot s^{-1}$. Отримані конструктивні, кінематичні та експлуатаційні параметри можуть бути успішно використані в конструкторських бюро при проєктуванні перспективних машин для збирання різних коренеплідних культур, в науково-дослідних установах та університетах при проведенні сучасних досліджень в галузі агроінженерних наук

Ключові слова: гичка; залишки; план-матриця; оптимальні параметри; гумові лопаті

Machinery & Energetics
Vol. 14, No. 3. 2023

Journal homepage:
https://technicalscience.com.ua/en

UDC 621.313.33:621.318.122
DOI: 10.31548/machinery/3.2023.34

Stefan Junge*
Doctor of Technical Sciences, Professor
Berlin University of Applied Sciences
13353, 10 Luxemburger Str., Berlin, Germany
https://orcid.org/0000-0002-8045-4103

Nikolay Zablodskiy*
Doctor of Technical Sciences, Professor
National University of Life and Environmental Sciences of Ukraine
03041, 15 Heroiv Oborony Str., Kyiv, Ukraine
https://orcid.org/0000-0001-8889-8158

Natalya Zaiets
Doctor of Technical Sciences, Professor
National University of Life and Environmental Sciences of Ukraine
03041, 15 Heroiv Oborony Str., Kyiv, Ukraine
https://orcid.org/0000-0001-5219-2081

Roman Chuenk
PhD in Technical Sciences, Associate Professor
National University of Life and Environmental Sciences of Ukraine
03041, 15 Heroiv Oborony Str., Kyiv, Ukraine
https://orcid.org/0000-0002-9339-9764

Stanislav Kovalchuk
Postgraduate Student
National University of Life and Environmental Sciences of Ukraine
03041, 15 Heroiv Oborony Str., Kyiv, Ukraine
https://orcid.org/0000-0002-1194-3464

The screw-type electrothermomechanical converter as a source of multiphysical influence on the technological environment

Abstract. In ensuring the reliability of electromechanical converters in harsh conditions, the problem of increasing the energy efficiency of their application through structural, functional, and thermal integration with the technological environment is present. Thus, the research aims to determine the conditions of the direct multiphysical impact of a screw-type electromechanical converter on the technological environment. The method used is based on determining the list of features of screw-type electromechanical converters using the Comsol Multiphysics software, and a combination of three-dimensional and two-dimensional finite element models limited to the rotor with the inclusion of blades in the computational domain. Two variants of forming an algorithm for the multiphysical impact on the technological environment were studied: local concentration of the impact in certain areas of the rotor and uniform distribution along the rotor surface of temperature, pressure, magnetic induction, and electric field strength. The regularities of the distribution of magnetic

Article's History: Received: 03.04.2023; Revised: 12.07.2023; Accepted: 11.08.2023.

Suggested Citation:
Junge, S., Zablodskiy, N., Zaiets, N., Chuenko, R., & Kovalchuk, S. (2023). The screw-type electrothermomechanical converter as a source of multiphysical influence on the technological environment. *Machinery & Energetics,* 14(3), 34-46. doi: 10.31548/machinery/3.2023.34.

*Corresponding author

induction on the outer surface of the ferromagnetic rotor at different azimuthal locations of the frontal parts of adjacent stators have been established. The distribution of the normal component of the magnetic flux density at the contact with the process medium in the form of rutile product or ilmenite concentrate is determined. The consumed electric energy is distributed in the stator tooth zone and the zone of electromagnetic field penetration into the rotor. Eddy currents are concentrated at the penetration depth from the rotor's inner surface, with the penetration depth depending on the thermal state and sliding mode. The electric field intensity on the rotor's outer surface reaches 0.8 V/m in the areas opposite the stator crowns and depends on the current activity of the phases at a given moment. Controlling the thermal and speed regime of the rotor can be used to create conditions for bioenergy stimulation on its surface in places of contact with the medium or to support the process of electrode heating of the technological medium. The adequacy of the mathematical models proposed for numerical modelling to the experimental data of the prototype of the screw electromechanical converter was confirmed, with deviations not exceeding 9.5%. The obtained results can be used to predict the optimal indicators of electromagnetic and heat transfer processes in screw electromechanical converters associated with the technological environment

Keywords: magnetic induction; eddy currents; temperature field; electromagnetic field; thermogram, magnetic permeability

INTRODUCTION

Most electromagnetic devices (EMDs) are characterised by the simultaneous action of electromagnetic, thermal, vibration, mechanical and acoustic fields not only on the electromagnetic core of the device but also on the technological environment. These EMDs contain continuously moving or stationary parts with the required electrical conductivity and magnetic properties that are in direct contact with the process medium - solid, liquid, gaseous and multiphase objects that are actively or passively used in the technological process of production or use of products. An urgent problem is the drying and processing of wet dispersed waste from food production, which can then be effectively used as fertiliser, livestock feed or biofuel (Bulgakov *et al.*, 2020).

A special category of EMDs is represented by solid rotor induction motors (SRIMs), which, due to their rigid construction and integrity, can operate at the highest required rotational speeds. These machines can be used in aggressive and humid environments and integrate design and functionality with the process. All types of energy dissipation in such machines are used to process raw materials. For example, in screw electromechanical converters (SEMCs), an external massive rotor can contact the processing medium and create multiphysical processes for processing raw materials (Zablodskiy *et al.*, 2021).

T. Wolnik & T. Jarek (2022) compared the losses, power factors, and efficiency of induction motors with a solid and shielded rotor magnetic circuit. It was found that the increase in total losses of the solid rotor is primarily due to the growth of eddy current losses in the presence of higher harmonics and subharmonics in the magnetic flux harmonic spectrum. The comparison of design parameters and weight reveals that the solid rotor has a simplified design and manufacturing technology and a lower weight, especially for motors with an external rotor.

To increase the power factor, V. Kaplun *et al.* (2022) suggested using internal capacitive compensation of the reactive power of an induction motor. A winding with two parallel windings in each phase is used, one of which forms the main winding that is connected to the power supply network. The other parallel winding in the core slots is offset relative to the main winding and forms an additional winding that is switched on according to the scheme of a rotary autotransformer to an electric capacitance. A comparison of the modelling results of the basic and improved motors indicates the possibility of increasing energy efficiency and torque when using internal capacitive reactive power compensation.

C.A. Wengerkievicz *et al.* (2022) analysed the possibilities of determining the loss distribution of an induction machine with a two-phase stator winding and a massive groove-less rotor by testing according to standard methods used for squirrel-cage induction motors. Even if a high operating frequency is required, the tests are carried out at a reduced frequency and voltage to avoid the influence of time harmonics. It is proposed to adjust the loss distribution to take into account the effect of high slip without load, as well as to analyse parasitic losses during load tests. The final test results are extrapolated to establish nominal conditions. According to C. Mellak *et al.* (2022), motors with a solid rotor have higher mechanical and thermal stability, and better stator current to electromagnetic torque ratio at high slip, which makes them suitable for compressor production, railway electric transport, and medicine.

However, there are applications where efficiency may not be the most important parameter. In this case, the technological environment may have high temperature, pressure and humidity or a limited volume. To predict losses, A. Laidoudi *et al.* (2020) proposed an analytical model that is combined with a thermal model to predict the temperature in different parts of the machine and the effect of temperature on parameters important for EMD performance.

A wide range of technological processes with heavy temperature loads exist that require the direct coupling of rotating parts of EMDs with actuators. M.M. Mazlan *et al.* (2019), and F. Campuzano *et al.* (2019) proved the

effectiveness of using a screw converter in the processing of bulk and plastic substances. The influence of hydrolysis parameters on the mixing torque was investigated for single- and twin-screw electromechanical converters by C. Feng *et al.* (2019). In these studies, regression models were developed to establish a correlation between system parameters and time-varying parameters. M. Mushtruk *et al.* (2020) investigated the issue of high energy consumption associated with machining in an electromechanical screw converter.

A feature of the considered methods and results of studies of electromechanical converters is the stationary temperature conditions of the surrounding cooling medium. However, for screw-type electromechanical converters (SEMCs) for technological purposes, studies with nonlinear changes in the load-cooling medium become relevant. The second important feature of the design and application conditions of the SEMC is that the presence of a wide range of harmonics in the distribution of its resulting magnetic field, which forms eddy current losses, is a useful component for ensuring the temperature regime in the rotor-technological environment system. At the same time, the electromagnetic system of the SEMC should provide the required electromechanical characteristics and overall efficiency. As such, along with solving the problem of ensuring the reliability of electromechanical converters in harsh environments, a scientific demand for improving the energy efficiency of their use through structural, functional, and thermal integration with the technological environment is present. Thus, the research aims to determine the conditions of the direct multiphysical influence of an electromechanical screw-type converter on the technological environment.

MATERIALS AND METHODS

The research was carried out at the Educational and Research Institute of Energy, Automation and Energy Saving of the National University of Life and Environmental Sciences of Ukraine in 2020-2022. The object of the study was electromagnetic, electromechanical, and thermal processes in the electromagnetic system of the screw electromechanical converter (SEMC) and the areas of direct contact of the external massive rotor screw with the technological environment. Two variants of forming an algorithm for the multiphysical influence on the technological environment in accordance with the technological process were considered: the first variant is the local concentration of such impact in certain areas of the rotor; the second variant is the uniform distribution along the rotor surface of temperature, pressure, magnetic induction, and electric field intensity. Numerical modelling was carried out for the SEMC, a fragment of the electromagnetic system design which is shown in Figure 1.

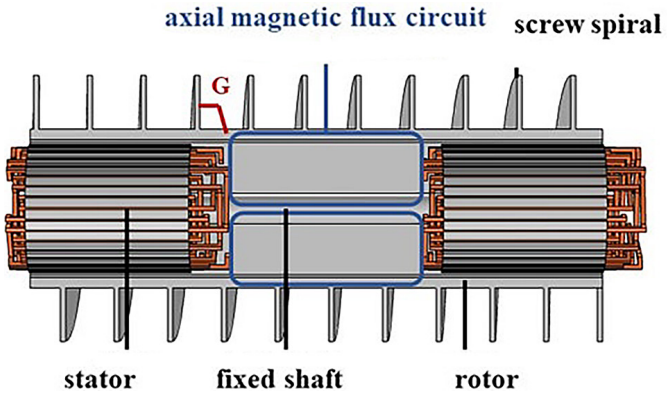

Figure 1. The SEMC electromagnetic system
Note: blue contours show the circulation of the longitudinal magnetic flux in the intermodule zone; G – outer surface of the rotor with the rotor helical blades (ribs)
Source: compiled by the authors

A method based on the numerical determination of the characteristics of the SEMC using a combination of three-dimensional and two-dimensional finite element models, limited by the rotor with the inclusion of blades in the computational domain is applied. Considering the identity of electromagnetic and thermal processes occurring on the stator-common rotor modules of the electromagnetic system of the SEMC, the simulation was carried out for one of them in the Comsol Multiphysics software environment (AC/DC Module User's Guide, COMSOL Inc., Burlington, MA, USA, 2018). The numerical analysis of the electromagnetic field was carried out using a mathematical model (MM) and the spatial distribution of the grid of an electromechanical screw-type device for the hydrolysis processing of feathers (Fig. 2).

The operating loading and cooling medium are in direct contact with the screw rotor. Depending on the loading mode of the SEMC, the process medium can be represented in the following types: at idle (system warm-up mode) - air; at the main operating mode - a continuous heterogeneous medium using averaged characteristics (specific conductivity, magnetic and dielectric constant).

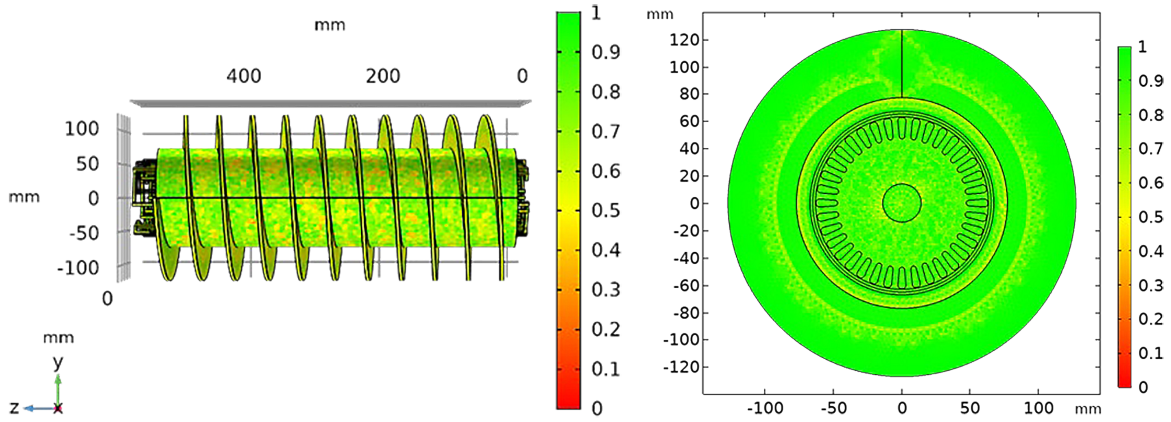

Figure 2. Finite element mesh in the design domain
Source: N. Zablodskiy *et al.* (2021)

Considering these properties of the technological environment, other vectors of electric induction and magnetic field strength were introduced to account for all the induced currents, namely: polarisation current of bound charges; free carrier current; eddy current of magnetisation:

$$D(r,t)=E(r,t)+4\pi P(r,t);\ H(r,t)=B(r,t)+4\pi M(r,t), \quad (1)$$

where $P(r,t)=\int_{-\infty}^{t} j(r,t)\,dt$ – a polarisation density vector that combines induced currents of all types; $M(r,t)$ – the magnetisation vector of the operating environment.

When modelling the main mode of operation of the SEMC, ilmenite and rutile with a specific electrical conductivity of $10^{-1} \leqslant \rho \leqslant 10_4$ S/m were considered as a heterogeneous medium surrounding the screw rotor, which differs in magnetic properties: ilmenite is weakly magnetic (specific magnetic susceptibility $24 \cdot 10^{-7}$ m^3/kg), and rutile is non-magnetic (specific magnetic susceptibility $0.25 \cdot 10^{-7}$/kg).

Considering the factor of the discrete location of the stators, an important stage of research was to determine the electromagnetic and thermal characteristics of the intermodule section of the rotor. For the second variant of forming an algorithm for the multiphysical impact on the technological environment, namely, the uniform distribution along the rotor surface of temperature, pressure, magnetic induction, and electric field strength, a method based on the numerical determination of the transverse and longitudinal edge effect of a common rotor for two SEMC stators using a combination of three-dimensional and two-dimensional finite element models was proposed. These effects, by matching the magnetic fluxes of the frontal parts of adjacent stators, are used in the numerical model of the SEMC to ensure uniformity of the rotor temperature field in the intermodule zone and increase the energy performance of the SEMC.

The distribution of a plane electromagnetic wave in the intermodule zone during the passage of an alternating magnetic flux $\dot{\Phi}_m$ along a steel rotor cylinder was considered (Fig. 1). Since the average diameter of the hollow cylindrical rotor of the screw SEMC is an order of magnitude greater than its thickness, and the rotor thickness b of the SEMC prototype exceeds the penetration depthΔ_{ew}, the influence of wave curvature and reflection can be neglected, and a flat electromagnetic field can be assumed to penetrate the rotor in the intermodule zone from both sides.

To verify the modelling results, two prototypes of the SEMC with different azimuthal arrangements of the fronts of adjacent stators were tested: the prototype – an arbitrary azimuthal arrangement of the fronts of adjacent stators; the second prototype - magnetic fluxes of the fronts of adjacent stators coordinated in space and time. The nominal data of the SEMC are power consumption P = 1900 W; supply voltage U = 80 V; current consumption I = 30 A; power factor cos φ = 0,65; number of poles – 6; rotation frequency n = 180 rpm. Figure 3 shows the components of the prototype SEMC with the definition of the zones for measuring electromagnetic and temperature parameters.

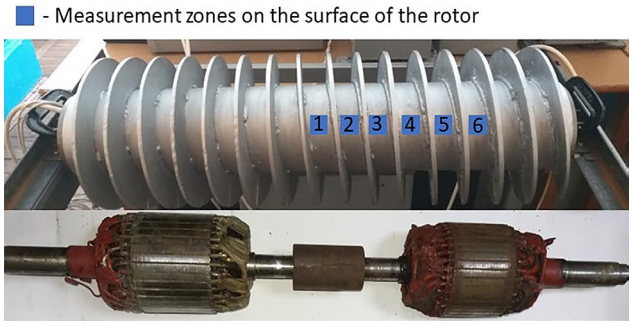

Figure 3. Distribution of measurement zones of electromagnetic and temperature parameters on the surface of the outer rotor of the mock-up sample of the SEMC
Note: the figure shows the corresponding arrangement of the system of adjacent stators placed in the outer rotor cavity
Source: compiled by the authors

Measurements of electromagnetic and temperature parameters on the prototypes were performed in short-circuit mode (braked rotor) with the supply voltage reduced to the level at which the rated current is achieved.

The following measuring devices were used in the empirical studies: Tenmars TM-191 Magnetic Field Meter (manufactured in Taiwan), designed to measure ultra-low frequency electromagnetic fields from 30 Hz to 300 Hz; Tenmars TM-190 Multi-Field EMF Meter (Taiwan) – a device for measuring high-frequency electromagnetic fields in the frequency range from 50 MHz to 3.5 GHz and low-frequency electric and magnetic fields in the frequency range of 50-60 Hz; infrared, optical pyrometer BENETECH GM533A (China), measuring range -50-530°C, visibility index 12: 1, thermal radiation coefficient 0.1-1, spectrum 5-14 μm; thermal imager Xintest HTI HT-18 (country of origin China), thermal sensitivity 0.07°C, temperature range: -20°C--300°C, image capture frequency 8 Hz, wavelength range 8-14 μm.

RESULTS AND DISCUSSION

The research methodology allowed us to establish a wide range of parameters and regularities through modelling and experimental measurements, but this section presents primarily the results of determining the conditions for the direct multiphysical influence of the screw-type electromechanical converter on the technological environment. Figure 4 shows the distribution of magnetic field induction in the stator plane of a separate SEMC module. The levels of magnetic induction in the stator tooth zone do not exceed 1.4 T, which indicates the absence of saturation zones and is explained by the low voltage value on the winding phases. The highest values of magnetic induction (up to 2.8 T) are observed on the side of the inner surface of the rotor at the depth of penetration Δ of the electromagnetic field into the rotor array. In the array and on the outer surface of the rotor, which is in direct contact with the process medium, 6 wide and 6 narrow zones are formed in a circular pattern alternating in a circle following the number of poles. On the outer surface, the magnetic field induction levels for the wide (opposite the poles) and narrow zones are 0.6 T and 0.1 T, respectively.

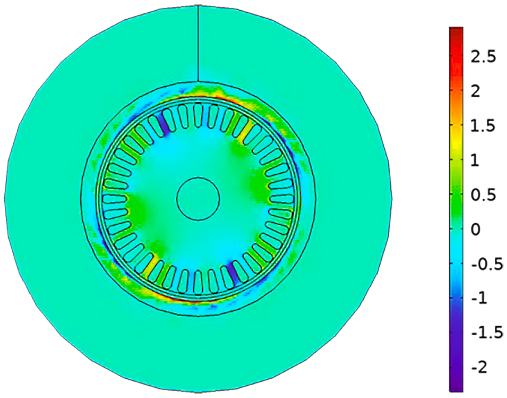

Figure 4. Induction of a magnetic field in the stator plane of a single module of an SEMC
Note: scale dimension – T
Source: compiled by the authors

The distribution of the normal component of the magnetic flux density of the SEMC coincides with the results of modelling electromechanical converters of the submersible type for oil production technologies in terms of the levels of magnetic induction in the stator tooth zone, on the inner and outer surfaces of the rotor, and at the depth of electromagnetic wave attenuation in the rotor ferromagnetic body (Zablodskiy *et al.*, 2014).

With an increase in the supply voltage, the magnetic flux penetrates much deeper into the rotor, as noted by C.A. Wengerkievicz *et al.* (2022), but in this case, the study concerns a massive hollow rotor with helical blades (fins) external to the stator. Since the array of the external solid rotor of the SEMC is simultaneously conductive for magnetic flux and eddy currents, the nature of the distribution of electromagnetic parameters in it differs significantly from induction machines with a shielded rotor.

Figure 5 shows the distribution of the normal component of the magnetic flux density for the cross-section of the SEMC module in the presence of contact with the process medium in the form of rutile product or ilmenite concentrate.

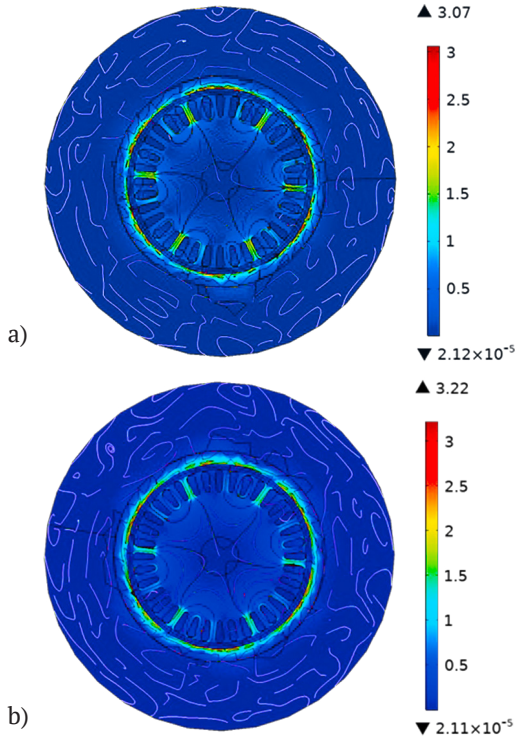

Figure 5. Magnetic flux density during SEMC operation
Note: scale dimension - T; a) – with rutile product; b) – with ilmenite concentrate
Source: compiled by the authors

Rutile product slightly weakens the external magnetic field in the rotor surface area and deviates from the rotor surface, while ilmenite concentrate, on the contrary, strengthens the magnetic field and adheres tightly to the rotor surface.

The SEMC can be used for heating up to 110°-120°C and transporting it to the production of commercial rutile concentrate, as well as preheating non-conductor industrial products before feeding them to an electrostatic separator to produce zircon product.

Figure 6 shows a three-dimensional image of the magnetic induction distribution on the outer surface of the ferromagnetic rotor at different azimuthal locations of the stator fronts. The magnetic induction on the surface of the rotor sections covered by the corresponding stator magnetic cores is 0.6 T. The magnetic field induction levels on the outer surface of the SEMC rotor in the intermodule zone are much lower and are in the range of 0.2-0.35 T.

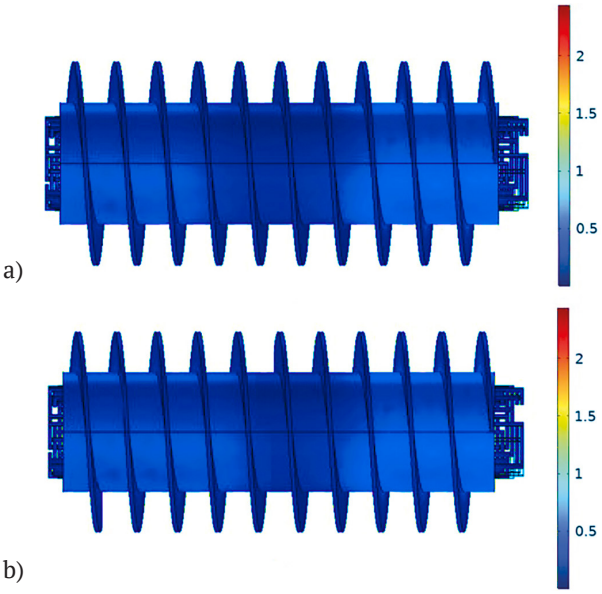

Figure 6. Three-dimensional image of the magnetic field induction distribution on the rotor surface with different azimuthal arrangements of the stator frontal parts

Note: scale dimension – T; a) – arbitrary azimuthal location of the frontal parts of adjacent stators; b) – magnetic fluxes of the frontal parts of adjacent stators coordinated in space and time

Source: compiled by the authors

At the same time, the length of the section with this level of magnetic induction is half as long for the variant of the magnetic fluxes of the frontal parts of adjacent stators coordinated in space and time compared to the variant of the arbitrary azimuthal arrangement of the frontal parts of adjacent stators. This indicates that the coordination in space and time of the magnetic fluxes of the frontal parts of adjacent stators creates conditions for the formation of a variable magnetic flux along the steel rotor cylinder (Fig. 1) and, accordingly, the excitation of eddy currents in the intermodule zone. It is necessary to determine the regularity of changes in the intensity of the electric and magnetic fields along the rotor cross-section, in which the outer surface has a lateral branch corresponding to the screw turn cross-section. The position of this branch changes no more than the screw turn pitch, making one revolution around the rotor circumference. Following Figure 7, the electromagnetic wave propagates perpendicular to the hollow rotor surface between the outer and inner surfaces in the intermodule zone. In the same direction, through the inner and outer surfaces, energy flows into the rotor array, which is given by the Poynting vector $\bar{P}$, caused by the electric and magnetic field components perpendicular to it and tangent to the surface.

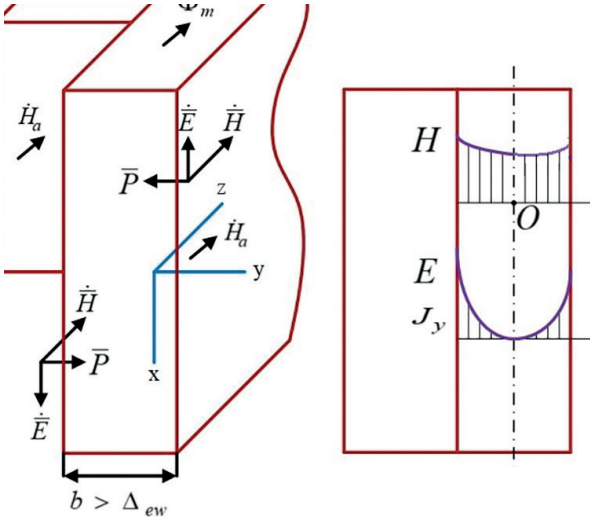

Figure 7. Distribution of electromagnetic field components and density of eddy currents in the array of the intermodule zone of the SEMC rotor

Note: $\dot{E}$ і $\dot{H}$ – amplitude values of the electric and magnetic field intensity vectors, respectively; H_a – axial component of the magnetic field strength; $\bar{P}$ – Poynting vector; Φ_m – magnetic flux; b – rotor thickness; Δ_{ew} – electromagnetic wave penetration depth; J_y – eddy current density along the rotor thickness

Source: compiled by the authors

The electric field causes conduction current and heating of the rotor mass, and the field amplitudes decay as the electromagnetic wave propagates deeper into the metal. The final conductivity of the rotor causes the presence of a tangential component of the electric field E_τ when current flows on its surface. The electric field strength and eddy current density decrease according to the law:

$$j(y) = \gamma E_\tau(y) = \gamma E_\tau(y) exp(-a_j y), \quad (2)$$

where a_j – wave propagation constant.

The amplitude values of the electric $\dot{E}$ and magnetic $\dot{H}$ field intensity vectors, as well as the wave propagation constant a_j, will be different when the wave penetrates the boundaries of the hollow rotor surfaces in the presence of a lateral branch in the form of ribs on the outer surface of the rotor. The temperature distribution T is determined as a solution to the equation as follows:

$$\lambda\Delta T - c\rho\frac{\partial T}{\partial t} = -Q, \quad (3)$$

where λ, c, p – respectively thermal conductivity, heat capacity and density of the material; Q – specific heat emissions. The heat emission in the rotor array is calculated by the formula:

$$Q = {J_z^2}/{\gamma(T)}, \quad (4)$$

where the electrical conductivity of the rotor iron at each point depends on the temperature T. For a two-dimensional modelling problem, equation (3) is presented in the following form:

$$\lambda\frac{\partial^2 T}{\partial x^2} + \lambda\frac{\partial^2 T}{\partial y^2} - cp\frac{\partial T}{\partial t} = Q. \quad (5)$$

The interconnection of electromagnetic and thermal processes is manifested in the mutual influence of temperature, electrical conductivity, eddy current density and specific heat emissions, which is reflected in formulas (3-4). Boundary and initial conditions are set for equation (5). When constructing the mathematical model, it was assumed that the main heat transfer from the rotor to the bulk material was carried out in the form of heat flow through the outer surface G (Fig. 1). This assumption is met by the second-order boundary condition, which sets the average value of the heat flux at the boundary of the computational domain:

$$q|_G = \frac{1}{R_{2H}}\int_{s'} Q ds = \frac{1}{R_{2H}}\int_{s'}\left[{J_z^2}/{(\gamma)T}\right] ds, \quad (6)$$

where R_{2H} – outer rotor radius; S' – outer radius of the rotor area of integration. Expression (6) also determines the relationship between the electromagnetic and thermal tasks.

The study considers the effect of temperature on the nature of electromagnetic processes. Approximately, the process of penetration of an electromagnetic field wave into the rotor array along the y-coordinate with a harmonically varying magnetic flux in time can be represented by the following expression:

$$J(y) = J_{m e^{-ky}}, \quad (7)$$

where $k = \sqrt{\omega\mu/2\rho}$; ω is the angular frequency of the field change; μ is the magnetic permeability; ρ is the resistivity, which varies with temperature according to the known law $\rho = \rho_0[1 + \alpha(T - T_0)]$, where ρ_0 is the resistivity at temperature T_0. The dependence of the magnetic permeability of steel on temperature is more complex and is determined by empirical dependencies. The differential equation for determining the temperature increase of the surface of a ferromagnetic rotor and the corresponding temperature increase of the medium $\Delta T_{en.m}$ is as follows:

$$R_r\frac{d(\Delta T_r)}{dt} + \Delta T_r = \Delta T_{en.m}, \quad (8)$$

where R_r is the thermal time constant of the rotor design zone; $\Delta T_{en.m}$ is the temperature increase of the medium; ΔT_r is the temperature increase of the rotor. The thermal time constant of a ferromagnetic rotor:

$$R_r = \frac{m_r c_r}{2\cdot G_{TCR}}, \quad (9)$$

where m_r, c_r – mass and specific heat capacity of the rotor material, respectively; G_{TCR} – rotor thermal conductivity. The thermal conductivity G_{TCR} is calculated for a homogeneous cylindrical wall with heat sources and heat dissipation through the outer wall, considering the helical rotor blades (fins):

$$G_{TCR} = \frac{2\pi\cdot r^2\cdot l_r}{\frac{1}{\alpha_1}+\frac{r_2-r_1}{\lambda}+\frac{1}{\alpha_2[1+A_{0S}(k_{0S}-1)]}}, \quad (10)$$

where l_r – rotor length; r_1, r_2 – inner and outer radii of the cylindrical rotor, respectively; λ – thermal conductivity of the rotor material; α_1, α_2 – are, respectively, the heat transfer coefficient on the un-finned surface of the rotor wall and the finned surface of the rotor; A_{0S} – finning efficiency factor; k_{0S} – the coefficient of finning of the rotor surface, equal to the ratio of the total area of the finned surface to the area of the smooth rotor surface. The proposed method for calculating the magnetic field and thermal parameters is advisable to implement for an end-arc squirrel-cage induction motor with an electrically conductive rotor. Unlike the method used by A.P. Rashchepkin *et al.* (2017), the modularity of the rotor design and the combination of the rotor with the working body were considered.

The rotor of the SEMC performs the functions of an actuator and is used as a direct drive, in which a wide range of rotational speeds can be formed without a semiconductor converter. Similar results were achieved in the works of P.J. Holik *et al.* (2007), and B. Virlan *et al.* (2013), which present a comprehensive study of the performance of an induction motor (IM) with an external rotor and a multipole stator winding.

In recent years, a large number of studies have focused on methods to improve the energy efficiency of SRIM. In comparison with the results of V.M. Sundaram *et al.* (2015), and M.V. Cistelecan *et al.* (2010), the proposed design, modelling, and experimental studies of the SEMC provide comparable performance at high slip in terms of average/pulsating torque with a significant reduction in the total copper consumption, considering the spatial harmonics of the magnetomotive force in the air gap, including saturation effects.

The magnetic field created on the outer surface of the rotor must be rotating. Therefore, this effect can be considered as a kind of electromagnetic stirrer (Zablodskiy *et al.*, 2021). In the case of using such a field, for example, in liquid media, eddy currents arise that create their magnetic field and interact with the rotating stator field, which contributes to more intense heat and mass transfer in the liquid (Smith, 2015).

Figure 8 shows thermograms of the outer surface of the rotor of the SEMC prototype with an arbitrary azimuthal arrangement of the fronts of adjacent stators and with the magnetic fluxes of the fronts of adjacent stators coordinated in space and time.

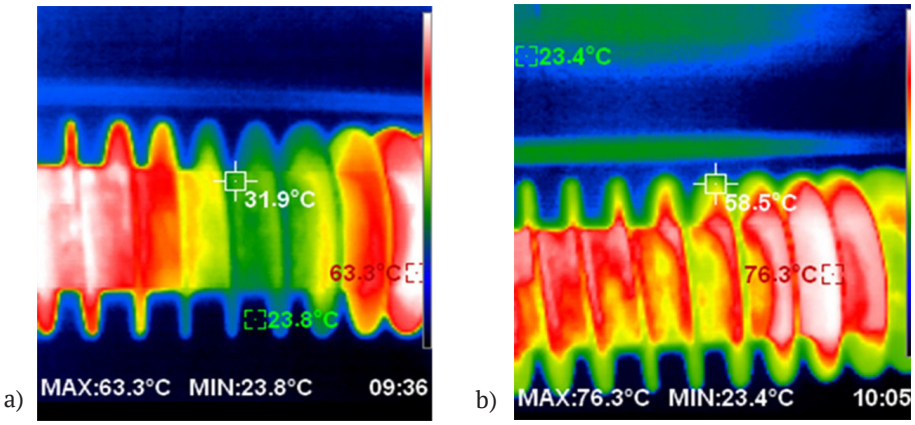

Figure 8. Thermogram of the outer surface of the rotor of the prototype SEMC
Note: the thermograms were recorded after 7 minutes of operation in the short-circuit mode at a voltage of U = 73V. 2; a) prototype with an arbitrary azimuthal arrangement of the frontal parts of adjacent stators; b) prototype with magnetic fluxes of the frontal parts of adjacent stators coordinated in space and time
Source: compiled by the authors

It is noticeable that in the case of magnetic fluxes of the frontal parts of adjacent stators coordinated in space and time, a certain uniformity of temperature field distribution along the rotor length, including the intermodule zone, is achieved. Figure 9 shows the distribution of current density (z-component) in the cross-section of the SEMC module. The eddy currents are concentrated at the penetration depth from the rotor inner surface, with the current penetration depth $\Delta = 1/k$ depending on the thermal state and sliding mode of the SEMC:

$$\Delta = \sqrt{2\rho_0[1 + \alpha(T - T_0)]/\omega\mu}. \qquad (11)$$

In contrast to C. Wengerkievicz *et al.* (2022), who acquired results using two-dimensional finite element modelling, our work considers the regime of large slips up to 80%. The difference in the distribution of eddy currents at slips close to the idle stroke and slips corresponding to the full screw loading regime was noted. The magnetic permeability μ of the rotor material is not constant, so its magnetic saturation is considered. For structural carbon steels, the values are in the range of strong fields ($H = 2 \cdot 10^{-3}$--$12 \cdot 10^{-3}$ A/m) have slight fluctuations when heated to temperature 400°C, and then begin to decrease, reaching unity at the Curie point temperature.

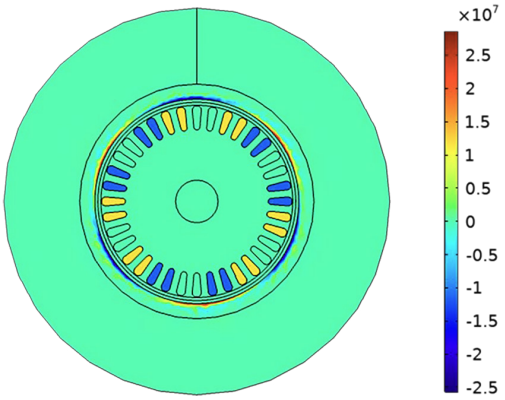

Figure 9. Distribution of current density (z-component) in the cross-section of the SEMC module, A/m^2
Source: compiled by the authors

The determination of the current density distribution in the end regions is problematic due to the lack of special methods and models. The method proposed by M. Jagiela *et al.* (2012), which is based on the numerical determination of the dimensionless rotor end coefficient using a combination of three-dimensional and two-dimensional finite element models, was developed for high-speed induction motors with a solid rotor and does not consider the operation of an electromagnetic system with several stators and a common rotor. To form an analytical method for calculating the magnetic field and electromagnetic field energy distribution in the intermodule space of the SEMC, it may be advisable to use Maxwell's system of equations for the quasi-stationary regime and integral transformations into Fourier series along the azimuthal coordinate (Rashchepkin *et al.*, 2017).

The distinctive feature of the SEMC is the conversion of the concept of "power losses", which are determined by standard loss allocation procedures, for example, for induction motors, into the concept of "dissipative energy component". In the SEMC, all types of dissipative energy (electrical and magnetic) are attributed to useful (in this case, thermal) energy. Figure 10 shows the distribution of electrical energy density for the cross-section of a SEMC module.

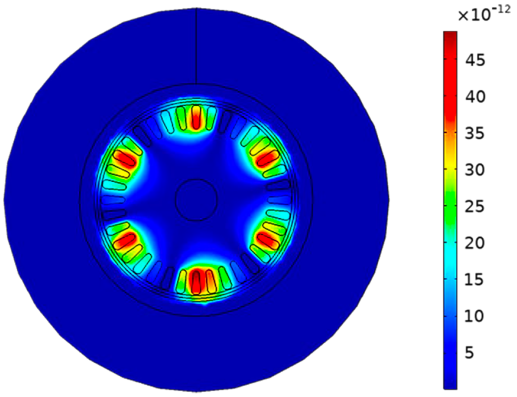

Figure 10. Electric energy density for the cross-section of the SEMC module, J/m^3
Source: compiled by the authors

It can be seen that the main electrical energy consumed is distributed in the stator tooth zone and the zone of electromagnetic field penetration into the rotor. The methods of loss segregation proved to be appropriate by tests with a locked rotor and no load, which was used by C. Mellak *et al.* (2022) in experimental studies of induction motors with smooth solid rotors. Table 1 shows the experimental data of the prototype of the SEMC. Magnetic induction, electric field intensity, and electromagnetic radiation flux density were measured in the short-circuit mode at the minimum possible distance of 1 mm from the rotor surface of the SEMC.

Table 1. Experimental data of the prototype sample of the SEMC

Measurement area	Parameters			
	Magnetic induction, mT	Electric field strength, V/m	Density of electromagnetic radiation flux, mW/m²	Temperature, (Fig. 3)
1	60	0.03	0.7	48
2	100	0.03	0.9	51
3	170	0.03	1.8	62
4	400	0.2	523	74
5	380	0.15	520	76.2
6	410	0.15	525	76.3

Note: the temperature distribution is given for the variant with the magnetic fluxes of the frontal parts of adjacent stators coordinated in space and time
Source: compiled by the authors

A. Wasak *et al.* (2019) noted that a rotating magnetic field is used as a tool to improve the properties of enzymes. At the interfaces of matter, the Hall effect in the presence of a magnetic field promotes intense interaction of the electric fields of bulk ion charges and electric charges of the interface. Therefore, it was important to determine the distribution of the normal component of the electric field strength for the cross-section of the SEMC module, especially on the rotor's outer surface. Figure 11 shows the distribution of the normal component of the electric field intensity for the cross-section of the SEMC module.

The electric field intensity on the rotor's outer surface reaches 0.8 V/m in the areas corresponding to the location of the stator crowns and depends on the current activity of the phases at the moment. Thus, the control of the rotor thermal and speed regime makes it possible to create conditions for bioenergy stimulation on its surface in places of contact with the medium or to maintain the process of its electrode heating.

Considering the objective reason for the remote location of the device sensors, we extrapolated the data for measuring magnetic induction, electric field strength, and electromagnetic radiation flux density of the SEMC prototype. The adequacy of the mathematical models proposed for the numerical modelling of the experimental data of the SEMC prototype was confirmed (Table 1). The deviations do not exceed 9.5%. Based on the results of the simulation, Figure 12 shows the distribution of electromagnetic forces acting in the air gap of the SEMC.

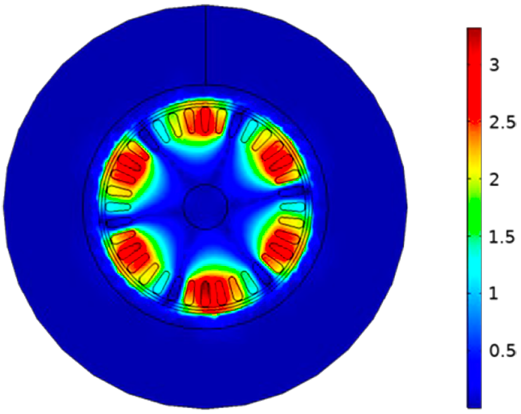

Figure 11. Distribution of the normal component of the electric field intensity for the cross-section of the SEMC module, V/m^3

Source: compiled by the authors

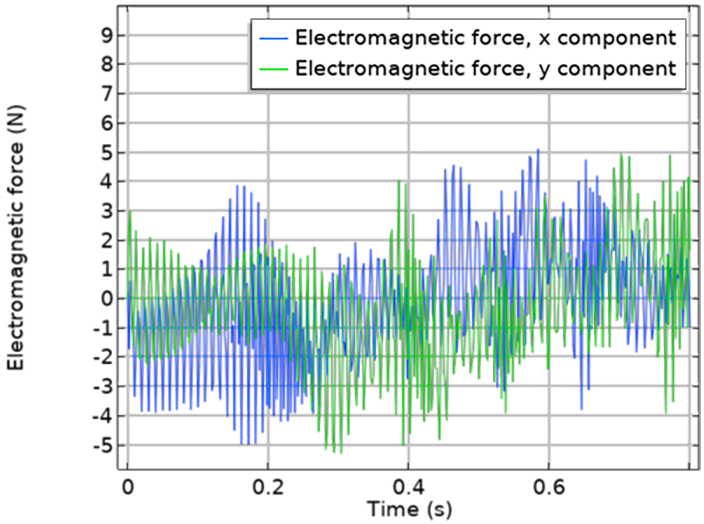

Figure 12. Distribution of electromagnetic forces

Source: compiled by the authors

The frequency range of electromagnetic forces is 90-120 Hz and significantly exceeds the frequency of the stator supply current. The data of the study by V. Bulgakov *et al*. (2020) also indicate that under the influence of vibration, materials undergo transformations whose properties depend on the vibration intensity, and, for example, keratin materials go into a state of fluidisation. In addition, the determination of the distribution of electromagnetic forces and, accordingly, electromagnetic moments allow, in comparison with the calculations of P. Singha & K. Muthukumarappan (2016) to improve the accuracy of estimating the effect of hydrolysis parameters on the mixing torque for single- and twin-screw electromechanical converters.

The found regularities of the distribution of surface parameters and characteristics of the electromagnetic field of the SEMC are confirmed by the results of the study by T.Y. Chen *et al.* (2017) create the basic conditions for the formation of the necessary modes of processing substances, substrates and the technological environment. A certain part of biopolymers does not have a strictly ordered crystal structure but has a dissipative fractal structure or a certain level of relative order, for example, the paramagnetic downy mass of birds. High molecular weight compounds, such as lignins and their substrates, have a structure of several interconnected levels.

The regularities of the distribution of eddy currents and components, of the electromagnetic field under variations in the length of the intermodule zone and the parameters of the helical winding require careful study. However, consideration of real processes of electromagnetic interaction with the medium, which include not only the processing of the technological environment utilizing electromagnetic disturbances, but also the processes of destruction of its structure, generation of its electromagnetic oscillations, and ion exchange, can be demonstrated in future work on metrologically and hardware-improved laboratory samples.

CONCLUSIONS

Using the proposed research methodology and the results of modelling and experimental studies, it was confirmed that the screw-type electromechanical converter can be considered as a source of multiphysical influence on the environment in the formation of technological operations for the processing of substances and technogenic waste. Depending on the loading mode of the SEMC, the technological environment can be represented in the following types: at idle (system warm-up mode) – air; at the main operating mode – a continuous heterogeneous environment using averaged characteristics (specific conductivity, magnetic and dielectric constant).

To consider the properties of the technological environment, it is proposed to introduce into the mathematical model vectors of electric induction and magnetic field intensity, which are different in content, and consider all the above currents, namely: eddy current; polarisation current of bound charges; free carrier current. To form an algorithm for the multiphysical influence on the technological environment, namely, the uniform distribution along the rotor surface of temperature, pressure, magnetic induction, and electric field strength, a method based on the numerical determination of the transverse and longitudinal edge effect of a common rotor for two stators of a SEMC using a combination of three-dimensional and two-dimensional finite element models is proposed. The regularities of the magnetic induction distribution on the outer surface of a ferromagnetic rotor at different azimuthal locations of the stator frontal parts are established. In the case of coordinated space and time magnetic fluxes of the frontal parts of adjacent stators, a certain uniformity of the temperature field distribution along the rotor length, including the intermodule zone, is achieved.

The electric field intensity on the rotor's outer surface reaches 0.8 V/m in areas corresponding to the location of the stator tooth crowns and depends on the current activity of the phases at the moment. Controlling the thermal and speed regime of the rotor makes it possible to create conditions for bioenergy stimulation on its surface in places of contact with the medium or to support the process of electrode heating of the technological medium. Further research will be devoted to the development of designs and control systems for industrial models of screw electromechanical units and energy-saving technologies based on them.

ACKNOWLEDGEMENTS

This work was supported by the Ministry of Education and Science of Ukraine (№ 0123U102165).

CONFLICT OF INTEREST

The authors declare no conflict of interest.

REFERENCES

[1] AC/DC module user's guide, COMSOL Inc. (2018). Retrieved from https://doc.comsol.com/5.4/doc/com.comsol.help.acdc/ACDCModuleUsersGuide.pdf.

[2] Bulgakov, V., Sevostianov, I., Kaletnik, G., Babyn, I., Ivanovs, S., Holovach, I., & Ihnatiev, Y. (2020). Theoretical studies of the vibration process of the dryer for waste of food. *Rural Sustainability Research*, 44(339), 32-45. doi: 10.2478/plua-2020-0015.

[3] Campuzano, F., Brown, C.R., & Martínez, J.D. (2019). Auger reactors for pyrolysis of biomass and wastes. *Renewable and Sustainable Energy Reviews*, 102, 372-409. doi: 10.1016/j.rser.2018.12.014.

[4] Chen, T.Y., Wang, B., Wu, Y.Y., Wen, J.L., Liu, C.F., Yuan, T.Q., & Sun, R.C. (2017). Structural variations of lignin macromolecule from different growth years of Triploid of *Populus tomentosa* Carr. *International Journal of Biological Macromolecules*, 101, 747-757. doi: 10.1016/j.ijbiomac.2017.03.146.

[5] Cistelecan, M.V., Ferreira, F.J., & Popescu, M. (2010). Three phase tooth-concentrated multiple-layer fractional windings with low space harmonic content. In *2010 IEEE Energy Conversion Congress and Exposition* (pp. 1399-1405). Atlanta: IEEE. doi: 10.1109/ECCE.2010.5618267.

[6] Feng, C., Li, Z., Wang, Z., Wang, B., & Wang, Z. (2019). Optimizing torque rheometry parameters for assessing the rheological characteristics and extrusion processability of wood plastic composites. *Journal of Thermoplastic Composite Materials*, 32(1), 123-140. doi: 10.1177/0892705717744828.

[7] Holik, P.J., Dorrell, D.G., & Popescu, M. (2007). Performance improvement of an external-rotor split-phase induction motor for low-cost drive applications using external rotor can. *IEEE Transactions on Magnetics*, 43(6), 2549-2551. doi: 10.1109/TMAG.2007.893304.

[8] Jagiela, M., & Garbiec, T. (2012). Determination of best rotor length in solid-rotor induction motor with axial slitting. *Archives of Electrical Engineering*, 61(2), 267-276. doi: 10.2478/v10171-012-0022-2.

[9] Kaplun, V., Makarevych, S., & Chuenko, R. (2022). Modelling of asynchronous motor with split stator windings on the principle of a rotary autotransformer. *Przeglad Elektrotechniczny*, 98(3). doi: 10.15199/48.2022.03.10.

[10] Laidoudi, A., Duchesne, S., Morganti, F., & Velu, G. (2020). High-power density induction machines with increased windings temperature. *Open Physics*, 18(1), 642-651. doi: 10.1515/phys-2020-0131.

[11] Mazlan, M.M., Talib, R.A., Mail, N.F., Taip, F.S., Chin. N.L., Sulaiman, R., Shukri, R., & Mohd Nor, M.Z. (2019). Effects of extrusion variables on corn-mango peel extrudates properties, torque and moisture loss. *International Journal of Food Properties*, 22, 54-70. doi: 10.1080/10942912.2019.1568458.

[12] Mellak, C., Deuringer, J., & Muetze, A. (2022). Impact of aspect ratios of solid rotor, large air gap induction motors on run-up time and energy input. *IEEE Transactions on Industry Applications*, 58(5), 6045-6056. doi: 10.1109/TIA.2022.3180030.

[13] Mushtruk, M., Gudzenko, M., Palamarchuk, I., Vasyliv, V., Slobodyanyuk, N., Kuts, A., Nychyk, O., Salavor, O., & Bober, A. (2020). Mathematical modeling of the oil extrusion process with pre-grinding of raw materials in a twin-screw extruder. *Potravinarstvo Slovak Journal of Food Sciences*, 14, 937-944. doi: 10.5219/1436.

[14] Rashchepkin, A.P., Karlov, O.M., & Kryshchuk, R.S. (2017). Structure of magnetic field of the axial arc-stator induction motor with solid bimetallic disc rotor. *Proceedings of the Institute of Electrodynamics of the National Academy of Sciences of Ukraine*, 47, 28-36.

[15] Singha, P., & Muthukumarappan, K. (2016). Effects of processing conditions on the system parameters during single screw extrusion of blend containing apple pomace. *Journal of Food Process Engineering*, 40(4), 1-11. doi: 10.1111/jfpe.12513.

[16] Smith, C.W. (2015). Electromagnetic and magnetic vector potential bio-information and water. *Homeopathy*, 104(4), 301-304. doi: 10.1016/j.homp.2015.08.006.

[17] Sundaram, V.M., & Toliyat, H.A. (2015). A fractional slot concentrated winding (FSCW) configuration for outer rotor squirrel cage induction motors. In *2015 IEEE International Electric Machines & Drives Conference* (pp. 20-26). USA: IEEE. doi: 10.1109/IEMDC.2015.7409031.

[18] Virlan, B., Benelghali, S., Simion, A., Livadaru, L., Outbib, R., & Munteanu, A. (2013). Induction motor with outer rotor and ring stator winding for multispeed applications. *IEEE Transactions on Energy Conversion*, 28(4), 999-1007. doi: 10.1109/tec.2013.2279841.

[19] Wasak, A., Drozd, R., Jankowiak, D., & Rakoczy, R. (2019). Rotating magnetic field as tool for enhancing enzymes properties-laccase case study. *Scientific Reports*, 9(1), 1-9. doi: 10.1038/s41598-019-39198-y.

[20] Wengerkievicz, C.A., Batistela, N.J., Sadowski, N., Huguet, T., & Lefèvre, Y. (2022). Experimental loss segregation in a solid rotor induction motor. *Journal of Microwaves, Optoelectronics and Electromagnetic Applications*, 21, 584-597. doi: 10.1590/2179-10742022v21i4268098.

[21] Wolnik, T., & Jarek, T. (2022). Solid rotor core vs. lamination rotor core in fractional-slot pmsm motor with high power density. *Energies*, 15(15), article number 5729. doi: 10.3390/en15155729.

[22] Zablodskiy, N., Chuenko, R., Gritsyuk, V., Kovalchuk, S., & Romanenko, O. (2021). The numerical analysis of electromechanical characteristics of twin-screw electromechanical hydrolyzer. *In 2021 11th International Conference on Advanced Computer Information Technologies (ACIT)* (pp. 130-135). Deggendorf: IEEE. doi: 10.1109/ACIT52158.2021.9548392.

[23] Zablodskiy, N., Pliugin, V., & Gritsyuk, V. (2014). Submersible electromechanical transformers for energy efficient technologies of oil extraction. In *Progressive technologies of coal, coaled methane, and ores mining* (pp. 223-227). Boca Raton: CRC Press.

Стефан Юнге
Доктор технічних наук, професор
Берлінський університет прикладних наук
13353, вул. Люксембурзька, 10, м. Берлін, Німеччина
https://orcid.org/0000-0002-8045-4103

Микола Миколайович Заблодський
Доктор технічних наук, професор
Національний університет біоресурсів і природокористування України
03041, вул. Героїв Оборони, 15, м. Київ, Україна
https://orcid.org/0000-0001-8889-8158

Наталія Анатолієвна Заєць
Доктор технічних наук, професор
Національний університет біоресурсів і природокористування України
03041, вул. Героїв Оборони, 15, м. Київ, Україна
https://orcid.org/0000-0001-5219-2081

Роман Миколайович Чуєнко
Кандидат технічних наук, доцент
Національний університет біоресурсів і природокористування України
03041, вул. Героїв Оборони, 15, м. Київ, Україна
https://orcid.org/0000-0002-9339-9764

Станіслав Ігорович Ковальчук
Аспірант
Національний університет біоресурсів і природокористування України
03041, вул. Героїв Оборони, 15, м. Київ, Україна
https://orcid.org/0000-0002-1194-3464

Електромеханічний перетворювач шнекового типу як джерело мультифізичного впливу на технологічне середовище

Анотація. При забезпечення надійності роботи електромеханічних перетворювачів у важких умовах, виникає проблема підвищення енергоефективності їх застосування шляхом структурної, функціональної і теплової інтеграції з технологічним середовищем. Тому метою дослідження було визначення умов безпосереднього мультифізичного впливу електромеханічного перетворювача шнекового типу на технологічне середовище. Застосовано метод, який заснований на чисельному визначенні в програмному середовищі Comsol Multiphysics характеристик шнекових електромеханічних перетворювачів з використанням комбінації тривимірних і двовимірних моделей кінцевих елементів, обмежених ротором з внесенням лопатей до розрахункової області. Досліджувались два варіанта формування алгоритму мультифізичного впливу на технологічне середовище: локальна концентрація впливу на певних ділянках ротора і рівномірний розподіл вздовж поверхні ротора температури, тиску, магнітної індукції, напруженості електричного поля. Встановлені закономірності розподілу магнітної індукції на зовнішній поверхні феромагнітного ротора при різному азимутальному розташуванні лобових частин суміжних статорів. Визначено розподіл нормальної складової щільності магнітного потоку при наявності контакта з технологічним середовищем у вигляді рутілового продукту або ільменітового концентрату. Споживана електрична енергія розподілена в зубцевій зоні статора та зоні проникнення електромагнітного поля в ротор. Вихрові струми сконцентровані на глибині проникнення від внутрішньої поверхні ротора, при цьому глибина проникнення залежить від теплового стану та режиму ковзання. Напруженість електричного поля на зовішній поверхні ротора досягає 0,8 V/m на відповідних до розташування коронок зубців статора ділянках і залежить від струмової активності фаз в даний момент. Регулювання температурного та швидкісного режиму ротора дає можливість на його поверхні в місцях контакту з середовищем створювати умови біоенергетичної стимуляції або підтримувати процес низькоамперного електролізу імпульсами невисокої напруги в тонкому шарі. Підтверджена адекватність математичних моделей, які були запропоновані для чисельного моделювання, експериментальним даним макетного зразка шнекового електромеханічного перетворювача, відхилення не перевищують 9,5%. Отримані результати дозволяють прогнозувати оптимальні показники електромагнітних та теплообмінних процесів у шнекових електромеханічних перетворювачах, пов'язаних з технологічним середовищем

Ключові слова: магнітна індукція; вихрові струми; температурне поле; електромагнітне поле; термограма; магнітна проникність

Machinery & Energetics
Vol. 14, No. 3. 2023

Journal homepage:
https://technicalscience.com.ua/en

UDC 519.23
DOI: 10.31548/machinery/3.2023.47

Victor Melnik*
Doctor of Technical Sciences, Professor
State Biotechnological University
61002, 44 Alchevskikh Str., Kharkiv, Ukraine
https://orcid.org/0000-0002-1176-2831

Alexei Zelensky
Postgraduate Student
State Biotechnological University
61002, 44 Alchevskikh Str., Kharkiv, Ukraine
https://orcid.org/0000-0001-9819-9086

Andrew Zelensky
Postgraduate Student
State Biotechnological University
61002, 44 Alchevskikh Str., Kharkiv, Ukraine
https://orcid.org/0000-0002-0364-5571

Design of centrifugal radial fans using regression analysis methods

Abstract. With the development of scientific and technological progress in agriculture, the use of operational and mathematical modelling for effective solution of problems and resource conservation in the field of agricultural engineering is relevant. Therefore, the purpose of the study was to determine the optimal parameters of the centrifugal radial fan of a pneumatic precision seed drill by constructing a new mathematical model of the process of its operation. This was achieved by applying mathematical modelling methods when planning multi-factor experiments. As a result, a complex of automated experiments has been defined, which leads to a significant increase in the productivity of scientific work. A statistical representation of the experiment is established, which allows moving to a multi-factor active experiment, in which it is possible to separate the influence of factors from the noise background and make a transition to statistical methods for analysing the results. This allowed predicting the optimal characteristics of the centrifugal radial fan of the precision seed drill. In the course of this study, a new regression equation was compiled in the form of a first-degree polynomial, which determines the influence of each of the factors on the magnitude and value of the response. The coefficients of the polynomial are determined, the significance of the coefficients is estimated, and the adequacy of the proposed model is checked. After obtaining the regression equation, it became possible to graphically construct the dependence of the response function on impact factors. A fractional factor experiment was also performed, which determined the values of the parameters of the object's state Y for all possible combinations of levels of variation of the factors X_i. Based on the established functional relationship between the output parameter of the fan, a regression equation of the following form is obtained: $P_v = P_v(n, \beta_1, \beta_2, z)$. This predicted the receipt of the total pressure P_v(Pa), when setting different values of independent quantities n, β_1, β_2 and z. The application of the obtained analytical dependencies significantly simplified the determination of optimal design parameters of pneumatic systems for the development and construction of modern technical seed drills

Keywords: mathematical model; multi-factor process; pressure; frequency of rotational motion; installation angles; number of blades

Article's History: Received: 22.03.2023; Revised: 23.06.2023; Accepted: 11.08.2023.

Suggested Citation:
Melnik, V., Zelensky, A., & Zelensky, A. (2023). Design of centrifugal radial fans using regression analysis methods. *Machinery & Energetics,* 14(3), 47-60. doi: 10.31548/machinery/3.2023.47.

*Corresponding author

INTRODUCTION

Improving agricultural products and optimising the use of resources is an urgent issue. Pneumatic seed drill systems, in particular fans, play an important role in the sowing process, affecting seed distribution and crop cultivation. Optimisation of their operation involves selecting the optimal geometric parameters of various system components, including the impeller, stator, pipes, and other elements. D.C. Montgomery *et al*. (2023) define a model as an artificial system that reflects, with a certain degree of accuracy, the main properties of the object under study – the original. The model is in a certain correspondence with the object under study can replace it during research, and allows getting information about it. The paper notes that when studying an object, two problems are set: extreme and interpolation. When solving an extreme problem, the conditions of the process are determined to ensure that the optimal value of the selected parameter is obtained (the existence of an extremum of a certain function). When studying a multi-factor process, setting up all possible experiments to obtain a mathematical model is associated with a huge complexity of the experiment, since the number of all possible experiments is large.

Methods of mathematical planning of an experiment allow simultaneously considering the influence of several factors on the object under study. They are based on the mathematical theory of the experiment, which determines the conditions for optimal behaviour of the object under study, including incomplete knowledge of the physical essence of the phenomenon. Mathematical methods of experiment planning allow considering and optimising complex systems and processes, ensuring high efficiency of the experiment and accuracy in determining the factors under study. These methods were used by such researchers as J. Frost (2020), who made significant contributions to the interpretation of experimental results and verification of the correctness of initial prerequisites, planning techniques in laboratory and industrial settings, as well as block planning in the methodology for building scientific research.

F. Tanzim *et al*. (2022) present the developed model for predicting the width of the fan used in the sprayer. The researchers developed a complete factor experiment with a broad analysis of factors affecting the dynamic sputtering index. Based on this, a linear regression model was obtained to calculate the fan width, which varies within 2.5 cm to maintain the production tolerance. The model was tested statistically and experimentally so that it could eliminate trial and error to save time and money. However, the technical parameters of the working bodies that perform this technological process are not considered. Effectiveness is evaluated only by the final result, and therefore, research and the suggestion of broad boundaries are rather questionable here.

Y. Wang *et al*. (2022) applied the Fourier random feature method to detect nonlinear relationships between data samples. In addition, when studying the regression coefficient matrix, the low-rank components of this explicit feature space are simultaneously extracted to reduce the redundancy effect. It is also not possible to use this method to study the optimal parameters of technical systems. The possibility of introducing an appropriate surrogate model for modelling objective functions, subject to its solution, was presented by V.T. Nadikto (2019), S. Nitri Asomani *et al*. (2020). In this study, a sampling method was used to obtain the values of the objective function, and an artificial neural network and a generalised regression neural network were used as surrogate models for approximating the objective function in the design space. This study has all the features of modern analytical research, but it will be quite difficult to optimise the parameters of any technical system using a surrogate model.

And only in the paper by X. Ping *et al*. (2021), based on experimental studies, theoretical analysis, and machine experiments, a controlled model for predicting isoentropic efficiency for a multi-stage centrifugal pump is constructed. The S-fold cross-validation algorithm is used to improve model data analysis and control capabilities. In addition, the accuracy of model prediction is improved by smoothing coefficient circulation screening technology. Based on this, the prediction accuracy of the optimised model and the unoptimised model is determined. Thus, the results of the study presented in this paper can be partially applied to the analytical study of centrifugal fans.

Thus, a brief analysis of literature sources indicates the widespread use of methods for constructing mathematical models that work based on random processes and the use of correlation analysis in the study of complex technical systems. The purpose of the study was to obtain by constructing a new mathematical model of a computational experiment to determine the optimal parameters of the studied workflow carried out by a centrifugal radial fan.

To build a new mathematical model of the fan, it was necessary: to determine the design and analyse the operation of the pneumatic system of the seed drill, in particular the fan; to substantiate the choice of the most influential input factors and the most significant output variables of the experiment; to make a choice of the mathematical model by which experimental data will be provided; to substantiate the choice of the optimality criterion; to substantiate the choice of the experiment plan; to conduct an experiment and process the results; to analyse the work performed.

MATERIALS AND METHODS

An experimental factor mathematical model was used to optimise the parameters. The experimental factor mathematical model, unlike the theoretical ones, is not based on physical laws describing the processes that occur in objects, but represents some formal dependences of the initial parameters on the internal and external parameters of design objects (Nadikto, 2019).

When constructing the experimental factor model, the technical system that was designed was presented in the

form of a cybernetic system, the so-called "black box" system (Fig. 1), which was fed with some vectors $X=(X_1, X_2, .., X_k)$ and $W=(W_1, W_2, .., W_l)$ of independent values, and variable values were observed and recorded at the output $y_1, y_2, ..., y_m$ of vector components $Y=(Y_1, Y_2, .., Y_m)$ of dependent values, where k, l, m – number of elements, respectively, of vectors X, W and Y.

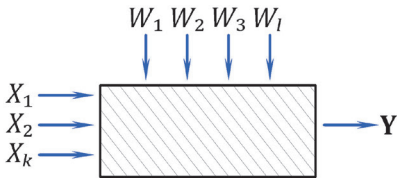

Figure 1. "Black box" system
Source: H. Beloev *et al*. (2021)

During experiments, changes in the values of $x_1, x_2, ..., x_k$ and $W_1, W_2, ..., W_l$ of the quantities X_α, ($\alpha = 1, 2, ..., k$) and W_β, ($\beta = 1, 2, ..., l$) led to a change in the original dependent values $y_1, y^2, ..., y_m$ of components Y_γ, ($\gamma = 1, 2, ..., m$) of vector Y. To build a factor model, these changes were recorded and their necessary statistical processing was performed to determine the model parameters.

During a physical experiment with variables X_α, it was possible to control them by changing their values x_α according to the specified law. Variables W_β, – unmanaged ones that acquired random values W_β. Values x_α and W_β of variables X_α and W_β, can be monitored and registered. Variables X_α, ($\alpha = 1, 2, ..., k$) are actually controlled manageable factors, and the parameters W_β, ($\beta = 1, 2, ..., l$) are controlled unmanageable factors. Factors X_α are controlled and changed as deterministic variables, factors W_β, – unmanageable and randomly changed over time. Space of controlled variable factors X_α, ($\alpha = 1, 2, ..., k$) and uncontrolled W_β, ($\beta = 1, 2, ..., l$) created a factor space as a result of the study (Arkes, 2023).

Output vector Y was a vector of dependent variables of the modelled object, i.e., it is a vector of response functions. Dependency of each component Y_γ, ($\gamma = 1, 2, ..., m$) vector Y from factors X_α, ($\alpha = 1, 2, ..., k$) and W_β, ($\beta = 1, 2, ..., l$) was a response function. The geometric representation of the response function in this paper forms the response surface. Accordingly, the number of response functions was equal to the number of vector components Y.

In computational experiments, the object of this research was a theoretical mathematical model, based on which it is necessary to obtain an experimental factor model. To determine it, the type of mathematical relations between factors X_α, W_β and a review Y_γ were determined, and numerical parameter values were set. Here, the parameters are coefficients of the equations of the factor model. The problems of determining model parameters were fully formalised and solved by regression analysis methods.

To obtain an adequate mathematical model, certain experimental conditions were met. It was assumed that the model will then be adequate, due to the fact that in a reasonable interval of variation of factors X_α, ($\alpha = 1, 2, ..., k$) obtained using the value model y_γ, response functions Y_γ, ($\gamma = 1, 2, ..., m$) differ from the true ones by no more than a given amount. The purpose of planning the experiment was also to obtain maximum information about the properties of the object under study with a minimum of experiments (time and resources spent).

In addition, the following provisions were immediately noted: a complete picture of the properties of the response surface can only be obtained if a dense discrete grid of factor values is used, covering the entire factor space. The choice of the structure of the factor model is based on postulating a certain degree of smoothness of the response surface. Therefore, to reduce the number of experiments, a small number of points of the plan were taken, according to which the implementation of the experiment is carried out.

However, the sets $\{y_1\}, \{y_2\}, ..., \{y_m\}$ of values of response functions Y_γ, ($\gamma = 1, 2, ..., m$) in experiments conducted at one point of the plan (with fixed values $x_1, x_2, ..., x_k$ factors X_α, ($\alpha = 1, 2, ..., k$), with a large level of random disturbances, can have large discrepancies. Therefore, the lower the perturbation level, the more accurate the factor model is. In other words, $y_1, y_2, ..., y_m$ is not the same as Y_α, ($\alpha = 1, 2, ..., m$). Value $w_1, w_2, ..., w_l$ ov unmanaged parameters W_β, ($\beta = 1, 2, ..., l$) are inherently random. So for fixed values $x_1, x_2, ..., x_k$ due to variation $w_1, w_2, ..., w_l$ in each repetition of the experiment, it is possible to get different values $y_1, y_2, ..., y_m$ of response functions Y_γ, ($\gamma = 1, 2, ..., m$). That is, a fixed set of parameters $\{x_\alpha\}$, ($\alpha = 1, 2, ..., k$) will correspond to two sets of sets $\{w_1\}, \{w_2,\} ..., \{w_l\}$ and $\{y_1\}, \{y_2\}, ..., \{y_m\}$, where the number of elements in each set $\{w_\beta\}$ and $\{y_\gamma\}$ is equal to the number of repeatability of the experiment.

Here, separately, it was necessary to focus on the features of computational and full-scale experiments. Unmanaged parameters in a field experiment W_β, ($\beta = 1, 2, ..., l$) change in accordance with objective processes, and therefore, at the same fixed values of input factors $\{x_\alpha\}$, ($\alpha = 1, 2, ..., k$) in each new repetition of the experiment, a new unique set of values $\{w_\beta\}$ and $\{y_\gamma\}$ will be obtained. Moreover, there are two possible options in a computational experiment. The first option is implemented if, first, the values of $\{w_\beta\}$ are justified in a certain way and always remain fixed, and, secondly, the algorithm of the computational experiment itself is completely deterministic and does not contain a pseudo-random component. In this case, the repetition of the experiment did not make sense, because the random component was completely excluded. The second option was implemented when at least one condition was met, or an algorithm of a computational experiment containing a pseudo-random component or values $\{w_\beta\}$ are modelled in a pseudo-random way. In this case, the second option was implemented, although the specifics of applying methods of mathematical modelling of random variables were not considered separately.

Further, these provisions of the improved methodology were implemented for their further application in solving a specific problem. First of all, in the general case, it can

be argued that there is a functional relationship between independent variables and the output of the process of the following type:

$$(Y\gamma = f(X, W), (\gamma = 1, 2, ..., m). \quad (1)$$

The least squares method was used to solve this problem (to approximate experimental data). This method allows constructing an optimal estimate of the moments of the distribution of the experimental error in a certain sense and solving the question of whether the resulting model is adequate (i.e., one that properly corresponds to reality).

Since the study introduced restrictions in the context of searching for only one response function $Y \in \{Y_\gamma\}$ from the full set of functions $\{Y_\gamma\}$, $(\gamma = 1, 2, ..., m)$ vector components Y, and given that the parameters W_β, $(\beta = 1, 2, ..., l)$ are not manageable and, moreover, it was not planned to fix them, it became possible to further simplify the idea of functional dependence (1) to the following form:

$$Y = f(X). \quad (2)$$

Thus, the number of objective functions was limited to one and a limit was introduced on the number of parameters that were considered and, accordingly, included in the mathematical model that was planned to be obtained.

A mathematical model of the process was constructed from experimental data. The process of determining the explicit type of regression equation is called regression analysis. For different mathematical plans of the experiment, regression equations may contain different components. Namely:

1) for first-order plans, the regression equation includes effects and paired interactions:

$$y = b_0 + \sum_{i=1}^{k} b_i x_i + \sum_{i=1}^{k-1} \sum_{j=i+1}^{k} b_{ij} x_i x_j, \quad i, j = 1,2, ..., k, \quad i < j, \quad (3)$$

2) for second-order plans, the regression equation includes effects, pairwise interactions, and quadratic effects:

$$y = b_0 + \sum_{i=1}^{k} b_i x_i + \sum_{i=1}^{k} \sum_{j=i}^{k} b_{ij} x_i x_j, \quad i, j = 1,2, ..., k, \quad i \le j, \quad (4)$$

where b_0 – free term of the regression equation; b_i, b_{ij} – coefficients of the regression equation; x_i – value of factors; k – now and in the future, in accordance with the Pareto principle, this is the number of significant controlled manageable factors considered during the experiment, which is less than the total number of controlled manageable factors, according to the previous definition k.

The resulting expressions (3) and (4) were analysed. Thus, coefficients for independent variables indicate the strength of the influence of factors. The larger the numerical value of the coefficient, the more the factor affects. If the coefficient has a plus sign, then the optimisation parameter increases as the factor value increases, and if it is negative, then, on the contrary, it decreases. The value of the coefficient corresponds to the contribution of this factor to the value of the optimisation parameter when the factor moves from zero to the upper or lower level. Sometimes it is convenient to evaluate the contribution of a factor during the transition from the lower to the upper level. The contribution defined in this way is the effect of a factor and is sometimes referred to as the main or main effect.

RESULTS AND DISCUSSION

Initially, a physical model of the impeller of a centrifugal radial fan was built, which has an outer diameter of 400 mm, the inner diameter of the impeller air inlet – 135 mm, and the width of the impeller itself – 35 mm. The direction of rotational movement with the angular speed of the impeller is shown by an arrow. The blades of the impeller itself have a curved shape, which is regulated by the angles at the inlet and outlet of the blade. These angles were measured between two tangent lines: the first – to the contour of the blade, and the second – to the circle of rotation. Figure 2 shows the angles, respectively, at the input, which is 70° and the output is equal to 140°. The thickness of the blades was 1 mm. In the future, in the process of constructing a regression model of a centrifugal radial fan, the angles of installation of the impeller blades, the number of blades installed on it, and the speed of rotational motion were supposed to change.

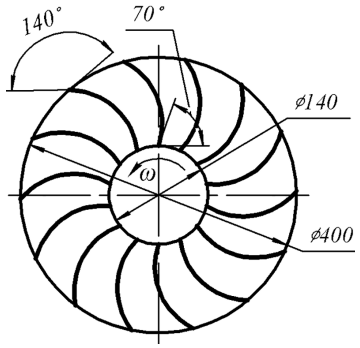

Figure 2. Centrifugal radial fan impeller
Source: compiled by the authors

Next, a mathematical model of the fan impeller was constructed. According to the above method, the following factors were selected as independent variables to investigate the operation process and the dependence of the geometric parameters of a centrifugal radial fan: X_1 – fan impeller rotation frequency, rpm; X_2 – blade installation angle at the impeller inlet, deg.; X_3 – blade installation angle at the impeller outlet, deg; X_4 – number of impeller blades, pcs.

Now, when considering the operation of a centrifugal radial fan, the influence of many factors $\{X_\alpha\}$, $(\alpha = 1, 2, ..., k)$ on the response function Y was first analysed (2). The Box-Wilson method was chosen to solve this optimisation problem. Among the plans of an extreme experiment, the simplest is the plan of a complete factor experiment, the implementation of which determines the value of the response function Y for all possible combinations of levels of variation of factors X_i, $(i = 1, 2, ..., k)$. First, the number of experiments that needed to be conducted in order to carry out a pilaf factor experiment was determined. It is equal to:

$$N = 2^k = 2^4 = 16, \quad (5)$$

where k – the number of experimental factors that are considered in the developed model, 2 – the number of levels.

Two values were set for each factor: maximum and minimum. In this value field, each factor can change continuously or discretely. The boundaries of factor values form a region in a multidimensional space – a hypercube, i.e., the value x_i of factors X_i lie inside this area. For the convenience of processing the results of the study, coding of independent input factors was introduced X_i:

$$x_i = \frac{x_i - x_i^{(0)}}{\Delta x_i}, \ i = 1, 2, \ldots, k, \quad (6)$$

where $X_i^{(0)}$ – basic level.

$$X_i^{(0)} = 0.5(X_i^{\min} + X_i^{\max}), \ i = 1, 2, \ldots, k, \quad (7)$$

where $X_i^{\min}$ and $X_i^{\max}$ – the lower and upper values of the input factors of the experiment; ΔX_i – variation interval of i-th factor:

$$\Delta X_i = \frac{X_i^{\max} - X_i^{\min}}{2}, \ i = 1, 2, \ldots, k. \quad (8)$$

Variation interval ΔX_i of input factors X_i was selected within 0.05...0.3 of the possible range of variation of the i-th factor. In encoded form, the value of factors x_i acquire normalised values: +1 or –1. It is established that in order to build a response surface, it is necessary to conduct N (5) experiments. For the convenience of planning the experiment, it was necessary to draw up a plan and a planning matrix for the four-factor experiment in accordance with which the research was conducted.

At the beginning, a detailed study of the process was not required, and the local area of the experiment around the main level was used as a start for moving to the extremum region. Therefore, initially, instead of a complete factor experiment, a fractional factor experiment was used. Using a fractional factor experiment, the linear terms of the regression equation were estimated. The plan of a fractional factor experiment is actually a fractional replica of a complete factor experiment. The number of experiments that needed to be performed for semi-replicas was determined using the following expression:

$$N = 2^{k-p} = 2^{4-1} = 8, \quad (9)$$

where p – number of linear effects. Thus, the number of experiments is reduced by half compared to the full factor experiment, according to calculations based on expression (5).

To obtain a linear model, it was recommended to choose fractional replicas with a higher resolution, i.e., replicas that have linear effects mixed with interaction effects close to zero. When choosing a fractional replica, it is important to consider the saturation of the plan, that is, the ratio between the number of experiments and the number of coefficients that are determined based on the results of these experiments. The number of experiments in the matrix of a saturated fractional replica is equal to the number of coefficients of the linear model. Next, a semi-replicas of the fractional factor experiment type 2^{4-1} with a generating ratio $x_4 = x_1x_2x_3$ was used. Then the defining contrast and the corresponding score were given by the following relations:

$$\begin{aligned} 1 &= x_1x_2x_3x_4, & x_1 &= x_2x_3x_4, \\ x_2 &= x_1x_3x_4, & x_3 &= x_1x_2x_4, \\ x_4 &= x_1x_2x_3, & x_1x_2 &= x_3x_4, \\ x_1x_3 &= x_2x_4, & x_1x_4 &= x_2x_3. \end{aligned} \quad (10)$$

This planning provided a rating system of this type:

$$\begin{aligned} b_1 &\to \beta_1 + \beta_{234}, & b_2 &\to \beta_2 + \beta_{134}, \\ b_3 &\to \beta_3 + \beta_{124}, & b_4 &\to \beta_4 + \beta_{123}, \\ b_{12} &\to \beta_{12} + \beta_{34}, & b_{13} &\to \beta_{13} + \beta_{24}, \\ & & b_{14} &\to \beta_{14} + \beta_{23}, \end{aligned} \quad (11)$$

where the sample coefficients of the process model parameters b_1, b_2, b_3, b_4, b_{12}, b_{13} and b_{14} are only estimates for theoretical coefficients $\beta_1, \beta_2, \beta_3, \beta_4, \beta_{12}, \beta_{13}, \beta_{14}, \beta_{123}, \beta_{124}, \beta_{134}, \beta_{23}, \beta_{24}, \beta_{234}, \beta_{34}$, which are the mathematical expectation for the relevant factors.

Triple and higher-order interactions are much more likely than double interactions to be zero, and they are usually ignored, respectively. The semi-replication of the type 2^{4-1}, defined by the generating relation $x_4 = x_1x_2x_3$, allowed obtaining separate estimates of four linear effects and three joint estimates of paired interactions. Separate estimates are b_1, b_2, b_3, and b_4, and triple interactions – β_{234}, β_{134}, β_{124} and β_{123} are neglected due to their insignificance. In the future, such a replica will be designated as for a fractional factor experiment 2^{4-1}_{IV}.

The initial conditions of the experiment were established and, accordingly, the intervals of variation of independent variables (input factors) were set (Table 1), which were used to determine the transition from natural variables X_1, X_2, X_3 and X_4 to code variables x_1, x_2, x_3, and x_4, which were accepted at the ends of the value intervals +1 or –1.

Table 1. Intervals of variation of independent variables, initial conditions of the experiment

Name and designation of values		Controlled parameters (factors): actual and encoded value							
		X_1	x_1	X_2	x_2	X_3	x_3	X_4	x_4
Variation interval	ΔX_i	350	–	20	–	30	–	6	–
Upper level	$X_i^{\max}$	5,350	1	70	1	140	1	26	1

Continued Table 1.

Name and designation of values		Controlled parameters (factors): actual and encoded value							
		X_1	x_1	X_2	x_2	X_3	x_3	X_4	x_4
Main level	$X_i^{(0)}$	5,000	0	50	0	110	0	20	0
Lower level	$X_i^{\min}$	4,650	−1	30	−1	80	−1	14	−1

Source: compiled by the authors

After selecting the experiment plan, the main levels and intervals of varying factors, the transition to the experiment was made. Each row of the matrix is an experimental condition. To avoid systematic errors, it is recommended to conduct experiments provided for by the matrix in a random sequence. The procedure for conducting experiments should be selected from the table of evenly distributed random numbers. In general, experiments are recommended to be conducted randomly. However, to reduce the time spent on conducting experiments, they are sometimes grouped, that is, several experiments are performed simultaneously. Conditions for conducting experiments (experiment plan) for a fractional factor experiment $2_{4\text{-}1IV}$ are shown in Table 2. In this table, according to the sequence of experiments u, combinations of factors are ordered at two levels.

Table 2. Conditions for performing a fractional factor experiment $2^{4\text{-}1}_{IV}$ – combinations of factor values (encoded and actual) for all experiments

u	x_1	X_1	x_2	X_2	x_3	X_3	x_4	X_4
1	−1	4.650	−1	30	1	140	1	26
2	1	5.350	−1	30	1	140	−1	14
3	−1	4.650	1	70	1	140	−1	14
4	1	5.350	1	70	1	140	1	26
5	−1	4.650	−1	30	−1	80	−1	14
6	1	5.350	−1	30	−1	80	1	26
7	−1	4.650	1	70	−1	80	1	26
8	1	5.350	1	70	−1	80	−1	14

Source: compiled by the authors

The results of the experiments are shown in Table 3, where y_{u1}, y_{u2}, y_{u3} and y_{u4} – value of the response function Y (2) for $n = 4$ repetitions of experiments (parallel observations) in each u-th point in the experiment planning matrix; $\bar{y}_u$ – average value of the response function (optimisation parameter) for the experiment by number u; $\sigma_2\{y_u\}$ – sample variance for the experiment by number u, which is calculated using the equation:

$$\sigma^2\{y_u\} = \frac{1}{(n-1)} \sum_{i=1}^{n} (\bar{y}_u - y_{ui})^2. \qquad (12)$$

Table 3. Results of the fractional factor experiment $2^{4\text{-}1}_{IV}$

u	y_{u1}	y_{u2}	y_{u3}	y_{u4}	$\bar{y}_u$	$\sigma^2\{y_u\}$
1	10.020	10.060	10.780	10.920	10.445	222.233
2	12.860	12.390	12.270	11.980	12.375	134.167
3	10.160	10.530	10.240	10.650	10.395	54.166.7
4	13.350	14.030	14.160	14.420	13.990	208.333
5	9.730	9.279	9.089	8.970	9.260.25	103.317
6	12.900	12.530	12.440	12.100	12.492.5	108.092
7	8.588	8.276	8.190	7.986	8.260	62.605.3
8	13.290	13.770	13.920	14.020	13.750	104.600
					Σ→	997.514
					max→	222.233

Note: Σ – the sum of sample variance values for all experiments; max – the maximum value of the sample variance
Source: compiled by the authors

Values $\sigma^2\{y_u\}$ were calculated for all points of the matrix plan, and the calculation results were entered in Table 3. Since the number of repetitions of experiments (parallel observations) in each u-th point in the matrix, the planning of the experiment is the same and equal to n, then the uniformity of variance at each level of factors can be checked by the Cochrane criterion. To do this, it was necessary to compare the calculated value G^a of the Cochrane

criterion with its tabular value G^b, which is found from the reference table for known values of the total variance value N and the number of degrees of freedom. If the following condition:

$$G^a < G^b, \quad (13)$$

is performed, then there are grounds to assert that the variances are homogeneous and, accordingly, the experiments are reproducible. The calculated value G^a of the Cochrane criterion was calculated by the formula:

$$G^a = \frac{\max\{\sigma^2\{y_u\}\}}{\sum_{u=1}^{N}\sigma^2\{y_u\}}, \quad (14)$$

where N – total number of points in the plan of the experiment matrix ($u = 1, 2, \ldots, N$); max $\{\sigma^2\{y_u\}\}$ – maximum value of the sample variance from the set N of experiments; $\sum_{u=1}^{N}\sigma^2\{y_u\}$ – sum of sample variances for N experiments. As a result, the following numeric value G^a of the Cochrane criterion was obtained:

$$G^a = 0.22279. \quad (15)$$

Tabular value G^b could also be approximated by the Fischer distribution. To determine the tabular value G^b of the Cochrane criterion, p level of significance was initially selected. The following value is obtained:

$$p = 0.05 \quad 16)$$

and the calculated number of degrees of freedom f has the following value:

$$f = n - 1 = 3. \quad (17)$$

Further, considering that the number of experiments (points in the plan of the experiment matrix) is:

$$N = 8, \quad (18)$$

the corresponding value G^b of the Cochrane criterion was calculated or selected from the reference table:

$$G^b = G(p; f; N) = 0.43075. \quad (19)$$

Given the value G^a, according to expression (15) and G^b according to expression (19), it was found that the condition $G^a < G^b$ according to expression (13) is fulfilled, which means that there is every reason to assert that the variances are homogeneous and, accordingly, the experiments are reproducible. Further, according to Table 3, the overall average variance was determined, that is, the variance of the reproducibility of the experiment:

$$\sigma^2\{\bar{y}\} = \frac{1}{N}\sum_{u=1}^{N}\sigma^2\{y_u\} = 124{,}689. \quad (20)$$

The error of the experiment (root-mean-square deviation) was determined as follows:

$$\sigma^2\{\bar{y}\} = \frac{1}{N}\sum_{u=1}^{N}\sigma^2\{y_u\} = 124{,}689. \quad (21)$$

The coefficients of the desired regression equation (4) were calculated using the following equations:

$$b_0 = \frac{1}{N}\sum_{u=1}^{N}\bar{y}_u, \quad (22)$$

$$b_i = \frac{1}{N}\sum_{u=1}^{N}\bar{y}_u x_i, \ i = 1, 2, 3, 4, \quad (23)$$

$$b_{1i} = \frac{1}{N}\sum_{u=1}^{N}\bar{y}_u x_1 x_i, \ i = 2, 3, 4, \quad (24)$$

where x_i – encoded values of experimental factors.
The calculation results are shown in Table 4.

Table 4. Calculated values of the coefficients of the regression equation, according to expression (4)

b_i	Value	b_i	Value
b_0	11,370.97	b_4	–74.09
b_1	1,780.91	b_{12}	490.34
b_2	227.78	b_{13}	–390.66
b_3	430.28	b_{14}	163.47

Source: compiled by the authors

Further, it was defined that: $\sigma^2\{b_i\}$ – variance of the regression coefficient error b_i provided that ($i = 0, 1, \ldots, 14$), and also considering that the number of experiments n (number of repetitions) at all points of the plan of the experiment matrix are the same and are equal to:

$$\sigma^2\{b_i\} = \frac{\sigma^2\{\bar{y}\}}{Nn} = 3{,}896.54. \quad (25)$$

Standard deviation $\sigma\{b_i\}$ of the error variance of regression coefficient b_i was determined by the equation:

$$\sigma\{b_i\} = \sqrt{\frac{\sigma^2\{b_i\}}{Nn}} = 62.42, \quad (26)$$

calculated value of the root-mean-square deviation of the variance $\sigma\{b_i\}$ is the same applies to all regression coefficients.

The significance of the regression coefficients was determined using t^b – the Student's tabular t-test and its value is compared with the calculated value t^a. Values were calculated for each regression coefficient t^a using equation:

$$t_i^a = \frac{|b_i|}{\sigma\{b_i\}}, \ i = 0, 1, \ldots, 4, 12, 13, 14, \quad (27)$$

where $|b_i|$ – calculated values of the regression coefficient (Table 4), which were taken modulo; $\sigma\{b_i\}$ – root-mean-square deviation of the variance of regression coefficients.

Tabular t^b value of the Student's t-test for the level of significance $q = 5\%$ and the degrees of freedom were determined using the following expression:

$$f_{St} = N(n-1) = 24, \quad (28)$$

next: $t^b = 2.1199$. For each regression coefficient, the values t^a were determined and compared to t^b. It was found that if the calculated value is $t^a > t^b$, then the regression coefficient is statistically significant and can be used in the future calculations. If the calculated value is $t^a < t^b$, then the regression coefficient is statistically insignificant and is discarded without recalculating other coefficients. Calculated values t^a of the regression coefficients according to expression (27) were entered in Table 5.

Table 5. Calculated values t^a

t_i^a	Value	t_i^a	Value
t_0^a	182.162	t_4^a	1.18698
t_1^a	28.53	t_{12}^a	7.85527
t_2^a	3.649	t_{13}^a	6.40246
t_3^a	6.89307	t_{14}^a	2.61876

Source: compiled by the authors

From the data in Table 5, it can be seen that all calculated values of the regression coefficient t_i^a, except for t_4^a, are significant. Instead, $t_4^a = 1.18698$ is an insignificant, and therefore, corresponding term $b_4 x_4$ in equation (4) was ignored. Statistical insignificance of the regression coefficient b_i can be caused by the following factors:

1) factor variation interval ΔX_i is selected small;

2) main level of the factor X_{0i} is close to the point of partial extremum;

3) big error of the experiment due to unaccounted factors;

4) there is no connection of factors with the initial value $\bar{y}_u$.

Interpretation of the regression equation is important both for understanding the process and for making decisions during optimisation. A special case occurs when using saturated plans. With the significance of all regression coefficients, nothing can be said about the adequacy or inadequacy of the model. A function whose coefficient values do not differ significantly is called symmetric with respect to the coefficients. However, it should be noted that a successful choice of variation intervals can make any linear function symmetric for significant factors. But at the first stage of planning, it is not always possible to get a symmetric function. If the function is sharply asymmetric (the coefficients differ by an order of magnitude), then it is more profitable to run the experiment again, changing the variation intervals, rather than moving along a gradient. As a result of the conducted research, the regression equation is further obtained in the form of a polynomial of the following form:

$$\hat{Y} = 11{,}370.97 + 1{,}780.91 \cdot 1 + 227.78 \cdot x_2 + \\ + 430.28 \cdot x_3 + 490.34 \cdot x_1 x_2 - 399.66 \cdot x_1 \cdot x_3 + \\ + 163.47 \cdot x_1 \cdot x_4, \quad (29)$$

where $\hat{Y}$ – mathematical expectation of the optimisation parameter indicator; x_1, x_2, x_3, and x_4 – process factors that were studied. The mathematical model obtained has the form of a first-degree polynomial (29) (Kononyuk, 2010). The coefficients of the polynomial, according to expression (29), are known. Next, the adequacy of the model was checked in accordance with the obtained regression equation according to the form of expression (29). For this purpose, the variance of the adequacy of the model was determined using the following equation:

$$s_{ag}^2 = \frac{n}{N-l} \sum_{u=1}^{N} (\bar{y}_u - \hat{y}_u)^2 = 326{,}594.47, \quad (30)$$

where N – total number of points in the plan of the experiment matrix; l – number of significant coefficients; $\bar{y}_u$ – arithmetic mean with n experiments (Table 3) at the point with the number ($u = 1, 2, ..., N$); $\hat{y}_u$ – the mathematical expectation of the optimisation parameter calculated by the regression equation according to expression (29).

The adequacy of the model was checked by comparing the calculated value F^a of Fischer's criterion with a tabular value F^b according to this equation (Kononyuk, 2010):

$$F^a < F^b(f_1; f_2), \quad (31)$$

where f_1 and f_2 – degrees of freedom. Further, the degrees of freedom were determined using the following expressions:

$$f_1 = N - l = 1, \quad (32)$$

$$f_2 = N(n-1) = 24. \quad (33)$$

Calculated value F^a and tabular value F^b of the Fischer criterion, respectively:

$$F^a = 2.619267. \quad F^b = 4.259677. \quad (34)$$

As can be seen from the numeric values of expressions (34) calculated value of the Fischer criterion F^a turned out to be less than the tabular value F^b and, accordingly, the hypothesis of adequacy of the model according to expression (29) is accepted. After substituting expressions (6) into equation (29), the return to natural variables X_i was made, and the obtained regression equation in explicit (decoded) form, which has such a relationship between the factors:

$$Y = -11{,}817.78 + 4.21 \cdot X_1 - 338.61 \cdot X_2 + 204.34 \cdot X_3 - 390 \cdot X_4 + \\ + 0.07 \cdot X_1 \cdot X_2 - 0.038 \cdot X_1 \cdot X_3 + 0.078 \cdot X_1 \cdot X_4. \quad (35)$$

The regression equation (35) was rewritten, considering that: Y corresponds to the pressure generated by the fan P_v(Pa); X_1 – fan impeller rotation frequency n (rpm); X_2 – blade installation angle at the impeller inlet β_1 (deg.); X_3 – blade installation angle at the impeller outlet β_2 (deg.); X_4 – number of impeller blades z (pcs). As a result, the following equation was obtained:

$$P_v = -11{,}817.78 + 4.21 \cdot n - 338.61 \cdot \beta_1 + 204.34 \cdot \\ \cdot \beta_2 - 390 \cdot z + 0.07 \cdot n \cdot \beta_1 - 0.038 \cdot n\beta_2 + 0.078 \cdot n \cdot z. \quad (36)$$

Further, it was established to what extent each of the factors n, β_1, β_2 and z affects the pressure generated by the centrifugal radial fan P_v. The value of each coefficient in equation (36) is a quantitative measure of this effect. The higher the coefficient, the stronger the influence of the factor. "Plus" sign at n indicates that with an increase in the values of this factor, the value P_v increases, and the "minus" sign at β_1 and z indicates that when they increase, the pressure P_v decreases. The effects of the interaction of factors are important. In the obtained equation (36), such an interaction is significant and has a positive sign for the interaction $(n \cdot \beta_1)$ and $(n \cdot z)$. With the effect of interaction of factors $(n \cdot \beta_2)$, there is a negative sign that reduces the final pressure value P_v.

The condition was accepted that P_v according to expression (36), is a function n, that is $P_v = P_v(n)$, where n – an independent variable, and β_1, β_2 and z – parameters. From the full set of properties, the common between the variable n and parameters β_1, β_2 and z is that they can all change, and the difference is that n changes continuously, and β_1, β_2 and z – discretely. In this case, expression (36) was rewritten as a linear equation of the following form:

$$P_v(n) = A \cdot n + B, \quad (37)$$

where

$$A = 4.21 + 0.07 \cdot \beta_1 - 0.038 \cdot \beta_2 + 0.078 \cdot z, \quad (38)$$

$$B = 11{,}817.78 + 338.61 \cdot \beta_1 - 204.34 \cdot \beta_2 + 390 \cdot z, \quad (39)$$

$$\{\beta_1, \beta_2, z\} = \text{const}. \quad (40)$$

Now previously independent variables β_1, β_2, and z have all the features as parameters included in linear equation (37) and, accordingly, determine the value of the coefficients A according to expression (38) and B according to expression (39). Expression (37) was then analysed. The coefficient A according to expression (38) indicates that: firstly, P_v grows regardless of its size B according to expression (39), it is proportional to growth n provided that $A > 0$; secondly, P_v decreases regardless of the value B according to expression (39), it is proportional to growth n provided that $A < 0$; and finally, thirdly, P_v does not depend on the value n provided that $A = 0$, and the value B according to expression (39), it indicates the value of P_v. It can be concluded that the first option is physically justified and it was further considered. To investigate the relationship between β_1 and P_v, the regression equation (36) was rewritten in the same way as the previous case (38-40) in the following form:

$$P_v(\beta_1) = C_1 \cdot \beta_1 + D_1, \quad (41)$$

where:

$$C_1 = 0.07 \cdot n - 338.61, \quad (42)$$

$$D_1 = -11{,}817.78 + 4.21 \cdot \text{n} + 204.34 \cdot \beta_2 - 390 \cdot \text{z} - \\ - 0.038 \cdot \text{n} \cdot \beta_2 + 0.078 \cdot \text{n} \cdot \text{z}, \quad (43)$$

$$\{n, \beta_2, z\} = \text{const}. \quad (44)$$

The calculations performed have established that in the case when $C_1 = 0$ according to the expression (42) n will have the following meaning:

$$n|_{C_1=0} = 4{,}837.286 \text{ rpm}. \quad (45)$$

Value P_v does not depend on β_1 and it is fully defined by a set of parameters:

$$\{\text{n}, \beta_2, z\}. \quad (46)$$

When:

$$n < n|_{C1=0} \text{ and } C_1 < 0, \quad (47)$$

relationship between β_1 and P_v is inversely proportional, and in the case when:

$$n > n|_{C1=0} \text{ and } C_1 > 0, \quad (48)$$

– directly proportional.

Further, a graphical dependency analysis was performed using a personal computer (36). For this purpose, a number of surfaces were considered that illustrate the dependence P_v from n, β_1, β_2 and z, provided that two of the four factors listed remain fixed. When considering the first option, when the value of factors $\beta_2 = 110°$ and $z = 20$ pcs. remain fixed, values n varies from 4,650 to 5,350 rpm, and β_1 varies from 30° to 70° (Fig. 3).

From expression (36) and from the surface shape $P_v(n, \beta_1)|_{\beta_2=110°;\ z\ =\ 20}$ (Fig. 3) it follows that within the full range of angle values $\beta_1 \in [30;70]$ deg, value P_v monotonically increases and proportional to the value $n \in [4650; 5350]$. When β_1 is fixed, the relationship between n and P_v is linear. A fixed speed of rotation of the impeller within $n \in [4{,}650; n|_{C_1=0}]$ increasing the angle $\beta_1 \in [30; 70]$ leads to a decrease in the value P_v, and at $n \in [n|_{C_1=0}; 5{,}000]$, and when the $\beta_1 \in [30; 70]$ increases, P_v also incleases. Therefore, the surface $P_v(n, \beta_1)|_{\beta_2=110°;\ z=20}$ (Fig. 3) has a rectilinear product parallel to the plane $(P_v n)$, but its angle of inclination relative to the horizontal varies depending on $\beta_1 \in [30; 70]$ and is defined as follows:

$$\arctan\left(\frac{\partial}{\partial n} P_v\right) = \arctan(C_1). \quad (49)$$

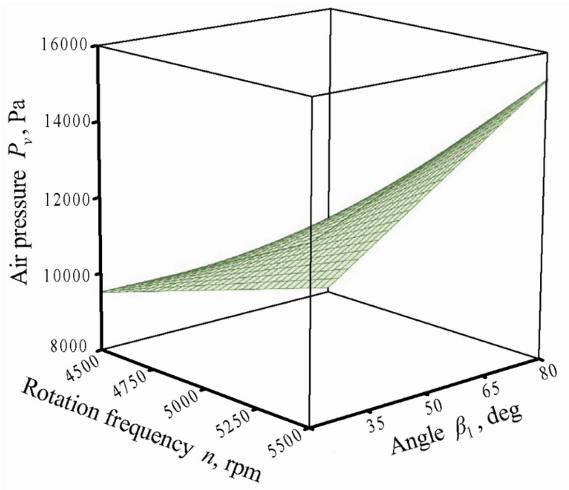

Figure 3. Dependence of the pressure generated by the fan on the impeller rotation speed and the angle of installation of the impeller blades at the inlet, with a fixed value of the angle of installation of the impeller blade at the outlet, and the number of blades

Note: P_v (Pa) – pressure, $n \in [4{,}650; 5{,}350]$ (rpm), $\beta_1 \in [30;70]$ deg, $\beta_2 = 110°$, $z = 20$ pcs

Source: compiled by the authors

The second option was considered, when the value of factors $\beta_1 = 50°$ and $z = 20$ pcs. remain fixed, value n varies from 4,650 to 5,350 rpm, and β_2 varies from 80° to 140° (Fig. 4).

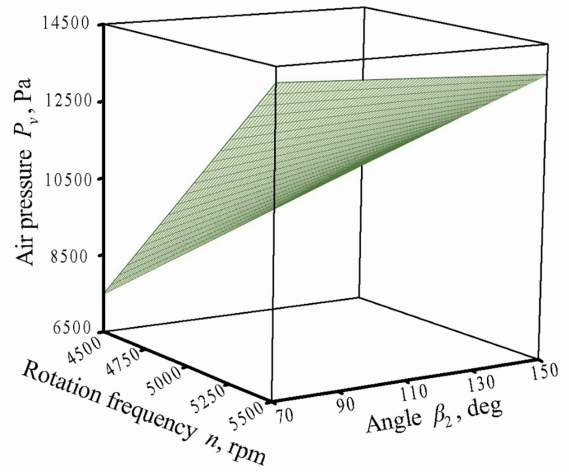

Figure 4. Dependence of the pressure P_v (Pa) generated by the fan on the impeller rotation speed and the angle of the impeller blades at the outlet at a fixed value of the impeller blade angle at the inlet, and the number of blades

Note: P_v (Pa) – pressure, $n \in [4{,}650; 5{,}350]$ (rpm), $\beta_2 \in [80;140]$ deg, $\beta_1 = 50°$, $z = 20$ pcs

Source: compiled by the authors

From the expression (36), as well as from the shape of the surface $P_v(n, \beta_2)|_{\beta 1=50°;\, z=20}$ (Fig. 4) it follows that the value P_v monotonically increases in proportion to the growth of $n \in [4{,}650; 5{,}350]$ for each fixed $\beta_2 \in [80; 140]$. In this case, the relationship between n and P_v is linear. The surface $P_v(n, \beta_2)|_{\beta 1=50°;\, z=20}$ (Fig. 4) has a straight line parallel to the plane $(P_v n)$, as in the previous case.

Next, the regression equation (36) is rewritten in linear form as before:

$$P_v(\beta_2) = C_2 \cdot \beta_2 + D_2, \tag{50}$$

where

$$C_2 = 204.34 - 0.038 \cdot n, \tag{51}$$

$$D_2 = -11{,}817.78 + 4.21 \cdot n - 338.61 \cdot \beta_1 - 390 \cdot z + \\ + 0.07 \cdot n \cdot \beta_1 + 0.078 \cdot n \cdot z, \tag{52}$$

$$\{n, \beta_1, z\} = \text{const}. \tag{53}$$

In the case when $C_2 = 0$, equation (50) and, accordingly, $n|_{C_2=0}$=5,377.368 rpm value P_v is independent of $\beta_2 \in [80; 140]$. When $n < n|_{C_2=0}$ and $C_2 > 0$, the relationship

between β_2 and P_v is directly proportional, and in the case of $n > n|_{C_2=0}$ and $C_2 < 0$ – inversely proportional (Chobal *et al.*, 2023). This is exactly the picture shown in Figure 4. Comparing the current situation with the previous Figure 3, it can be seen that the influence of angles β_1 and β_2 by the amount of P_v in a qualitative sense, it is a mirror image. Further, the third option was considered, when the value of factors $n = 5{,}000$ rpm and $z = 20$ pcs. remain fixed, values β_1 change from 30° to 70°, and β_2 – varies from 80° to 140° (Fig. 5).

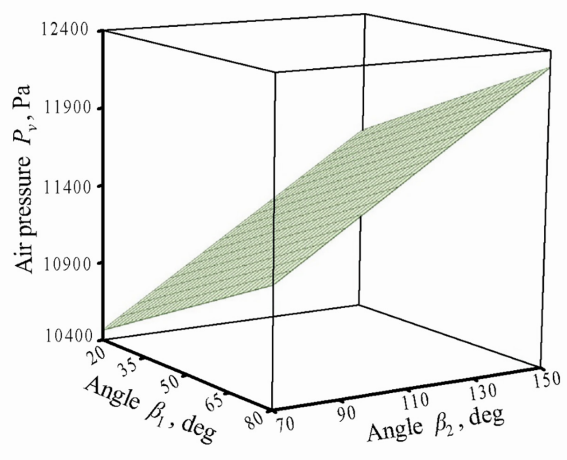

Figure 5. Dependence of the pressure P_v(Pa) generated by the fan on the angle of the impeller blades at the inlet and outlet at a fixed value of the fan impeller rotation frequency, and the number of blades

Note: P_v(Pa) – pressure, P_v deg, $\beta_2 \in [80;140]$ deg, $n = 5{,}000$ rpm, $z = 20$ pcs

Source: compiled by the authors

From the expression (36) and from the shape of the surface $P_v(\beta_1, \beta_2)|_{n = 5000;\ z=20}$ (Fig. 5) it follows that the value P_v monotonically increases in proportion to the increase in both angles $\beta_1 \in [30; 70]$ and $\beta_2 \in [80; 140]$. This situation fully corresponds to the patterns that were identified during the analysis of the surfaces shown in Figures 3 and 4. In the current case, the surface $P_v(\beta_1, \beta_2)|_{n = 5000;\ z=20}$ has a rectilinear line parallel to the plane (P_v β_1). The fourth option was considered as follows, when the value of factors $\beta_1 = 50°$ and $\beta_2 = 110°$ remained fixed, values n varied from 4,650 to 5,350 rpm, and the number of blades z changed from 12 to 28 pcs. The results obtained are shown in Figure 6.

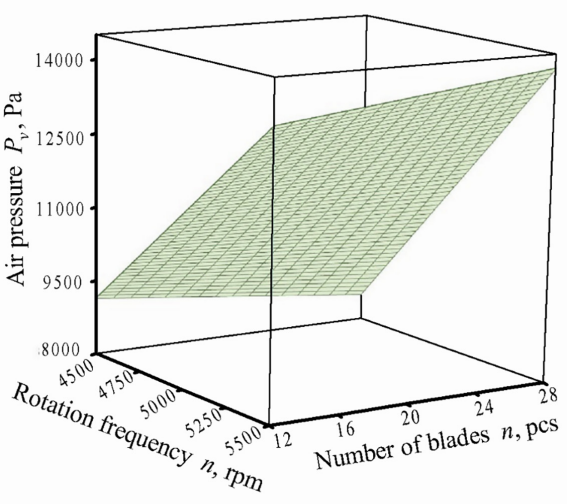

Figure 6. Dependence of the pressure P_v(Pa) generated by the fan on the impeller rotation speed and the number of blades at fixed values of the installation angles of the impeller blades at input and output

Note: P_v(Pa) – pressure, $n \in [4{,}650; 5{,}350]$ rpm, $z \in \{12, 16, \ldots, 28\}$, $\beta_1 = 50°$, $\beta_2 = 110°$

Source: compiled by the authors

From the expression (36) and from the shape of the surface $P_v(n, z)|_{\beta 1\ =\ 50°,\ \beta 2\ =\ 110°}$ (Fig. 6) it follows that in the qualitative sense, the nature of the influence of quantity z of impeller blades by the amount of pressure generated by it

P_v is similar to the regularities of the relationship between the angle β_1 and P_v, shown in Figure 3. At $n < 5{,}000$ rpm, the effect of the number of blades z on the pressure generated by the fan P_v is inversely proportional, and at $n > 5{,}000$ rpm – directly proportional. At $n = 5{,}000$ rpm, the impact of z on P_v is not observed.

Ultimately, the presented analysis of the obtained graph dependencies shown in Figures 3-6 gives grounds to assert that the obtained regressive model (36) is adequate to the working processes of a centrifugal radial fan of the considered design. Thus, precise and aggregated analytical dependencies and their graphical interpretations are found, which allow efficient and low-cost selection of optimal parameters of a centrifugal radial fan for any pneumatic seed drill.

Building a theoretical model involves conducting large and long-term research, since it is necessary to find out the nature of the microprocessors that the object has and describe them mathematically. R.B. Darlington & A.F. Hayes (2016) present the process model as a complex system of equations (a system of algebraic, ordinary differential equations, or partial differential equations). These systems of equations allow describing the processes occurring in the object very accurately and allow extrapolation at a point in the factor space where direct observation is impossible. Statistical models are obtained as a result of statistical processing of experimental data collected during the study.

Comparing the obtained scientific results with the results of known previous studies, it should be noted that G.J. Peng *et al*. (2021) also optimised the geometric parameters of the impeller of a multi-stage fan (pump) based on a rather complex and expensive experimental study. The obtained similar parameters, such as a smaller impeller diameter and fewer blades, require the use of a multi-stage design, which significantly increases the complexity and cost of the design.

H.C. Ding *et al.* (2020) also took a centrifugal fan as the object of research and installed five models of an impeller with different angles of release of the blades. Here, using computational hydrodynamics, the external characteristics of a centrifugal fan and the internal characteristics, including velocity, pressure, and turbulent energy distribution were obtained and compared in the middle plane of the fan impeller. In addition, pressure fluctuations around the impeller outlet as a function of external parameters were also analysed. However, there is no reason to consider the indicators obtained in this paper optimal, since the main methods of regressive analysis are not used here.

S.Q. Zhou *et al*. (2019) and Z.H. Li *et al*. (2020) considered a multi-blade centrifugal fan, which is characterised by a large number of blades (> 48) and their spiral installation on the drive shaft. It is established that the fluidity and noise characteristics of such a centrifugal fan depend on the type of spiral line and the geometry of the tongue at the spiral outlet. The origin and influence of a complex vortex structure near the spiral outlet of a multi-blade centrifugal fan are also investigated here. Due to the wide blade and short blade channel, the air flow maintains a large radial velocity in the blade channel. This continuous radial partial velocity causes vortices to form in the spiral release zone. A secondary flow close to the impeller is then generated from the centre to the sides along the volume. It is obtained that the current lines are divided into two parts (reverse and output) at the exit of the spiral. Although vortices near the spiral exit are complex, the main features of the flow behaviour caused by the vortex are clear. However, these obtained design and kinematic parameters of fans are not optimal, since they were also calculated without using correlation analysis. It is likely that even when developing specific designs of these centrifugal fans based on the application of the obtained parameters, it is necessary to conduct additional thorough experimental studies. And the application of the results obtained no longer requires any additional theoretical or experimental studies. This greatly simplifies obtaining fairly accurate design and kinematic parameters of the fan under study.

Many bladed centrifugal fans with different designs of impellers, blade profiles, grooves at the tip of the blade, etc., are considered in the papers by M. Kharati-Koopaee & H. Moallemi (2019), Z.Q. Xu *et al*. (2022) and F.N. Meng *et al*. (2023). Although correlation analysis methods are used here, their application is quite complex, expensive, and does not guarantee a fairly simple and accurate method proposed in this study. S. Tong *et al*. (2020), E.Ö. Aydın *et al*. (2022) considered a method for optimising the hydraulic efficiency of a ten-stage centrifugal pump. In accordance with the hydraulic loss model, a multi-criteria method for calculating optimisation based on constructed surrogate models is proposed. To determine the nonlinear relationship between key design variables and values of external characteristics of a centrifugal pump, this paper constructed a quadratic response surface, a radial basis Gaussian response surface, and three Kriging surrogate models using computer hydrodynamic modelling analysis. It is quite possible to switch from the study of a centrifugal pump to a centrifugal fan, but it still gives the effect that is used in this particular study. The authors of this well-known study have also built several models, but they are overwhelmingly based on hydraulic losses and applying them to generate air pressure will require significant additional transformations.

Based on the conducted comparative analysis, it can be argued that the developed method of designing centrifugal radial fans allows quite simply but also accurately determine the optimal design and kinematic parameters, which can be effectively used in the development and construction of various pneumatic systems that are widely used in the field of agricultural mechanisation.

CONCLUSIONS

The dependence of the total pressure P_v of the pneumatic system of the seed drill on the parameters of the main external factors present in its main body – the impeller – is analytically determined. For this purpose, a regression equation was derived that obeys the law of the first-degree polynomial equation. The high efficiency of applying the statistical theory of experiment planning in conducting computational studies instead of full-scale ones is proved.

In particular, the method of interpolation computational experiment is given. As a result, a functional relationship was established between the value of the total pressure generated by the fan P_v and independent variables: n – fan impeller rotation frequency; angles β_1 and β_2 of installations of each blade, respectively, at the inlet and outlet of the impeller; z – the number of impeller blades.

The resulting regression equation $P_v = P_v(n, \beta_1, \beta_2, z)$, Pa, shows that within the studied intervals, changes in independent quantities ($n \in [4{,}650; 5{,}350]$, rpm; $\beta_1 \in [30; 70]$, deg; $\beta_2 \in [80; 140]$, deg; $z \in [12, 16, \ldots, 28]$, pcs.) function $P_v = P_v(n, \beta_1, \beta_2, z)$ retains monotony, and therefore, the minimax optimisation experiment does not make sense. To obtain the required value of the total pressure generated by the fan P_v is enough to assign the corresponding values of independent values n, β_1, β_2 and z. Such a regression equation allows predicting response values based on the specified values of factors. The obtained analytical results allow effectively designing and constructing centrifugal radial fans with various technical indicators. In the future, the proposed methodological approach provides for the use to study and optimise processes in pneumatic systems not only in seed drills of various purposes and design in their development or improvement, but also in the study and design of pneumatic systems of other agricultural machinery and equipment of modern technical level.

The next stages in further research are the development of new physical models of pneumatic systems used in machines of various branches of agriculture and a fairly correct and accurate formalisation of their functioning depending on the input and output parameters, which will form the basis of their regression models built in the future. At the same time, there is a primary need to detail and establish the significance of individual factors, depending on the specific goals and features of further mathematical modelling.

ACKNOWLEDGEMENTS

None.

CONFLICT OF INTEREST

The authors declare no conflict of interest.

REFERENCES

[1] Arkes, J. (2023). *Regression analysis: A practical introduction*. New York: Routledge.
[2] Aydın, E.Ö., Tepe, E., & Balcan, C. (2022). Identification of determinants during the registration process of industrial heritage using a regression analysis. *Journal of Cultural Heritage*, 58, 22-32.
[3] Beloev, H., Adamchuk, V., Kaletnik, G., & Bulgakova, O. (2021). *The basis of scientific research in the field of agricultural engineering*. Ruse: Academic Publishing House Ruse University.
[4] Chobal, I., Chobal, O., Myslo, Yu., Petryshynets, I., & Rizak, V. (2023). Elastic-plastic properties of Li2B4O7 determined by nanoindentation. *Scientific Herald of Uzhhorod University. Series "Physics"*, 53, 53-63. doi: 10.54919/physics/53.2023.53.
[5] Darlington, R.B., & Hayes, A.F. (2016). *Regression analysis and linear models: concepts, applications, and implementation (methodology in the social sciences)*. London: Guilford Press.
[6] Ding, H.C., Chang, T., & Lin, F. (2020). The influence of the blade outlet angle on the flow field and pressure pulsation in a centrifugal fan. *Processes*, 8(11), article number 1422. doi: 10.3390/pr8111422.
[7] Frost, J. (2020). *Introduction to statistics: An intuitive guide for analyzing data and unlocking discoveries*. State College: Statistics by Jim Publishing.
[8] Kharati-Koopaee, M., & Moallemi, H. (2019). Effect of blade tip grooving on the performance of an axial fan at different tip clearances in the absence and presence of inlet guide vanes. *Proceedings of the Institution of Mechanical Engineers, Part A: Journal of Power and Energy*, 234(1), 72-84. doi: 10.1177/095765091985042.
[9] Kononyuk, A.E. (2010). *Fundamentals of scientific research. (General theory of experiment)*. Book 1. Kyiv. Establishment of Ukraine.
[10] Li, Z.H., Ye, X.X., & Wei, Y.K. (2020). Investigation on vortex characteristics of a multi-blade centrifugal fan near volute outlet region. *Processes*, 8(10), article number 1240. doi: 10.3390/pr8101240.
[11] Meng, F.N., Wang, L.J., Ming, W., & Zhang, H.X. (2023). Aerodynamics optimization of multi-blade centrifugal fan based on extreme learning machine surrogate model and particle swarm optimization algorithm. *Metals*, 13(7), article number 1222. doi: 10.3390/met13071222.
[12] Montgomery, D.C., Peck, E.A., & Vining, G. (2013). *Solutions manual to accompany introduction to linear regression analysis* (5th ed). Hoboken: Wiley.
[13] Nadikto, V.T. (2019). *Fundamentals of scientific research*. Kherson: Oldie-Plus.
[14] Nitri Asomani, S., Yuan, J., Wang, L., Appiah, D., & Adu-Poku, K.A. (2020). The impact of surrogate models on the multi-objective optimization of Pump-As-Turbine (PAT). *Energies*, 13(9), article number 2271. doi: 10.3390/en13092271.
[15] Peng, G.J., Hong, S.M., Chang, H., Zhang, Z.R., & Fan, F.Y. (2021). Optimization design of multistage pump impeller based on response surface methodology. *Journal of Theoretical and Applied Mechanics*, 59(4), 595-609. doi: 10.15632/jtam-pl/141939.
[16] Ping, X., Yang, F., Zhang, H., Zhang, J., Zhang, W., & Song, G. (2021). Introducing machine learning and hybrid algorithm for prediction and optimization of multistage centrifugal pump in an ORC system. *Energy*, 222, article number 120007. doi: 10.1016/j.energy.2021.120007.

[17] Tanzim, F., Kontos, E., & White, D. (2022). Generating prediction model of fan width by optimizing paint application process for Electrostatic Rotary Bell atomizer. *Results in Engineering*, 13, article number 100302. doi: 10.1016/j.rineng.2021.100302.
[18] Tong, S., Zhao, H., Liu, H., Yu, Y., Li, J., & Cong, F. (2020). Multi-objective optimization of multistage centrifugal pump based on surrogate model. *Journal of Fluids Engineering*, 42(1), article number 011101. doi: 10.1115/1.4043775.
[19] Wang, Y., Chen, L., Zhou, J., Li, T., & Yu, Y. (2022). Low-rank kernel regression with preserved locality for multi-class analysis. *Pattern Recognition*, 141, article number 109601. doi: 10.1016/j.patcog.2023.109601.
[20] Xu, Z.Q., Liu, X.M., Liu, Y., Qin, W.X., & Xi, G. (2022). Flow control mechanism of blade tip bionic grooves and their influence on aerodynamic performance and noise of multi-blade centrifugal fan. *Energies*, 15(9), article number 3431. doi: 10.3390/en15093431.
[21] Zhou, S.Q., & Li, Y.B. (2019). Volute characteristics of centrifugal fan based on dynamic moment correction method. *Proceedings of the Institution of Mechanical Engineers, Part A: Journal of Power and Energy*, 233(2), 176-185. doi: 10.1177/0957650918779856.

Віктор Іванович Мельник
Доктор технічних наук, професор
Державний біотехнологічний університет
61002, вул. Алчевських, 44, м. Харків, Україна
https://orcid.org/0000-0002-1176-2831

Олексій Петрович Зеленський
Аспірант
Державний біотехнологічний університет
61002, вул. Алчевських, 44, м. Харків, Україна
https://orcid.org/0000-0001-9819-9086

Андрій Петрович Зеленський
Аспірант
Державний біотехнологічний університет
61002, вул. Алчевських, 44, м. Харків, Україна
https://orcid.org/0000-0002-0364-5571

Проєктування відцентрових радіальних вентиляторів із застосуванням методів регресивного аналізу

Анотація. З розвитком науково-технічного прогресу в сільському господарстві актуальним є застосування операційно-математичного моделювання для ефективного вирішення завдань та ресурсозбереження в галузі сільськогосподарського машинобудування. Тому метою дослідження було визначення оптимальних параметрів відцентрового радіального вентилятора пневматичної сівалки точного висіву шляхом побудування нової математичної моделі процесу його роботи. Досягнення цього було здійснене шляхом застосування методів математичного моделювання при плануванні багатофакторних експериментів. В результаті визначено комплекс автоматизованого експерименту, що призводить до суттєвого підвищення продуктивності наукової роботи. Встановлено статистичне уявлення про експеримент, що дозволяє перейти до багатофакторного активного експерименту, в якому є можливість відокремити вплив факторів від шумового фону та здійснити перехід до статистичних методів аналізу результатів. Саме це дозволило отримати можливість прогнозування оптимальних характеристик відцентрового радіального вентилятора сівалки точного висіву. У процесі даного дослідження складено нове рівняння регресії у вигляді полінома першого ступеня, яке визначає вплив кожного із факторів на величину та значення відгуку. Визначено коефіцієнти полінома, проведено оцінку значущості коефіцієнтів та перевірку на адекватність запропонованої моделі. Після отримання рівняння регресії виникла можливість графічної побудови залежності функції відгуку від чинників впливу. Також проведено дробовий факторний експеримент, реалізуючи який визначено значення параметрів стану об'єкта Y при всіх можливих поєднаннях рівнів варіювання факторів X_i. На підставі встановленого функціонального взаємозвязку між вихідним параметром вентилятора одержане рівняння регресії наступного вигляду: $P_v = P_v(n, \beta_1, \beta_2, z)$. Це дало підстави прогнозувати отримання повного тиску P_v, (Па), при заданні різних значень незалежних величин n, β_1, β_2 та z. Застосування отриманих аналітичних залежностей суттєво спростило визначення оптимальних конструктивних параметрів пневматичних систем для розробки та конструювання сівалок сучасного технічного рівня

Ключові слова: математична модель; багатофакторний процес; тиск; частота обертального руху; кути установки; кількість лопаток

Machinery & Energetics
Vol. 14, No. 3. 2023

Journal homepage:
https://technicalscience.com.ua/en

UDC 631.11/.17:631.3
DOI: 10.31548/machinery/3.2023.61

Viacheslav Matsiuk
Doctor of Technical Sciences, Professor
National University of Life and Environmental Sciences of Ukraine
03041, 15 Heroiv Oborony Str., Kyiv, Ukraine
https://orcid.org/0000-0003-2355-2564

Viktoriia Opalko*
PhD in Technical Sciences, Associate Professor
National University of Life and Environmental Sciences of Ukraine
03041, 15 Heroiv Oborony Str., Kyiv, Ukraine
https://orcid.org/0000-0002-4209-1073

Liliya Savchenko
PhD in Technical Sciences, Associate Professor
National University of Life and Environmental Sciences of Ukraine
03041, 15 Heroiv Oborony Str., Kyiv, Ukraine
https://orcid.org/0000-0002-4336-4416

Oleg Zagurskiy
Doctor of Economics, Professor
National University of Life and Environmental Sciences of Ukraine
03041, 15 Heroiv Oborony Str., Kyiv, Ukraine
https://orcid.org/0000-0002-5407-8466

Nadiia Matsiuk
Assistant, MSc
National University of Life and Environmental Sciences of Ukraine
03041, 15 Heroiv Oborony Str., Kyiv, Ukraine
https://orcid.org/0000-0002-6922-3099

Optimisation of transport and technological system parameters of an agricultural enterprise in conditions of partial uncertainty

Abstract. At the stage of production of a wide range of agricultural products, to ensure the smooth operation of agricultural enterprises, it is necessary to solve the problems of fast and efficient delivery of relevant equipment, spare parts, and consumables with the rational use of available production resources. The research aims to improve the transport and technological system for the supply of orders in the form of consignments to meet the needs of the production activities of an agricultural enterprise. For this purpose, an simulation model was developed in the AnyLogic University Researcher environment using the Java compiler, since this toolkit allows simultaneously combining discrete-event and agent-based approaches. The model was implemented on the example of an enterprise of a separate subdivision of the National University of Life and Environmental Sciences of Ukraine "Agronomic Research Station". As a result, a comprehensive, optimisation mathematical model of the supply of goods on an extensive network of road routes using the agricultural

Article's History: Received: 07.04.2023; Revised: 17.07.2023; Accepted: 11.08.2023.

Suggested Citation:
Matsiuk, V., Opalko, V., Savchenko L., Zagurskiy, O., & Matsiuk, N. (2023). Optimisation of transport and technological system parameters of an agricultural enterprise in conditions of partial uncertainty. *Machinery & Energetics,* 14(3), 61-71. doi: 10.31548/machinery/3.2023.61.

*Corresponding author

enterprise's fleet of vehicles under conditions of partial uncertainty was obtained. In the course of experiments and calculations based on the real process of an agricultural enterprise, a range of values of the size of the truck fleet that meets the optimisation conditions has been found. It has been determined that the range of values close to the optimal size of the unloading truck fleet varies from 9 to 14 units. It has been established that the values of the optimisation criterion describing the average delivery time from the beginning of the need for an order to the moment of its delivery vary from 9.96 to 12.78 hours. The limit level of load of the transport and technological system is determined, at which the limit level of technological fault tolerance is ensured. It is 135 or more orders per year for each supplier with an estimated fleet of 12 trucks. The results of the study, such as the use of analytical tools and algorithms to optimise routes and allocate resources, can be used to improve transport efficiency, and help companies choose the most profitable and environmentally friendly routes for transportation

Keywords: agent-based simulation; vehicle fleet composition; technological fault tolerance; distribution logistics; component supply

INTRODUCTION

Global agricultural supply chains play a crucial role in ensuring the availability and accessibility of food for the world's population. As the world's population grows, demand for agricultural products is increasing, putting pressure on existing supply chains. By adopting technological innovations such as blockchain, vertical farm integration strategies, and precision agriculture, these supply chains will be better able to meet the needs of a growing global population and contribute to a more sustainable and equitable future (Latest agri-food trade report..., 2023).

The efficiency and performance of global agricultural supply chains are ensured by infrastructure components: transport systems, including road, rail and maritime networks, storage and warehousing systems, communications and connectivity that allow for information exchange, coordination, and digitalisation. Agricultural supply chains are complex networks that involve many stakeholders, including agricultural associations, farmers, cooperatives and agricultural processing organisations, wholesalers, retailers, and consumers.

M. De Bok & L. Tavasszy (2018) noted that modern agro-industrial enterprises are powerful high-tech industries with complex equipment that requires special and timely maintenance. To ensure the proper working condition of such equipment, enterprises periodically purchase spare parts from planned and unplanned deliveries, expendables and components, and other materials representing small and medium-sized consignments. The supply network through a variety of different suppliers is usually quite extensive. Coordinating and managing the movement of goods from the point of origin to the end customer is critical to success. R. Granillo-Macías (2021) argues that to ensure the efficiency and effectiveness of distribution logistics operations, several factors must be considered, including delivery efficiency, real-time tracking and visibility, regulatory compliance, technology, sustainability, and customer service.

The provision of transport services on an extensive network of routes, due to the need for unscheduled procurement, can be considered partially unpredictable. At the same time, according to L. Leng *et al.* (2020), and A. Bekrar *et al.* (2021), it can be seen that with significant volumes of deliveries, it is advisable to maintain its fleet of vehicles. In such cases, the issue of fleet optimisation always arises, both in terms of size and equipment. Thus, there is a certain scientific and applied task of developing models and methods for planning distribution logistics on the network of planned and unplanned purchases and deliveries under conditions of partial uncertainty. P.T.W. Lee *et al.* (2022), and G. Zhang (2023) have sufficiently covered the issues of improving the efficiency of transport processes and systems, optimising the technological parameters of supply chains, improving technological schemes and models of cargo flow management. A. Prokhorchenko *et al.* (2019) study the problem of the safe operation of critical transport infrastructure in conditions of partial uncertainty of the occurrence and elimination of the consequences of unauthorised interference. At the same time, these studies do not study the intra-technological conflicts inherent in the stochastic phenomena of transport processes. Stress test modelling, in particular agent-based simulations, is a fairly common practice in various fields of activity (Cichosz, 2020; Muñoz & Iglesias, 2021). However, such studies have not been conducted for transport and technological systems due to the accepted "safe" reliability threshold.

Thus, the issue of distribution logistics has been sufficiently studied, including with the help of agent-based simulation. However, there are not enough examples of optimisation of vehicle fleet parameters under conditions of partial uncertainty and stochasticity of transport processes. In addition, the issue of stress tests of the functioning of transport and technological processes has not been sufficiently studied. Therefore, the purpose of the study was to develop measures to improve the transport and technological system for the delivery of small consignments of goods under the condition of centralised fleet management. To achieve the goal of the plan, it was necessary to solve the following tasks: to develop a simulation model of the process of small consignments distribution under the condition of centralised management of the vehicle fleet; to optimise the parameters of the transport and technological system for small consignments distribution under the condition of centralised management of the vehicle fleet.

MATERIALS AND METHODS

One of the main indicators of the efficiency of logistics systems is the regularity and timeliness of delivery with the rational use of available production resources. The criterion for optimal planning and implementation of technological processes of cargo delivery is the average delivery time from the moment the order is required to be delivered to the moment it is delivered:

$$T_{avg} = f_{pr}(a_1, ..., a_n; p(a_1), ..., p(a_n)) \rightarrow \min, \quad (1)$$

where $a_1, ..., a_n$ – set of possible parameters of the fleet of vehicles, delivery routes, order conditions, suppliers working hours, etc.; $p(a_1), ..., p(a_n)$ – probabilistic description of the conditions for the use of the corresponding production resource and the conditions of the organization of supply.

The focus of optimisation was to reduce the selected indicator. The average delivery time was broken down into fixed and variable components:

$$T_{avg} = \overline{t}_{route} + \overline{t}_{technological\ downtime.} + \overline{t}_{unproductive\ downtime.}, \quad (2)$$

where $\overline{t}_{route}$ – truck driving time; $\overline{t}_{technological\ downtime}$ – technological downtime of trucks during scheduled operations: loading, unloading, etc.; $\overline{t}_{unproductive\ downtime}$ – time of unproductive downtime in the form of delays arising from technological conflicts due to the stochastic nature of transport and technological processes and the discrepancy between the processing capacity of the transport system and its loading volumes.

Elements $\overline{t}_{route}$ and $\overline{t}_{technological\ downtime}$ depend on the physical and technical characteristics of the transport system parameters, and therefore can be considered constant during operation. Whereas the element $\overline{t}_{unproductive\ downtime}$ is a variable component, which in most cases arises due to the unpredictability of the situation. Therefore, the optimisation of the objective function was to minimise the component $\overline{t}_{unproductive\ downtime}$ which theoretically, depending on the level of conflict, can vary within $\overline{t}_{tunproduct.downtime} = [0, \infty]$.

Given that the process of ordering components, spare parts, and other materials for the needs of agricultural companies is partially unpredictable, and this applies to both the possible delivery route and the time of the order, the entire technological process of order delivery and the use of vehicles was considered quasi-stochastic. Under such conditions, the request for the use of existing production resources (vehicles, staff time) should be optimal, and therefore their degree of use (utilisation) should be within limits:

$$\begin{aligned} \xi_r &\leqslant \varphi_{truck}(a_1, ..., a_n), \\ \xi_u &\geqslant \varphi_{truck}(a_1, ..., a_n), \end{aligned} \quad (3)$$

where φ_{truck} – the average load of vehicles, which corresponds to the part of the time of direct use of the vehicle relative to the total time of its operation; ξ_u – the limit of rational use of the selected production resource; ξ_r – limit of reliability (fault tolerance) of the use of the selected production resource.

At that time, the optimisation model was as follows:

$$\begin{aligned} &\overline{t}_{route} + \overline{t}_{technological\ downtime} + \overline{t}_{unproductive\ downtime} = \\ &= f_{pr}(a_1, ..., a_n; p(a_1), ..., p(a_n)) \rightarrow min \\ &\begin{cases} \xi_r \leq \varphi_{truck}(a_1, ..., a_n), \\ \xi_u \geq \varphi_{truck}(a_1, ..., a_n). \end{cases} \end{aligned} \quad (4)$$

Since the objective function had a significant set of parameters and was presented in an implicit form, one of the possible solutions to this problem was to develop and implement a simulation model. The simulation model represented the interaction of agents, most of which had a discrete-event formalisation (Table 1):

Table 1. Simulation model agents

Agent Name	Agent function	Agent task
Main	Base model agent	The main window of the model presentation.
Suppliers	The population of "Suppliers" agents with a set of coordinates on the suppliersPoints GIS map	Simulation of the work of suppliers of goods for the needs of agricultural production
BusinessProcess	Agent of the technological process of order delivery	Simulation of the process of receiving an order, planning, and organising the delivery of an order by a fleet of own trucks
Truck	The population of agents "Truck fleet"	Simulation of a fleet of vehicles ready for dispatch
Order	The population of agents of the "order" type	Simulation of an information order for the delivery of goods with a set of required characteristics: supplier, quantity of goods (cargo), terms of delivery.

Note: GIS – geographic information system
Source: compiled by the authors

The entire technological process of supplying own truck fleet begins with the receipt of an order, which can be formalised as an information message with a set of characteristics:

$$M=\{m_1,\ldots,m_n\}, \quad (5)$$

where m_1, ..., m_n – a set of information characteristics: point of departure, time of departure, amount of cargo, conditions of transportation, etc.

The information message is received by the dispatcher, after which the transport is planned as a sequence of organisational measures:

$$N=\{n_1,\ldots,n_n\}, \quad (6)$$

where n_1, ..., n_n – a set of organizational actions of the dispatching point, which is mostly associated with the choice of the required (according to the technical conditions of the M_i order) truck among currently available vehicles, documenting the route, etc.

The simulation model was implemented in the AnyLogic 8.7 environment using the Java compiler. The chosen development environment allows to implementation of business processes of goods supply through a combination of agent-based and discrete-event approaches. The main tools for modelling dynamic transport processes and recording changes in the state of system elements in each agent were the units of the *Enterprise* and *Ststchart* libraries built into *AnyLogic*.

The adequacy of the model was checked by comparing the results of the baseline experiment with the normative indicators of the work performed by the enterprise of the separate subdivision of the National University of Life and Environmental Sciences of Ukraine "Agronomic Research Station". The reliability of the results was ensured by determining the minimum number of replications and the minimum required modelling time. A level of reliability of at least 95% (with an error probability of no more than 5%) will be achieved with a minimum of ten replications and six months of simulation time.

RESULTS AND DISCUSSION

The *Enterprise library* allowed us to model various stages, such as the arrival of vehicles for loading, transportation to the unloading point, unloading, return with empty mileage, as well as all inter-operational downtime (Fig. 1).

Initial conditions and key parameters are summarised in Table 2.

Built-in GIS mapping technology was used to create a network of possible supply routes (Fig. 2).

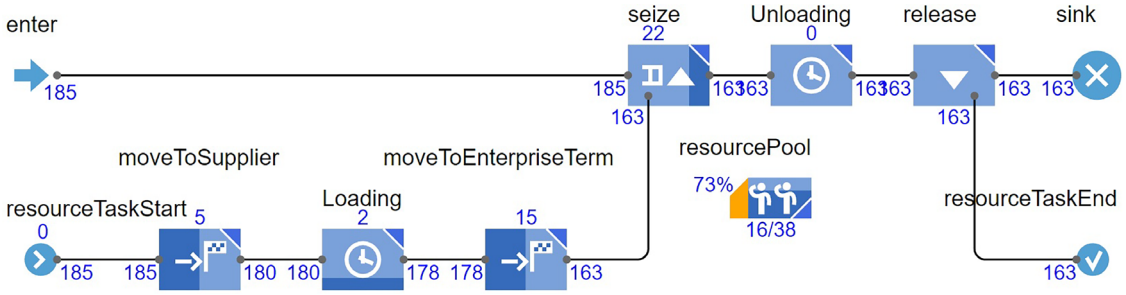

Figure 1. Discrete-event simulation of the technological process of order supply and turnover of trucks
Source: compiled by the authors

Table 2. Initial parameters of the simulation model implementation

Parameter	Value	Note
Supplier locations	Vinnytsia, Dnipro, Zhashkiv, Zhytomyr, Kyiv, Lviv, Kharkiv, Odesa, Sumy, Kherson, Zaporizhia, Khmelnytskyi, Cherkasy.	
Location of the company's cargo terminal	Pshenychne, Vasylkiv district, Kyiv region.	
The average intensity of orders from each supplier	1 in a week 52 in a year.	Exponential distribution
Drivers' working week, working conditions	5 days, irregular working hours.	
Average vehicle speed on the route	50 km/h	

Continued Table 2.

Parameter	Value	Note
Time spent by the vehicle at the loading point	8 hours	The distribution of the indicator is triangular [0.95*t*; *t*; 1.25*t*].
Average time spent at the unloading point	8 hours	The distribution of the indicator is triangular [0.95*t*; *t*; 1.25*t*].

Source: compiled by the authors

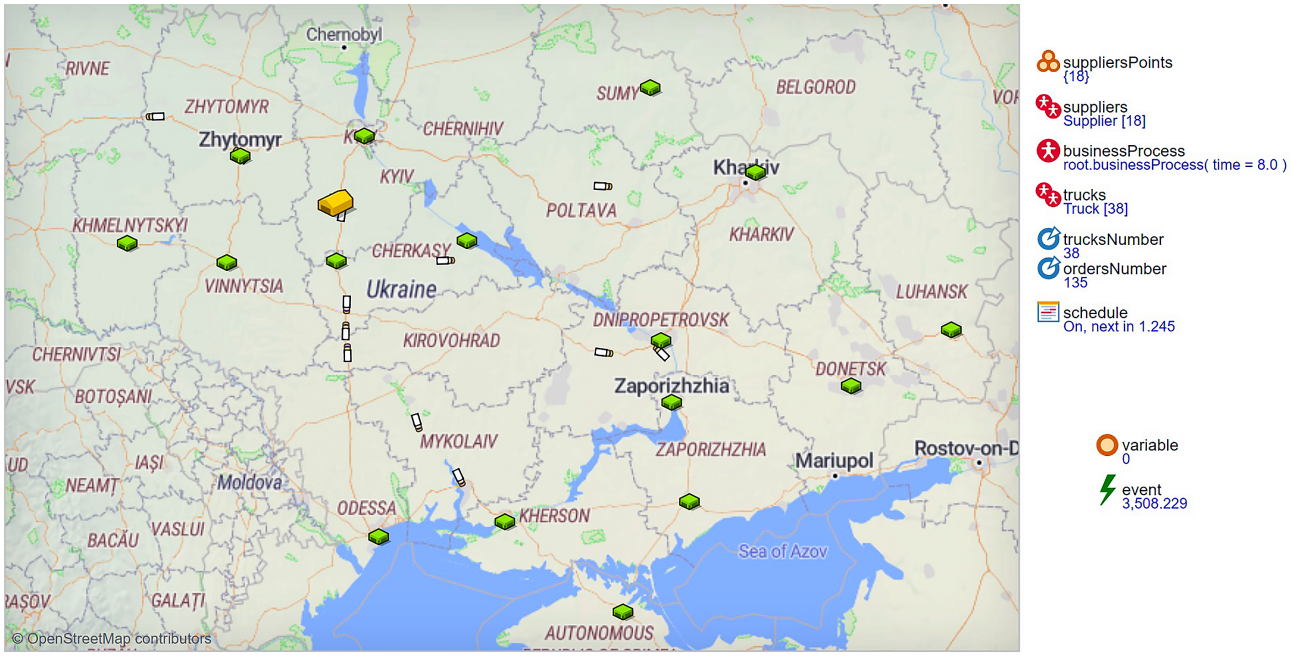

Figure 2. General view of the GIS map with supply points and possible routes at the presentation of the agent's Main
Source: compiled by the authors

The modelling of the emergence and formation of purchase orders is carried out by a population of Supplier agents (Fig. 3) using a discrete transition at a set intensity that simulates the random occurrence of the need to purchase goods according to an exponential distribution with an average intensity of *n* orders per week.

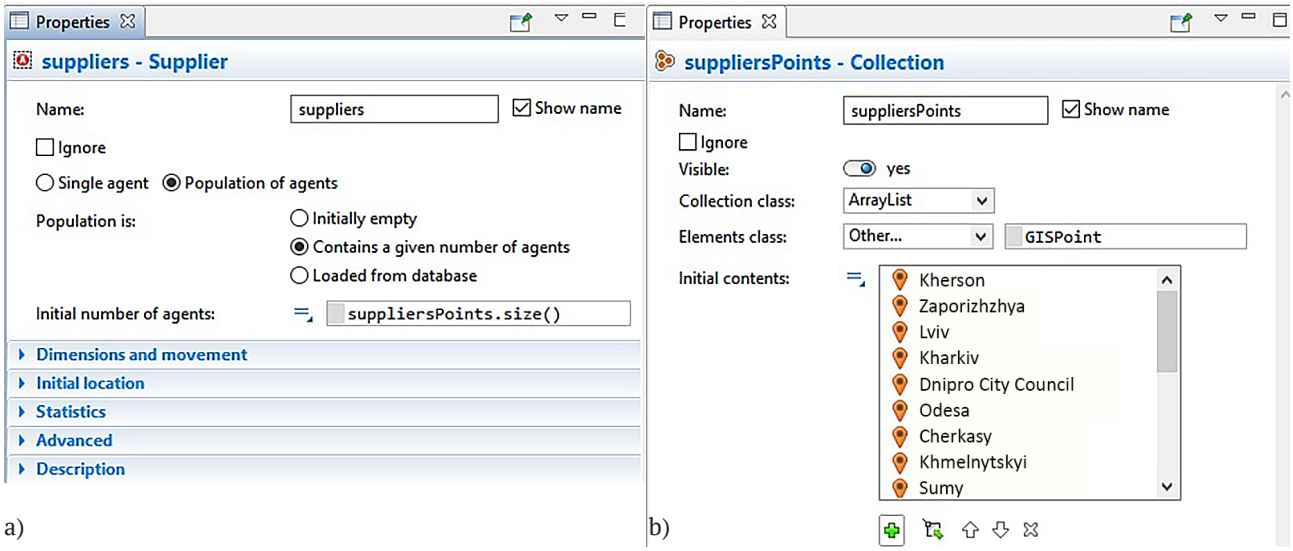

Figure 3. Discrete-event process of forming (generating) new supply orders in the agents of the population *Suppliers*
Note: a – agents of the population *Suppliers*; b – the process of forming new orders
Source: compiled by the authors

When the need for an order arises, a new agent of the *Order* type is generated using the corresponding Java code:

"Order order = **new** Order (**this**);
send (order, main.businessProcess);".

An instance of the *Order* class is passed to the *BusinessProcess* agent for processing. The simulation of the technological process of supplying goods by own car fleet is carried out in the *BusinessProcess* agent. The *seize* block simulates the processing of an order and the "seizure" of the necessary resources to process the order. The resource is a free truck that is located in the *resource pool* block – a fleet of vehicles.

In a situation where there are no available trucks, the order waits for its turn. If there is a free truck, control is transferred to the first subprocess, which simulates the first part of the truck's production cycle – driving to the loading point and loading: *resourceTaskStart* – the start of using a resource of the *truck* type.

The second subprocess begins with the *release* block and corresponds to the second half of the truck's production cycle – the return route and unloading of the order at its cargo terminal. To make the model more adequate, the simulation implements a scenario for scheduling access to the fleet of vehicles through the *scheduling* tool. This approach allows you to set the working hours of drivers during the days of the week.

To establish the optimal value of the number of trucks, an optimisation experiment was created in AnyLogic, based on the optimisation model (4). The model delivery time is defined as the time interval between the time a new order leaves the *Unloading* block and the time this order enters the *entered* block:

"dataTimeOrderIn.add(time() – timeInOrder);"

The validation of the software code was carried out step by step with the compilation of the Java code of all agents separately. The developed simulation models adequately simulate the transport and technological process of supplying orders from a plurality of suppliers on an extensive network of transport links. As a result of the development of the simulation model, it was possible to consider the variability of delivery routes in the conditions of the existing road transport infrastructure of Ukraine, as well as the Poisson nature of the receipt of orders for transportation.

As a result of the optimisation experiments and calculations based on the real process of an agricultural enterprise, a range of values of the indicator that meets the conditions of the optimisation model (4) was obtained (Fig. 4): from 9 to 14 trucks. At the same time, the average order delivery time, which is the optimisation criterion, varies from 9.96 to 12.78. For calculations, the option corresponding to the middle of the range was chosen, i.e., 12 trucks.

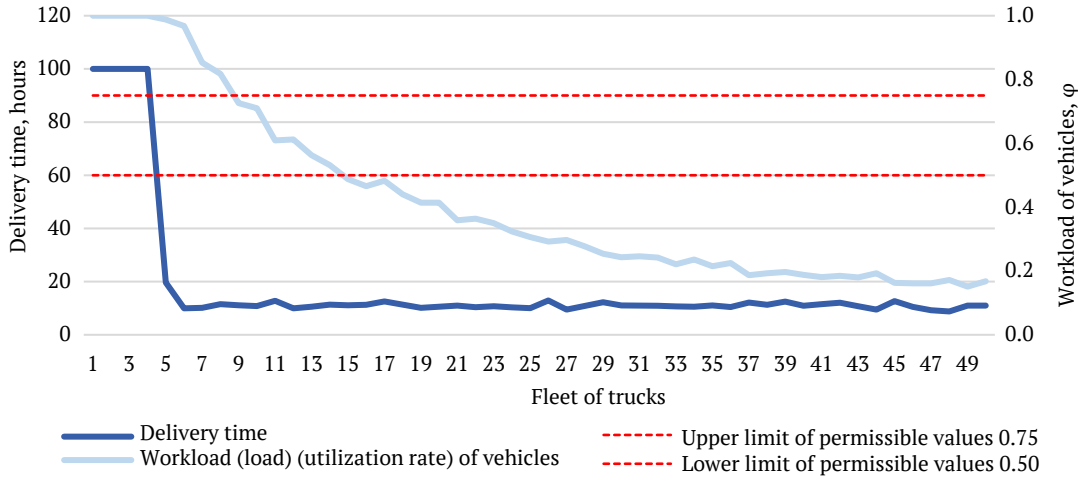

Figure 4. Dependencies of order delivery time and vehicle fleet loading on the working vehicle fleet
Note: delivery time is limited to 100 hours
Source: compiled by the authors

To determine the limit level of load, namely the intensity of orders, at which the transport and technological system of the enterprise will provide an appropriate level of fault tolerance, a sensitivity experiment of the model was conducted, in which the intensity of delivery orders was gradually increased with the estimated fleet of trucks (N_{cargo} = 12). As a result of a series of experiments, it was found that the queue of unfulfilled orders begins to grow significantly after the intensity of 140 orders per year (about 2.7 orders per week) (Fig. 5).

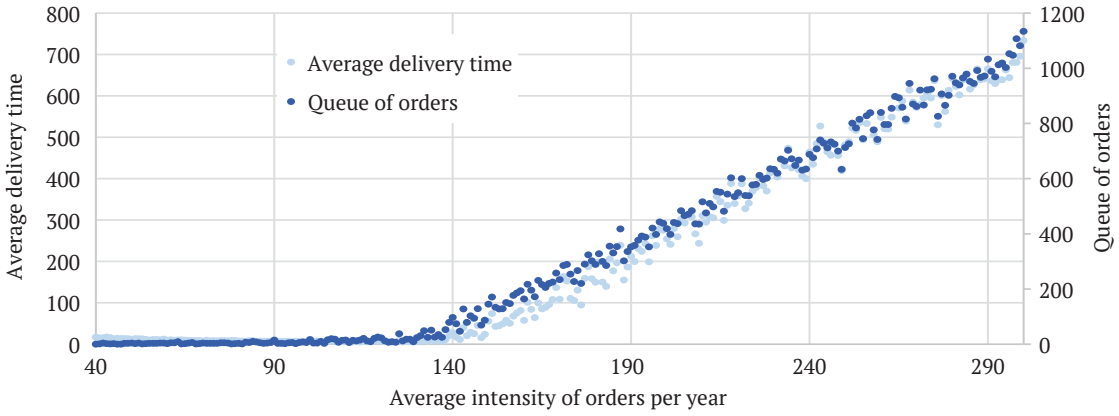

Figure 5. Dependence of the number of orders in the queue (at the end of the experiment) and the average delivery time on the average intensity of transportation

Source: compiled by the authors

A detailed analysis of the formation of the order backlog during the simulation period indicates a gradual increase in unfulfilled orders with an order intensity of 135 orders per year or more (Fig. 6).

At the same time, the value of the waiting time for an application for a free truck has an exponential distribution density, which confirms the naturalness of the process (Fig. 7).

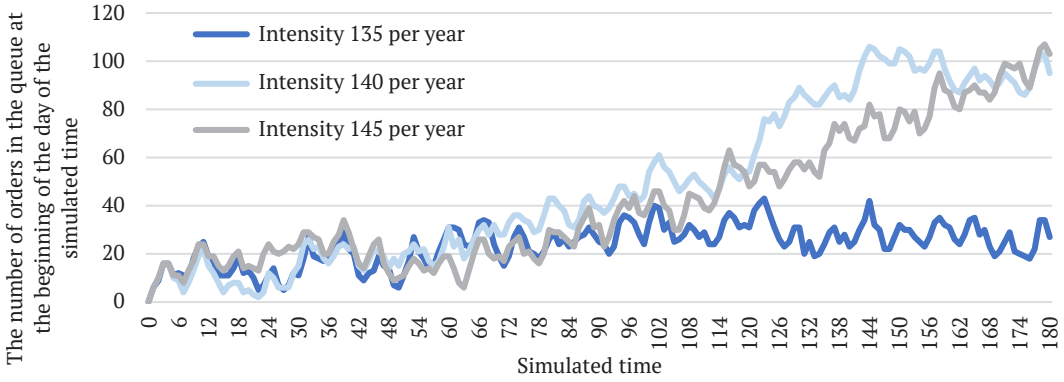

Figure 6. Dependence of the size of the order queue depends on the average intensity of receipt of transportation orders

Source: compiled by the authors

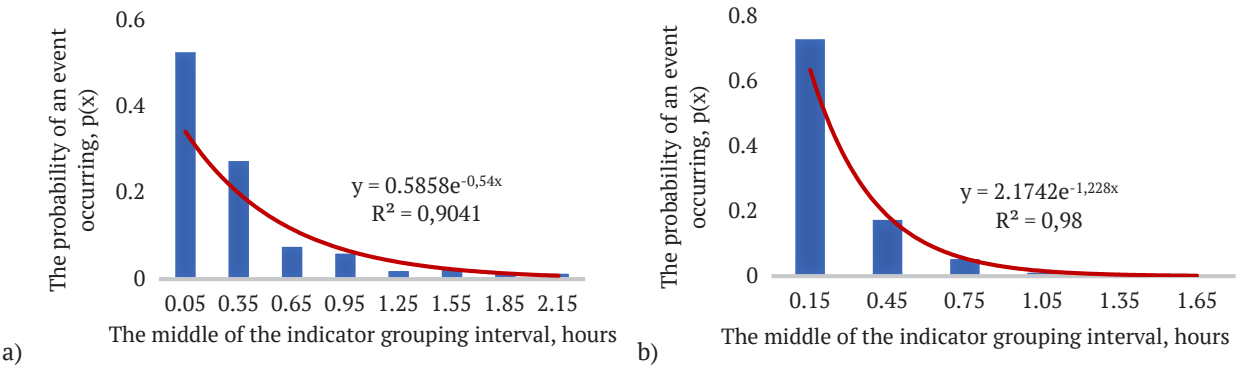

Figure 7. The probability density of the distribution of the waiting time for the execution of a transportation order due to the lack of a free truc

Note: a) for the calculated loading conditions on the system (number of vehicles 12, average intensity of orders 52 per year); b) For critical loading conditions on the system (number of vehicles 12, average intensity of orders 135 per year

Source: ompiled by the authors

Thus, it can be assumed that the maximum load of the transport and technological system of an enterprise with an estimated fleet of 12 trucks is 135 or more orders per year for each supplier. At the same time, the experimental models presented in these studies do not consider the complexity of multimodal transport, as noted by V. Shramenko *et al.* (2020). Only the last stage of delivery, the "last mile" stage, was considered. Therefore, it is impossible to state that the study of cargo delivery is complete, systematic and comprehensive, which, if possible, will be taken into account in further research.

Thus, the study systematically studied the problems of improving the efficiency of the transport and technological line using computer simulation, which made it possible to:

- consider the process as a single, complex and large transport system;
- to consider the slope of processes and phenomena, which minimised the abstractness of the model;
- to investigate the centralised management of the vehicle fleet and the issue of process resilience;
- establish the optimal parameters of the transport and technological process, considering a systematic approach.

However, the study could not consider:

- branching of delivery routes, considering the number of delivery points within each route;
- the process of transporting goods within the entire transport and technological line of multimodal supply chains.

Optimising transport routes is key to improving supply chain efficiency. One of the most modern and powerful tools for comprehensive optimisation of all key parameters of transport and technological systems of various types and levels is agent-based simulation (Liu *et al.*, 2022), including in the study of distribution logistics implementation conditions (Tang *et al.*, 2022; Alimohammadi & Behnamian, 2023), as well as based on GIS (geographic information system) components of the spatial orientation of transport infrastructure facilities on the ground (Chen *et al.*, 2021). At the same time, such models do not fully use the discrete-event approach, which allows for modelling technological subprocesses with a sufficient level of reliability.

In addition, the main feature of the developed model is the consideration of centralised fleet management. In other words, the model dynamically considers the possibility of changing the routes of trucks when organising the next flights and cargo delivery. A similar problem was solved by V. Matsiuk *et al.* (2021), where mainline locomotives were optimised for the delivery of iron ore concentrate. However, unlike these studies, this paper modelled the centralised management of trucks.

To study the resilience of the transport system, similar tools to the methods of queuing theory were used, as described by D. Ziemke *et al.* (2021). The methods of queuing theory were used to solve the scientific task of increasing the efficiency of processes to counter illegal and unauthorised interference with critical infrastructure. While the processes are similar, fleet management has certain differences, starting with greater discretion in events, sequencing (vehicles are serviced in a certain order) and less variation in the intervals of service requests and the duration of the service itself. Thus, the main value of this research is the focus on the problem of road transport of small consignments of goods in a wide variation of delivery routes under conditions of stochastic processes and systematic research.

At the same time, another rather powerful research tool, agent-based simulation, is gaining popularity. Simulation models developed based on this paradigm allow for the most comprehensive study of a wide range of activities, production, service, etc. For example, E. Derkenbaeva *et al.* (2023) presented the results of experiments with spatial microsimulation to predict the development of residential areas in one of the European countries. The agnostic approach made it possible to consider specific factors in human behaviour, such as the role of tenants and investors in shaping demand in the country's regions, and to forecast electricity consumption in the near future. Based on the study's findings, the researchers presented an effective decision-making support tool for the country's political leadership, including local authorities in the regions.

In another example, R. Faia *et al.* (2023) successfully addressed the problem of optimising the daily energy consumption of a region with intensive use of electric vehicles. With the help of the developed agent-based computer simulation, the researchers solved the problem of the optimal location of charging stations in the selected area. This problem successfully combines the approaches of linear programming and integral calculations in the process of parameter search.

The most similar results are obtained by O.V. Horbova & N.S. Murkovych (2021), as they present the results of experiments with agent-based simulation in the delivery of small consignments. At the same time, these studies are based on the task of a salesman and do not fully consider the simultaneous operation of several vehicles in the centralised organisation of transportation work.

In summary, the problem of distribution logistics is a complex and multifaceted issue that requires an integrated approach to overcome. By adopting a holistic approach, companies can ensure the success of their business and meet the ever-increasing demands of their customers.

CONCLUSIONS

A comprehensive optimisation (simulation) model for the delivery of orders on an extensive network of road routes by a truck fleet under conditions of partial uncertainty has been developed. The model is based on agent-based and discrete-event principles, considering the stochastic nature of the receipt of orders for transportation and the duration of the technological elements of the transportation process. The model was tested based on one of the operating units of the National University of Life and Environmental Sciences of Ukraine. This allowed the model to be adapted to the specific requirements and features of the enterprise in question, which contributed to higher

efficiency and accuracy of the results. The adequacy of the model was determined by comparing the performance indicators of the enterprise and the modelling results. The degree of reliability is 89%.

The results of the optimisation and sensitivity experiments of the model have established that, according to the criterion of the average delivery time of order and under the given initial conditions, there is a range of close to optimal values of the size of the truck fleet, namely from 9 to 14, while the optimisation criterion itself ranges from 9.96 to 12.78 hours. The average value of the specified range, namely 12 vehicles, was chosen as the calculated value.

The sensitivity experiment of the model, with the selected calculated value of the vehicle fleet, determined the maximum level of load on the transport and technological system, which ensures its efficient operation. The critical load of the system is the number of transport orders in the amount of 135 per year (from each supplier), which is 160% more than the existing level of orders of 52 per year. The density of the distribution of the waiting time for the fulfilment of transportation orders is approximated by an exponential distribution, which indicates sufficient fault tolerance of the process and, as a result, is evidence that the transport and technological supply system of the enterprise has a sufficient margin of safety.

Further research is needed to improve the simulation model since it did not consider the randomness of the formation of consignments of different sizes (weight and mass) and the different intensities of order formation in the supplier network.

ACKNOWLEDGEMENTS

None.

CONFLICT OF INTEREST

None.

REFERENCES

[1] Alimohammadi, M., Behnamian, J. (2023). Investigating digital transformation technologically enabled solutions in reverse logistics: A systematic review. *Environment, Development and Sustainability*. doi: 10.1007/s10668-023-03821-w.

[2] Bekrar, A., Cadi, A.A.E., Todosijevic, R., & Sarkis, J. (2021). Digitalizing the closing-of-the-loop for supply chains: A transportation and blockchain perspective. *Sustainability*, 13(5), article number 2895. doi: 10.3390/su13052895.

[3] Chen, Y., Huang, Z., Ai, H., Guo, X., & Luo, F. (2021). The impact of GIS/GPS network information systems on the logistics distribution cost of tobacco enterprises. *Transportation Research Part E: Logistics and Transportation Review*, 149, article number 102299. doi: 10.1016/j.tre.2021.102299.

[4] Cichosz, M., Wallenburg, C.M., & Knemeyer, A.M. (2020). Digital transformation at logistics service providers: Barriers, success factors and leading practices. *International Journal of Logistics Management*, 31(2), 209-238. doi: 10.1108/IJLM-08-2019-0229.

[5] De Bok, M., & Tavasszy, L. (2018). An empirical agent-based simulation system for urban goods transport (MASS-GT). *Procedia Computer Science*, 130, 126-133. doi: 10.1016/j.procs.2018.04.021.

[6] Derkenbaeva, E., Hofstede, G.J., van Leeuwen, E., & Halleck Vega, S. (2023). Simulating households' energy transition in Amsterdam: An agent-based modeling approach. *Energy Conversion and Management*, 294, article number 117566. doi: 10.1016/j.enconman.2023.117566.

[7] Faia, R., Ribeiro, B., Goncalves, C., Gomes, L., & Vale, Z. (2023). Multi-agent based energy community cost optimization considering high electric vehicles penetration. *Sustainable Energy Technologies and Assessments,* 59, article number 103402. doi: 10.1016/j.seta.2023.103402.

[8] Granillo-Macías, R. (2021). Logistics optimization through a social approach for food distribution. *Socio-Economic Planning Sciences*, 76, article number 100972. doi: 10.1016/j.seps.2020.100972.

[9] Horbova, O.V., & Murkovych, N.S. (2021). Research of complex processes based on Step-By-Step Modeling. *Science and Transport Progress*, 5(95), 51-59. doi: 10.15802/stp2021/252704.

[10] Latest agri-food trade report shows rebound of EU exports in February 2023. (2023). Retrieved from https://agriculture.ec.europa.eu/news/latest-agri-food-trade-report-shows-rebound-eu-exports-february-2023-2023-06-08_en.

[11] Lee, P.T.W., Hu, Z.H., Lee, S., Feng, X., & Notteboom, T. (2022). Strategic locations for logistics distribution centers along the Belt and Road: Explorative analysis and research agenda. *Transport Policy*, 116, 24-47. doi: 10.1016/j.tranpol.2021.10.008.

[12] Leng, L., Zhang, J., Zhang, C., Zhao, Y., Wang, W., & Li, G. (2020) A novel bi-objective model of cold chain logistics considering location-routing decision and environmental effects. *PLoS ONE,* 15(4), article number e0230867. doi: 10.1371/journal.pone.0230867.

[13] Liu, H., Jiao, L., Wang, F., & Zhang, X. (2022). Control optimization design of radio frequency identification technology in IoT express logistics distribution system. *Journal of Control Science and Engineering*, 2022, article number 3169032. doi: 10.1155/2022/3169032.

[14] Matsiuk, V., Galan, O., Prokhorchenko, A., & Tverdomed, V. (2021). An agent-based simulation for optimizing the parameters of a railway transport system. In *ICTERI-2021: Main Conference, PhD Symposium, Posters and Demonstrations* (Vol 3013, article number 20210121). Kherson, Ukraine.

[15] Muñoz, S., & Iglesias, C.A. (2021). An agent based simulation system for analyzing stress regulation policies at the workplace. *Journal of Computational Science*, 51, article number 101326. doi: 10.1016/j.jocs.2021.101326.
[16] Prokhorchenko, A., Parkhomenko, L., Kyman, A., Matsiuk, V., & Stepanova, J. (2019). Improvement of the technology of accelerated passage of low-capacity car traffic on the basis of scheduling of grouped trains of operational purpose. *Procedia Computer Science*, 149, 86-94. doi: 10.1016/j.procs.2019.01.111.
[17] Shramenko, V., Muzylyov, D., & Shramenko, N. (2020). Integrated business-criterion to choose a rational supply chain for perishable agricultural goods at automobile transportations. *International Journal of Business Performance Management*, 21(1/2), article number 166. doi: 10.1504/ijbpm.2020.10027634.
[18] Tang, W., Li, Z., Yu, Z., Qian, T., Lian ,X.,& Chen, X. (2022). Cost-optimal operation and recovery method for power distribution systems considering multiple flexible resources and logistics restrictions. *Sustainable Energy Technologies Assessments*, 49, article number 101761. doi: 10.1016/j.seta.2021.101761.
[19] Zhang, G., Dai, L., Yin, X., Leng, L., & Chen, H. (2023). Optimization of multipath cold-chain logistics network. *Soft Computing*. doi: 10.1007/s00500-023-09013-y.
[20] Ziemke, D., Charlton, B., Horl, S., & Nagel, K. (2021). An efficient approach to create agent-based transport simulation scenarios based on ubiquitous Big Data and a new, aspatial activity-scheduling model. *Transportation Research Procedia*, 52, 613-620. doi: 10.1016/J.TRPRO.2021.01.073.

Вячеслав Іванович Мацюк
Доктор технічних наук, професор
Національний університет біоресурсів та природокористування України
03041, вул. Героїв Оборони, 15, м. Київ, Україна
https://orcid.org/0000-0003-2355-2564

Вікторія Григорівна Опалко
Кандидат технічних наук, доцент
Національний університет біоресурсів та природокористування України
03041, вул. Героїв Оборони, 15, м. Київ, Україна
https://orcid.org/0000-0002-4209-1073

Лілія Анатоліївна Савченко
Кандидат технічних наук, доцент
Національний університет біоресурсів та природокористування України
03041, вул. Героїв Оборони, 15, м. Київ, Україна
https://orcid.org/0000-0002-4336-4416

Олег Миколайович Загурський
Доктор економічних наук, професор
Національний університет біоресурсів та природокористування України
03041, вул. Героїв Оборони, 15, м. Київ, Україна
https://orcid.org/0000-0002-5407-8466

Надія Олексіївна Мацюк
Асистент, магістр з транспортних технологій
Національний університет біоресурсів та природокористування України
03041, вул. Героїв Оборони, 15, м. Київ, Україна
https://orcid.org/0000-0002-6922-3099

Оптимізація параметрів транспортно-технологічної системи аграрного підприємства в умовах часткової невизначеності

Анотація. На етапі виробництва широкого спектру сільськогосподарської продукції для забезпечення безперебійної роботи аграрних підприємств необхідно вирішити задачі швидкої та ефективної доставки відповідного обладнання, запчастин, розхідних матеріалів при раціональному використанні наявних виробничих ресурсів. Метою дослідження було вдосконалення транспортно-технологічної системи постачання замовлень у вигляді партій вантажів на потребу виробничої діяльності аграрного підприємства. Для цього було розроблено імітаційну модель у середовищі AnyLogic University Researcher із використанням компілятора Java, оскільки цей інструментарій дозволяє одночасно поєднувати дискретно-подієвий та агентний підходи. Модель реалізовано на прикладі підприємства відокремленого підрозділу Національного університету біоресурсів і природокористування України «Агрономічна дослідна станція». В результаті була отримана комплексна, оптимізаційна математична модель постачання товарів на розгалуженій мережі автомобільних шляхів сполучення власним парком автотранспортних засобів агропідприємства в умовах часткової невизначеності. Під час проведення експериментів та обчислень на основі реального процесу аграрного підприємства було знайдено діапазон значень розміру парку вантажних автомобілів, що відповідає умовам оптимізації. Визначено, що діапазон близьких до оптимального значень розміру парку вивантажних автомобілів змінюється в межах від 9 до 14 одиниць. Встановлено, що значення критерію оптимізації, що описує середній час доставки від початку виникнення потреби в замовленні до моменту його доставки, змінюються в межах від 9,96 до 12,78 годин. Визначено граничний рівень навантаження транспортно-технологічної системи, при якому забезпечується граничний рівень технологічної відмовостійкості. Він складає 135 та більше замовлень у рік у кожного постачальника при розрахунковому парку вантажних автомобілів у 12 одиниць. Результати дослідження, такі як застосування аналітичних інструментів та алгоритмів для оптимізації маршрутів та розподілу ресурсів, можуть бути використані для підвищення ефективності транспорту, для допомоги підприємствам у виборі найбільш вигідних та екологічних маршрутів для перевезень

Ключові слова: агентна симуляція; склад парку транспортних засобів; технологічна відмовостійкість; дистрибутивна логістика; постачання комплектуючих

Machinery & Energetics
Vol. 14, No. 3. 2023

Journal homepage:
https://technicalscience.com.ua/en

UDC 629.359, 681.513.1
DOI: 10.31548/machinery/3.2023.72

Yuriy Romasevych*
Doctor of Technical Sciences, Professor
National University of Life and Environmental Sciences of Ukraine
03041, 15 Heroiv Oborony Str., Kyiv, Ukraine
https://orcid.org/0000-0001-5069-5929

Yaroslav Hubar
Postgraduate Student
National University of Life and Environmental Sciences of Ukraine
03041, 15 Heroiv Oborony Str., Kyiv, Ukraine
https://orcid.org/0009-0000-3651-866X

Propeller thrust tower crane slewing mechanism model identification

Abstract. Any study of the dynamics and control of mechanical systems is based on adequate mathematical models that contain the dynamic parameters of the system under study. Their evaluation, in particular for the tower crane boom system, is a particularly relevant scientific and practical problem, the solution of which will provide the basis for further calculations of the optimal modes of movement of the tower crane slewing mechanism. The research aims to determine the dynamic parameters of the installation (moment of inertia of the slewing mechanism J, torque of dry friction forces M_0, driving torque coefficient K_1) and to plan experimental studies. The experimental method, numerical optimization methods (in particular, the modified Rot-Ring-PSO method), and statistical methods were used to conduct the research. Based on the results of the experiments, the dynamic parameters of the mathematical model of the laboratory installation of the tower crane slewing mechanism with propeller thrust were identified. The criterion that evaluates the identification error of the parameters K_1, M_0, and J was formed and minimized using the Rot-Ring-PSO algorithm. Plots of the kinematic characteristics of the movement of the boom system in terms of the angle of rotation of the boom and the speed of rotation of the boom were constructed. When processing the experimental data, the dependence of the error values on the supply voltage of the propeller drive was revealed. The error in the boom rotation speed at the drive supply voltage of 90% (compared to the voltage variant of 40%) decreased by almost 15%, and the error in the boom rotation angle at the drive supply voltage of 90% (compared to the supply voltage variant of 40%) decreased by almost 3 times. The regularity has been confirmed that with an increase in the supply voltage, the error value of the system decreases. In the course of processing the experimental studies, the dynamic parameters of the installation were identified: $K_1 = 4.80 \cdot 10^{-8}$ V/(rpm)^2, $M_0 = 34.519$ Nm, $J = 24.21$ kgm^2. The obtained results will be used to optimise the plant's motion modes, and the developed identification algorithm can be used for other similar problems

Keywords: error; criterion, equipment; algorithm; crane

INTRODUCTION

Tower cranes are used in the construction of high-rise buildings and to move various loads on construction sites. These cranes must, first and foremost, be reliable, and have sufficient performance and high safety standards. This determines the relevance of studying the dynamic characteristics of tower cranes and optimising their operation for improving production processes.

One of the mechanisms of a tower crane is the slewing mechanism. Many scientists studied the optimal movement modes of this mechanism. As such, Patent of Ukraine

Article's History: Received: 03.05.2023; Revised: 21.07.2023; Accepted: 11.08.2023.

Suggested Citation:
Romasevych, Yu., & Hubar, Ya. (2023). Propeller thrust tower crane slewing mechanism model identification. *Machinery & Energetics,* 14(3), 72-78. doi: 10.31548/machinery/3.2023.72.

*Corresponding author

No. 131788 "The method of controlling the movement of the slewing mechanism of the tower crane" (2019) synthesises the optimal mode of movement of a tower crane. The peculiarity of this study is determined by the change in the speed of the crane's slewing mechanism being implemented using the derived optimal law of movement of the mechanism, which eliminates pendulum oscillations of the load and increases the reliability and capacity of the tower crane. V. Loveikin *et al.* (2020) analysed the process of starting the tower crane slewing mechanism, provided that the crane moves at a steady-state speed, and identified the most significant factors that affect the energy, dynamic, and kinematic processes of the system. A. Trąbka (2016) presented a comprehensive method for determining the parameters characterising the main structural components of cranes. Its novelty lies in the fact that the analysis ensures the detection of deficiencies even before the installation of components on the crane structure. F. Liu *et al.* (2021) determined the oscillation and oscillation characteristics of a tower crane. They proved that the mass of the load has little effect on the spatial angle of slewing during the lifting and tilting motion and that the intensity of the change in the angle of rotation increases with the height of the tower crane. M. Zhang *et al.* (2020) developed an adaptive crane motion controller based on a dynamic model of a tower crane that ensures accurate load positioning while eliminating pendulum oscillations of the load. R. Čápková *et al.* (2019) presented a study that considers the control of crane motion using a PID controller. R. Gao *et al.* (2013) presented a method for evaluating the braking process of a tower crane. It was based on a model of the dynamics of an elastic system. V. Loveikin *et al.* (2023) considered a method for minimising the driving torque of the trolley movement mechanism during a steady-state crane slewing. It is based on the developed mathematical model of the "tower crane-load" system and minimization of the optimisation criterion by synthesising optimal control. V. Loveikin *et al.* (2022), based on a dynamic system, investigated a method for minimising trolley motion oscillations during a steady crane slewing using the movement duration criterion. W. Chen *et al.* (2020) studied a tower crane scheme to assess the stability of the structure under variable wind loads using CFD (Computational Fluid Dynamics) and time-domain analysis of wind reactions. O. Grigorov *et al.* (2020) analysed the use of a hydrodynamic drive for the movement and slwing mechanism. As a result, compared to other drives, they proved that it is effective in operation. I. Gorbatyuk & O. Bulavka (2022) presented a method for determining dynamic loads during load hoisting using calculation schemes that reflect the actual operation of the mechanism.

Optimal control of the movement of tower crane mechanisms requires a mathematical model. Its definition is a mandatory problem. However, the identification of model parameters can be quite difficult. Therefore, the research aims to develop a methodology for identifying the parameters of the model of the tower crane slewing mechanism using a laboratory installation as an example.

MATERIALS AND METHODS

An experimental laboratory installation of a tower crane (Fig. 1) with a boom length (L = 3570 mm) at the National University of Life and Environmental Sciences of Ukraine was used for the study. In the installation, the worm gear slewing mechanism was replaced by a propeller-driven slewing mechanism.

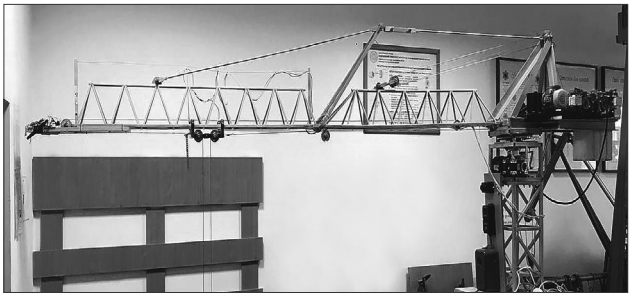

Figure 1. Experimental laboratory installation of a tower crane
Source: authors' photo

The propeller-driven slewing mechanism (Fig. 2) is installed at the end of the boom, which allows the experimental unit to reach the optimum speed and angle of rotation faster with less driving force and, accordingly, at a lower propeller speed.

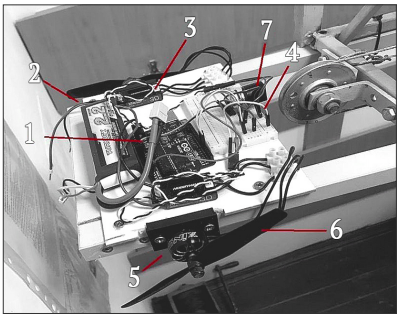

Figure 2. The structure of the propeller-driven slewing mechanism
Note: 1 – Arduino UNO board, 2 – Turnigy battery, 3 – Hobbywing XRotor Pro 25A driver, 4 – control block, 5 – iFlight XING-E Pro brushless motor, 6 – propellor, 7 – engine speed driver
Source: authors' photo

The list of equipment and its main technical characteristics used for the experiments: iFlight XING-E Pro brushless motor (China) (motor size 28.5x19.7 mm; weight 33.8 g; no-load current at 12.6 V 1.2 A; maximum power 800.5 W); Turnigy battery (China) (capacity 2200 mAh; voltage 11.1 V; dimensions: 104x27x35 mm); Hobbywing XRotor Pro motor driver (China) 25A (rated current 25 A; peak current for up to 10 seconds 40 A; frequency 50-500 Hz); AUTONICS E40S6-5000-3-T-24 incremental encoder (South Korea) (Fig. 3) (accuracy 5000 imp/rev, supply voltage 12-24 V).

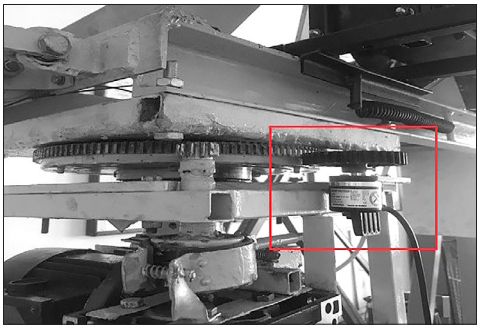

Figure 3. Incremental encoder location

Source: authors' photo

To record the data (supply voltage of the boom slewing mechanism drive, boom rotation angle, time), the Arduino UNO board (China) was used. The code was created using the Arduino IDE programming system. All data were obtained in numerical form and then processed in Wolfram Mathematica.

A data acquisition device m-DAQ 14 (Ukraine) and a laboratory power supply were used for data collection (Fig. 4).

Figure 4. Data recording device m-DAQ 14

Source: authors' photo

To conduct the experiments, the supply voltage to the actuator was increased from 10% of the nominal value to 100% in 10% increments. At 10 and 20% of the nominal voltage, the dry friction forces of the boom were greater than the thrust of the propeller, so these values were not used in the future. A total of 16 experiments were conducted with the motor supply voltage ranging from 30% to 100% of the nominal (12V) value.

It was proposed to use the following system of equations (mathematical model) to describe the motion of the laboratory installation:

$$\begin{cases} M_D = K_1 (PU_i)^2 L; \\ M_D - M_0 = J\ddot{\varphi}, \end{cases} \quad (1)$$

where K_1 – driving torque coefficient, H/(rpm)^2; P – drive speed ratio, rpm/V; U_i – nominal voltage that was applied to the motor on the i-th control cycle, B; L – boom length, m; M_0 – torque of dry friction forces, Nm; J – moment of inertia of the boom system, kgm^2; $\ddot{\varphi}$ – angular acceleration of the boom system, rad/s^2.

Model (1) was chosen as it well describes the physical phenomena occurring in the experimental setup (inertial, hydraulic, etc.). For example, as the motor supply voltage increases, the thrust of the propellers increases quadratically, which is the reason for the quadratic expression in the first equation (1). Unknown and requiring determination in the model (1) are the values of K_1, M_0, J. To determine them, a criterion was developed to describe the prediction error of model (1), i.e., the total deviation of the predicted data from the experimental data. This criterion is described by the following expression:

$$I = I_{\varphi.RMS} + I_{\varphi.max} + I_{\dot{\varphi}.RMS} + I_{\dot{\varphi}.max} = \sqrt{\sum_{i=1}^{690} (\varphi_{m.i} - \varphi_{e.i})^2} + \\ + \max(\varphi_{m.i} - \varphi_{e.i}) + \sqrt{\sum_{i=1}^{690} (\dot{\varphi}_{m.i} - \dot{\varphi}_{e.i})^2} + \max(\dot{\varphi}_{m.i} - \dot{\varphi}_{e.i}), \quad (2)$$

where $I_{\varphi.RMS}$ and $I_{\dot{\varphi}.RMS}$ – root mean square error values for the boom position and rotation speed; $II_{\varphi max}$ and $I_{\dot{\varphi}.max}$ – maximum (modulo) error values for the boom position and rotation speed; $\varphi_{m.i}$ and $\varphi_{e.i}$ – i-th values of the boom position obtained based on model (1) and experimental data, respectively; $\dot{\varphi}_{m.i}$ and $\dot{\varphi}_{e.i}$ – i-th values of the boom rotation speed were obtained based on model (1) and based on experimental data, respectively.

Criterion (2) was minimised using the Rot-Ring-PSO algorithm (Romasevych *et al.*, 2021) to identify the parameters K_1, M_0, and J.

RESULTS AND DISCUSSION

To illustrate the results, the plots (Fig. 5 and 6) and Table 1 are presented at 40% and 90% of the nominal supply voltage of the drives.

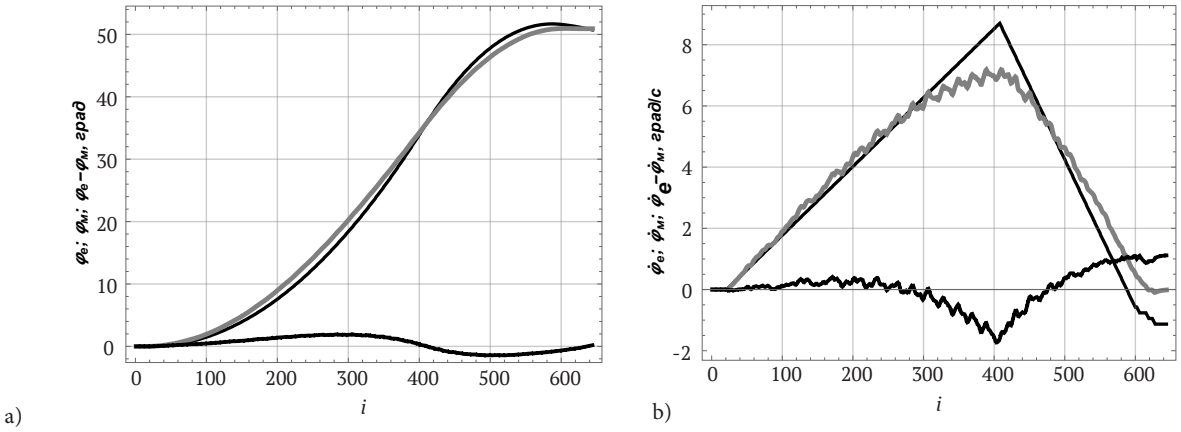

Figure 5. Plots of the kinematic characteristics of the boom system movement at a motor supply voltage of 40% of the nominal value

Note: a) by the angle of rotation of the boom, b) by the speed of rotation of the boom

Source: compiled by the authors

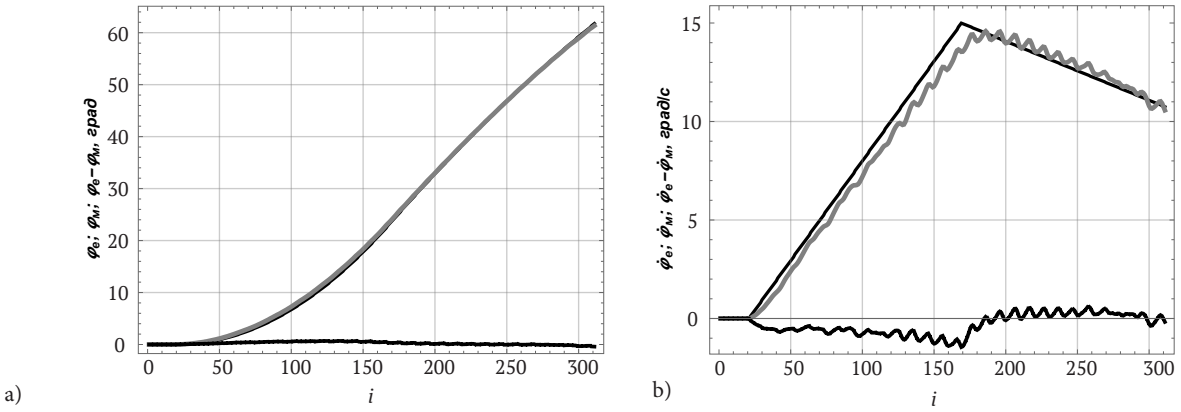

Figure 6. Plots of the kinematic characteristics of the boom system movement at a motor supply voltage of 90% of the nominal value

Note: a) by the angle of rotation of the boom, b) by the speed of rotation of the boom

Source: compiled by the authors

The black curve in Figure 5a shows a plot of changes in the angle of rotation of the boom system obtained using model (1). The grey curve represents the values obtained during the experiment. The dashed curve shows the plot of the prediction error of model (1), i.e., the difference between theoretical (predicted by model (1)) and experimental values. Figure 5b shows similar plots but for the boom slewing rate. Plots for the drive supply voltage level of 90% of the nominal value are shown in Figure 6. Figure 6a shows that the curves for the theoretical and experimental values of the boom angle of rotation coincide and their error is insignificant. A slight discrepancy between the curves is shown in Figure 6b. For a more detailed explanation of the results obtained, numerical data are provided (Table 1).

Table 1. Error-values at changes in drive voltage

Error name	Scale	Drive supply voltage, % of nominal value	
		40	90
Maximum (modulo) values			
Boom rotation speed	degrees/s	1.7317	1.4531
Boom position	degrees	1.9246	0.6965
Root mean square values			
Boom rotation speed	degrees/s	0.6374	0.5881
Boom position	degrees	1.1440	0.3503

Source: compiled by the authors

Table 1 shows that at 90% of nominal supply voltage, the maximum error in boom slewing speed is reduced by 15% (compared to 40% of nominal supply voltage). The maximum error in the boom slewing position at the same levels of drive supply voltage decreased by almost 3 times. Increasing the supply voltage of the drive has a negligible effect on the value of the RMS error in the boom slew rate. However, the factor of supply voltage has a significant effect on the RMS value of the boom position error, which decreased by almost 3 times when the supply voltage increased from 40% to 90% of the nominal value.

Comparing the values of the errors (Table 1), the increase in the motor voltage shows a tendency to reduce the error in the speed and angle of slewing of the installation. An increase in the supply voltage of the drive does not greatly affect the change in the error in the boom slewing speed, but at the same time, the error in the boom position decreases significantly with an increase in voltage.

Based on the data presented in Table 1, the error values at a drive supply voltage of 90% of the nominal value are small. This allows us to determine parameters $K_1 = 4.80 \cdot 10^{-8}$ W/(rpm)^2, $M_0 = 34.519$ Nm, $J = 24.21$ kgm^2 for this particular motor voltage level for further calculations of optimal driving modes.

H.M. Omar & A.H. Nayfeh (2005) developed a method for controlling crane mechanisms by installing two controllers. One of them provides system oscillation damping and the other provides trajectory control of the crane mechanisms. B. Jerman *et al.* (2004) presented a study of the dynamics of crane movement based on the developed mathematical model of a slewing crane.

V. Kovalenko *et al.* (2022) developed a control law for the crane control mechanism to rotate the boom with a load to a given angle φ in the shortest possible time, and at the end of the working cycle, the load should not oscillate. The problem of synthesising the laws of motion of the mechanism with optimal performance is solved by the methods of optimal control theory, namely, using the maximum principle. The basis is the differential equation of the mechanical system "boom crane – load". The common feature of this work is that it was conducted on a laboratory setup, the difference being that in our case the slewing mechanism is propeller-driven, while in the study mentioned above it is of the standard type, i.e., with a worm gearbox.

Yu. Romasevych *et al*. (2023) revealed the solution to the problem of trajectory avoidance when constructing the trajectory of a load moved by a tower crane by developing a methodology for synthesising consistent laws of motion of mechanisms. The commonality with the present study is the laboratory setup, even though the experiment was carried out using an accelerometer and a m-DAQ 14 data recording device. Thus, the laboratory setup is a fairly versatile tool for implementing the results of solving the problems of controlling tower crane mechanisms.

J. Ye & J. Huang (2022) solved the problem of controlling the movement of a tower crane boom based on the developed model of the installation. Moreover, the pendulum oscillations of the load and the influence of the movement (vibration) of the boom on them are considered. All experiments were carried out under ideal conditions in a laboratory setup, i.e., neglecting the aerodynamic effect and the influence of external weather factors. This confirms the applicability of the approach used in this study.

G. Yao *et al*. (2018) proposed to apply the finite element method and the Saint-Venant principle to conduct experiments to determine the stability of the installation structure. In contrast to this study, a 1:2 scale model of a tower crane installation was used instead.

The study of I. Doçi & S. Lajqi, (2018) aimed to determine the dynamic parameters of the tower crane slewing mechanism. This study is similar to the one cited above, although the authors additionally considered the oscillations of the plant.

CONCLUSIONS

The study involved the selection of measuring and recording equipment for experimental studies to identify a model of a laboratory installation of a tower crane with an improved slewing mechanism with propeller thrust. To determine the dependence of the angle and speed of the boom slewing from time, as well as the value of the voltage applied to the propeller drive, a code was developed in the Arduino IDE programming system.

Using the Rot-Ring-PSO algorithm, the minimum RMS values of the prediction errors of the model of the tower crane slewing mechanism (in terms of speed and angle of rotation of the boom) were determined. All calculations were performed at different motor supply voltages. It was found that at a lower motor supply voltage, the error increases, and at a higher one, it decreases. In particular, the error values are as follows: maximum boom rotation speed -1.45 deg/s, RMS -0.59 deg/s, maximum boom rotation angle -0.69 degrees, RMS -0.35 degrees.

The data obtained in the course of processing the experimental studies allowed us to identify the dynamic parameters of the plant $K_1 = 4.80 \cdot 10^{-8}$ W/(rpm)^2, $M_0 = 34.519$ Nm, $J = 24.21$ kgm^2, which will be used to implement the optimal modes of movement of the laboratory tower crane installation.

In the future, it is necessary to carry out theoretical calculations of the dependence of the boom slewing speed on the parameters that affect it: the mass of the load, trolley position on the crane boom, and the length of the rope.

ACKNOWLEDGEMENTS

None.

CONFLICT OF INTEREST

None.

REFERENCES

[1] Čápková, R., Kozáková, A., & Minar, M. (2019). Experimental modelling and control of a tower crane in the frequency domain. *Journal of Mechanical Engineering*, 69(3), 17-26. doi: 10.2478/scjme-2019-0025.

[2] Chen, W., Qin, X., Yang, Z., & Zhan, P. (2020). Wind-induced tower crane vibration and safety evaluation. *Journal of Low Frequency Noise, Vibration and Active Control*, 39(2), 297-312. doi: 10.1177/1461348419847306.

[3] Doçi, I., & Lajqi, S. (2018). Rotational motion of tower crane – dynamic analysis and regulation using schematic modeling. *International Scientific Journal "Mathematical Modeling"*, 2(1), 21-25.

[4] Gao, R., Yang, J., Luo, G., & Yan, C. (2013). The simulation of rotary motion of the flexible multi-body dynamics of tower crane. *Advanced Materials Research*, (655-657), 281-286. doi: 10.4028/www.scientific.net/AMR.655-657.281.

[5] Gorbatyuk, Ie., & Bulavka, O. (2022). Dynamic loads when lifting cargo by tower cranes. In *Collection of scientific papers "SCIENTIA" with Proceedings of the III International Scientific and Theoretical Conference* (pp. 119-120). Tel Aviv: European Scientific Platform.

[6] Grigorov, O., Anischenko, G., Petrenko, N., Strizhak, V., Turchyn, O., Strizhak, M., Okun, A., & Radchenko, V. (2020). Testing of hydrodynamic drive of cranes mechanisms. *Journal of Engineering Sciences and Innovation,* 5(4), 371-382.

[7] Jerman, B., Podrzaj, P., & Kramar, J. (2004). An investigation of slewing-crane dynamics during slewing motion – development and verification of a mathematical model. *International Journal of Mechanical Sciences*, 46(5), 729-750. doi: 10.1016/j.ijmecsci.2004.05.006.

[8] Kovalenko, V., Kovalenko, O., Stryzhak, V., Svirgun, V., & Stryzhak, M. (2022). Optimization of control of the tower crane slewing mechanism. *Bulletin of NTU "KhPI". Series of Automobile and Tractor Construction*, 1, 84-95, doi: 10.20998/2078-6840.2022.1.10.

[9] Liu, F., Yang, J., Wang, J., & Liu, Ch. (2021). Swing characteristics and vibration feature of tower cranes under compound working condition. *Shock and Vibration*, 2021, article number 8997396. doi: 10.1155/2021/8997396.

[10] Loveikin, V., Romasevych, Yu., Loveikin, A., Liashko, A., & Korobko, M. (2022). Minimization of high-frequency oscillations of trolley movement mechanism during steady tower crane slewing. *Scientific Bulletin, Series D*, 109, 31-44.

[11] Loveikin, V., Romasevych, Yu., Loveikin, A., Shymko, L., & Liashko, A. (2023). Minimization of the drive torque of the trolley movement mechanism during tower crane steady slewing. *Journal of Theoretical and Applied Mechanics,* 53, 19-33. doi: 10.55787/jtams.23.53.1.19.

[12] Loveikin, V.S., Romasevich, Yu.O., Kurka, V.P., Mushtin, D.I., & Pochka, K.I. (2020). Analysis of the start-up process of the tower crane slewing mechanism with a steady state motion mode of its load trolley. *Strength of Materials and Theory of Structures*, 105, 232-246. doi: 10.32347/2410-2547.2020.105.232-246.

[13] Omar, H.M., & Nayfeh, A.H. (2005). Anti-swing control of gantry and tower cranes using fuzzy and time-delayed feedback with friction compensation. *Shock and Vibration*, 12, 73-89. doi: 10.1155/2005/890127.

[14] Patent of Ukraine No. 131788 "The method of controlling the movement of the slewing mechanism of the tower crane". (2019, January). Retrieved from https://sis.ukrpatent.org/uk/search/detail/736599/.

[15] Romasevych, Yu., Loveikin, V., & Loveikin, Y. (2021). Development of new rotating ring topology of PSO-Algorithm. In *2021 IEEE 2nd KhPI Week on Advanced Technology (KhPIWeek)* (pp. 79-82). Kharkiv: IEEE. doi: 10.1109/KhPIWeek53812.2021.9569973.

[16] Romasevych, Yu.O., Loveikin, V.S., & Velykoivanenko, D.I. (2023). Construction of the laws of motion of the mechanisms for trolley movement and slewing of the tower crane. *Scientific Reports of NULES*, 102(2), 1-13. doi: dopovidi2(102).2023.020.

[17] Trąbka, A. (2016). Influence of flexibilities of cranes structural components on load trajectory. *Journal of Mechanical Science and Technology*, 14, 1-14. doi: 10.1007/s12206-015-1201-z.

[18] Yao, G., Xu, C., Yang, Y., Wang, M., Zhang, M., & Thabeet, A. (2018). Working mechanism of a high-performance tower crane attached to wall joints. *Journal of Engineering Science and Technology Review*, 11(1), 19-27.

[19] Ye, J., & Huang, J. (2022). Control of beam-pendulum dynamics in a tower crane with a slender jib transporting a distributed-mass load. In *IEEE Transactions on Industrial Electronics*, (vol. 70(1), pp. 888-897). Liverpool: IEEE. doi: 10.1109/TIE.2022.3148741.

[20] Zhang, M., Zhang, Y., Ouyang, H., Ma, Ch., & Cheng, X. (2020). Modeling and adaptive control for tower crane systems with varying cable lengths. In *Proceedings of the 11th International Conference on Modelling, Identification and Control, Lecture Notes in Electrical Engineering* (vol. 582, pp. 215-226). Singapore: Springer. doi: 10.1007/978-981-15-0474-7_21.

Юрій Олександрович Ромасевич
Доктор технічних наук, професор
Національний університет біоресурсів і природокористування України
03041, вул. Героїв Оборони, 15, м. Київ, Україна
https://orcid.org/0000-0001-5069-5929
Ярослав Сергійович Губар
Аспірант
Національний університет біоресурсів і природокористування України
03041, вул. Героїв Оборони, 15, м. Київ, Україна
https://orcid.org/0009-0000-3651-866X

Ідентифікація моделі установки механізму повороту баштового крана із пропелерною тягою

Анотація. Будь-які дослідження динаміки і керування механічних систем ґрунтується на адекватних математичних моделях, які містять динамічні параметри досліджуваної системи. Їх оцінка, зокрема для стрілової системи баштового крана, представляє собою окрему актуальну науково-прикладну задачу вирішення якої дасть підстави для подальших розрахунків оптимальних режимів руху механізму повороту баштового крана. Метою статті є визначення динамічних параметрів установки (момента інерції механізму повороту J, момента сил сухого тертя M_0, коефіцієнта рушійного момента K_1) та проведення планування експериментальних досліджень. Для проведення досліджень використано експериментальний метод, методи чисельної оптимізації (зокрема модифікований метод рою часток Rot-Ring-PSO), а також статистичні методи. За результатами проведених експериментів було ідентифіковано динамічні параметри математичної моделі лабораторної установки механізму повороту баштового крана із пропелерною тягою. Сформовано та за допомогою алгоритму Rot-Ring-PSO проведено мінімізацію критерію, який оцінює похибку ідентифікації параметрів K_1, M_0, J. Побудовано графіки кінематичних характеристик руху стрілової системи по куту повороту стріли та по швидкості повороту стріли. При обробці експериментальних даних виявлено залежність величин похибки від напруги живлення приводу пропелера. Похибка по швидкості повороту стріли при напрузі живлення приводу 90 % (у порівнянні з варіантом напруги в 40 %) зменшилась майже на 15 %, а по куту повороту стріли при напрузі живлення приводу 90 % (у порівнянні з варіантом напруги живлення 40 %) зменшилась, майже в 3 рази. Підтверджена закономірність, що при збільшенні напруги живлення зменшується величина похибки роботи системи. У ході обробки експериментальних досліджень отримано ідентифіковані динамічні параметри установки $K_1 = 4{,}80 \cdot 10^{-8}$ В/(об/хв)^2, $M_0 = 34{,}519$ Нм, $J = 24{,}21$ кгм^2. Отримані результати будуть використані для проведення оптимізації режимів руху установки, а розроблений алгоритм ідентифікації може бути використаний для інших подібних задачах

Ключові слова: похибка; критерій; обладнання; алгоритм; кран

Machinery & Energetics
Vol. 14, No. 3. 2023

Journal homepage:
https://technicalscience.com.ua/en

UDC 536.24
DOI: 10.31548/machinery/3.2023.79

Viktor Trokhaniak*
PhD in Technical Sciences, Associate Professor
National University of Life and Environmental Sciences of Ukraine
03041, 15 Heroiv Oborony Str., Kyiv, Ukraine
https://orcid.org/0000-0002-8084-1568

Valery Gorobets
Doctor of Technical Sciences, Professor
National University of Life and Environmental Sciences of Ukraine
03041, 15 Heroiv Oborony Str., Kyiv, Ukraine
https://orcid.org/0000-0003-1180-4509

Heat transfer and gas dynamics numerical modelling of compact pipe bundles of new design

Abstract. Weight and size characteristics, heat transfer efficiency across the surface, pressure losses in the flow paths for each heat transfer medium, and other parameters that characterise the heat exchanger play an important role in the development of new types of heat exchanger designs. This predefines the research relevance and the need for a solution. The research aims to develop and implement fundamentally new approaches to the design parameters of shell-and-tube heat exchangers, in which smooth-tube bundles are placed as compactly as possible in their crossflow. For this purpose, numerical modelling in the heat exchanger channels and studies of heat transfer and gas dynamics were carried out. The ANSYS Fluent software package was used to calculate the hydrodynamics and heat transfer in the tube bundle channels. Numerical modelling of hydrodynamics and heat transfer processes in the flow of a compact bundle of small-diameter pipes was carried out. The mathematical model includes the Navier-Stokes equation, the energy equation, and equations describing the turbulence of the external flow. The turbulence model k-ε was chosen as a model that describes turbulence in channels well. The results of numerical modelling showed a compact bundle of pipes at the outlet of the channels, with an average value of +20.1°C. Notably, the local temperature values near the channel walls are close to +30°C. The air velocity at certain points of the duct reaches 85.1 m/s. At the same time, the average air velocity in the cross-section of the channel is about 41.2 m/s at Re = 21420. It is demonstrated that the maximum values of local heat transfer coefficients for pipes in a compact bundle are observed in the areas where the flow joins the pipe surface and at the beginning of the boundary layer formation. The maximum values of the heat transfer coefficient reach up to 1335.5 W/m^2°C for the second and third rows, and at the front point of the first order, it is 1042.3 W/m^2°C. These results will improve the weight and dimensions of shell-and-tube heat exchangers and reduce their costs

Keywords: Navier-Stokes equation; Computational Fluid Dynamics; heat and mass transfer; intertubular channels; weight and dimensions

INTRODUCTION

A heat exchanger is a device used to efficiently transfer heat between two fluids (gas or liquid) to another. The use of heat exchangers in combination increases the efficiency of thermal management and energy saving of the system as a whole (Hojjat, 2020). According to P. Bichkar *et al.* (2018), shell-and-tube heat exchangers have many applications in air conditioning, chemical engineering, power plants, and aerospace. They are divided into two categories based

Article's History: Received: 28.02.2023; Revised: 30.05.2023; Accepted: 11.08.2023.

Suggested Citation:
Trokhaniak, V., & Gorobets, V. (2023). Heat transfer and gas dynamics numerical modelling of compact pipe bundles of new design. *Machinery & Energetics,* 14(3), 79-89. doi: 10.31548/machinery/3.2023.79.

*Corresponding author

on the direction of flow: straight tube and U-shaped. In straight-tube heat exchangers, the tube flow enters from one side of the heat exchanger and exits from the other side of the heat exchanger, but in U-tube heat exchangers, the flow enters the U-shaped tubes, returns, and exits from the same direction in which it enters.

Significant experimental and numerical research has been conducted on shell-and-tube heat exchangers to improve their efficiency (Wang *et al.,* 2020). In experimental studies, the cost of purchasing materials, parts, and the heat exchangers themselves is very high, so numerical modelling of heat exchangers using the commercial software package ANSYS. Fluent Theory Guide Release 18.2 (2017) is much more useful. This method considers all the details of geometry, and flow and can simulate the values of gas dynamics and heat transfer parameters at any point of the heat exchanger, but this method requires a lot of computer processing power.

M. Tayyab *et al.* (2020) claim that there are two ways to increase turbulence: active and passive. Active methods require the use of external energy, which can be mechanical, hydromagnetic or electrohydrodynamic (Alam & Kim, 2018). The use of extended surfaces called fins is a widely used passive method to increase heat transfer. M.T. Riaz *et al.* (2022) noted that the effective heat transfer area increases with the use of extended surfaces, which leads to flow turbulence, increasing the transfer rate. In the passive method, changing or improving the geometric properties of the flow path or adding intensifiers in the channel increases the intensity of turbulence in the fluid flow, resulting in an obvious increase in heat transfer rate. Passive methods of creating turbulence include twisted tubes, spiral strips, coils, and vortex flow generators (Feizabadi *et al.,* 2019; Talebi & Lalgani, 2021).

M.A. Jamil *et al.* (2020) used exergy-economic optimisation to improve the mass and thermal characteristics of heat exchangers. They achieved a reduction in heat exchange area by ~26.4%, capital cost by ~20%, operating cost by ~50%, total cost by ~22%, and flow cost by ~21%. T.-W. Lim & Y.-S. Choi (2020) developed the design and investigated the performance evaluation of a shell-and-tube heat exchanger utilising the cold energy of liquid natural gas on a ship washing the jacket of an internal combustion engine. The results of the cycle performance analysis show that R123 and R227e have the highest and lowest thermal efficiencies of approximately 17-23% and approximately 15-21%, respectively. R123 and R134a show the highest and lowest exergy efficiencies of approximately 25-31% and approximately 23-29%, respectively.

According to V. Gorobets *et al.* (2021), by varying the displacement of adjacent pipes in the transverse direction relative to the direction of flow in the channels, it is possible to improve the integrated characteristics of heat transfer on the surface of such bundles. Notably, these characteristics improve with an increase in the displacement of adjacent pipes, but at the same time, pressure losses in such channels increase. Therefore, when choosing the geometry of a curved channel, one should limit the offset value, which, for example, for a pipe diameter of 10 mm in a bundle should not exceed 1-3 mm. V.I. Trokhaniak *et al.* (2023) found that for such bundles, the intensification of heat transfer does not require the use of high-power pumping equipment for pumping the heat carrier in the intertube channels of the heat exchanger.

Development and recommendation of both new and improved design solutions for shell-and-tube heat exchangers with a compact arrangement of tube bundles is a highly relevant research topic and requires a solution.

The research aims to improve the known and develop new designs of shell-and-tube heat exchangers with compact placement of smooth-tube bundles in their crossflow and to numerically simulate the processes of heat and mass transfer in the channels of these heat exchangers.

MATERIALS AND METHODS

All studies were carried out based on the problematic scientific laboratory "Heat and Mass Transfer Processes and Alternative Energy Sources" at the Department of Heat and Power Engineering of the National University of Life and Environmental Sciences of Ukraine. A shell-and-tube heat exchanger with a rectangular cross-section, in which tube bundles are arranged in a traditional staggered order with a step of 1.5×1.5 ($s_1/D \cdot s_2/D$) and a compact configuration with their crossflow (Fig. 1) was considered. The heat exchanger uses a system of tubes in which adjacent tubes are in contact with each other and are displaced along the ordinate axes by a distance K relative to each other, where $0 < K < \sqrt{3}D/2$ distance meets the established condition $C \geqslant D + 5 \pm 0.1$ mm, where D is the outer diameter of the tubes. This is because modern and relatively cheap technologies for manufacturing such bundles are significantly complicated, with a distance between the tubes of less than 5 mm.

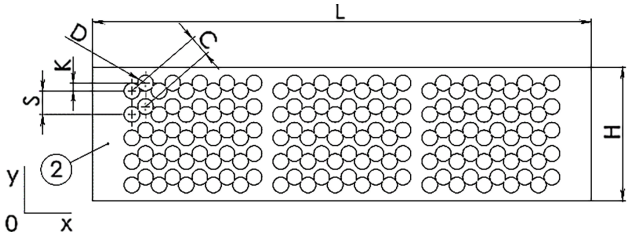

Figure 1. 1. Tube board with compact tube arrangement (top view)

Note: D – external tube diameter, m; S – width of the intertube passage, m; K – displacement of pipes along the ordinate axes, m; C – distance between pipes at displacement, m; L – length of the heat exchanger, m; H – heat exchanger width, m

Source: compiled by the authors

Numerical modelling of heat and mass transfer processes in the channels of heat exchangers of compact configuration was carried out using ANSYS software. Fluent theory guide. Release 18.2 (2017). The mathematical model is based on the Navier-Stokes equations (Khmelnik, 2010;

Marzouk *et al.* 2022) and the convective energy transfer equation. The standard k-ε turbulence model was chosen (ANSYS..., 2017).

The Navier-Stokes equations describing heat and mass transfer in heat exchange channels in a two-dimensional system are as follows:

- movement equation:

$$\begin{aligned}\rho\left(\frac{\partial u}{\partial t}+u\frac{\partial u}{\partial x}+v\frac{\partial u}{\partial y}\right)&=-\frac{\partial p}{\partial x}+\mu\left(\frac{\partial^2 u}{\partial x^2}+\frac{\partial^2 u}{\partial y^2}\right)\\ \rho\left(\frac{\partial v}{\partial t}+u\frac{\partial v}{\partial x}+v\frac{\partial v}{\partial y}\right)&=-\frac{\partial p}{\partial y}+\mu\left(\frac{\partial^2 v}{\partial x^2}+\frac{\partial^2 v}{\partial y^2}\right)\end{aligned}, \quad (1)$$

where ρ is the air density, kg/m3; μ is the dynamic air viscosity, Pa-s; p is the air pressure, Pa; u, v, is the vector field of air velocity, m/s; t is time, s;

- equation of continuity:

$$\frac{\partial u}{\partial x}+\frac{\partial v}{\partial y}=0; \quad (2)$$

- energy conservation equation:

$$\rho C_p\left(V_x\frac{\partial T}{\partial x}+V_y\frac{\partial T}{\partial y}\right)=\frac{\partial}{\partial x}\left(\lambda\frac{\partial T}{\partial x}\right)+\frac{\partial}{\partial y}\left(\lambda\frac{\partial T}{\partial y}\right), \quad (3)$$

where T is the temperature at a certain point, °C; λ is the thermal conductivity of air, W/m·°K; C_p is the specific heat capacity of air, J/kg·°K.

Boundary conditions were set (Fig. 1) at inlet:

$$x=0;\ W=W_0;\ T=T_{inlet}, \quad (4)$$

at output:

$$x=H;\ \frac{\partial W}{\partial x}=0, \quad (5)$$

tube walls:

$$T(x=x_{tube\_int})(y=y_{tube\_int})=T_{wall\_0}, \quad (6)$$

hull walls:

$$\left|\frac{\partial T_{wall\_case}}{\partial y}\right|_{y=0}=0, \quad (7)$$

adhesion conditions on the pipe wall:

$$x=x_{tube\_int};\ y=y_{tube\_int}, \quad (8)$$

adhesion conditions on the hull wall:

$$y=H;\ W=0;\ y=0. \quad (9)$$

For the standard k-ε turbulence model, the equations are as follows:

$$\begin{aligned}\frac{\partial}{\partial t}(\rho k)+\frac{\partial}{\partial x_i}(\rho k u_i)&=\frac{\partial}{\partial x_j}\left[\left(\mu+\frac{\mu_t}{\sigma_k}\right)\frac{\partial k}{\partial x_j}\right]+\\ &+G_k+G_b-\rho\varepsilon-Y_M+S_k\end{aligned} \quad (10)$$

and

$$\begin{aligned}\frac{\partial}{\partial t}(\rho\varepsilon)+\frac{\partial}{\partial x_i}(\rho\varepsilon u_i)&=\frac{\partial}{\partial x_j}\left[\left(\mu+\frac{\mu_t}{\sigma_\varepsilon}\right)\frac{\partial \varepsilon}{\partial x_j}\right]+\\ &+C_{1\varepsilon}\frac{\varepsilon}{k}(G_k+C_{3\varepsilon}G_b)-C_{2\varepsilon}\rho\frac{\varepsilon^2}{k}+S_\varepsilon\end{aligned}, \quad (11)$$

where G_k – generation of kinetic energy turbulence using velocity gradients; G_b – turbulence generation of kinetic energy from buoyancy; Y_M – dissipation contribution of the turbulence oscillating in the compressible to the total dissipation rate; $C_{1\varepsilon}$, $C_{2\varepsilon}$ and $C_{3\varepsilon}$ – constants; σ_k and σ_ε – turbulent Prandtl values for k and ε respectively.

The same boundary conditions apply in both cases. At the inlet of the heat exchanger, the mass flow rate is 0.25 kg/s at an initial temperature of T_{inlet} = +40°C. The height of the pipes is 200 mm, their outer diameter is 10 mm, and their wall thickness is 1 mm. For the coolant flowing inside the pipes, the following boundary conditions were set, which are typical for the flow of liquid coolants in channels of this type: the temperature on the inner surface of the pipes of the first section, starting from the entrance to the pipe bundle, is +11.46°C; for the second and third sections, respectively, +10.88°C and +10.3°C. The width of this channel between the pipes in this bundle configuration is 5 mm.

RESULTS

Results of numerical modelling of a staggered and compact tube bundle of a new design

Figures 2 to 4 below show the results of a numerical simulation in the traditional staggered heat exchanger channels. As can be seen in Figure 2, the temperature of the heat transfer medium drops as it approaches the outlet of the heat exchanger. At the outlet, the average temperature across the channel width is +19.3°C.

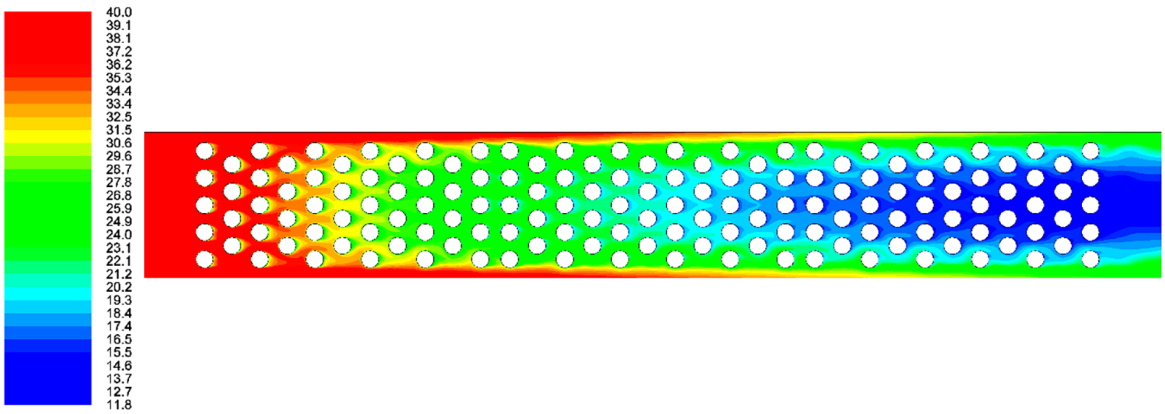

Figure 2. Temperature change in the heat exchanger staggered channel, °C

Source: V.I. Trokhaniak (2018)

The velocity field in the heat exchanger and the duct shows that in certain parts of the duct, the air velocity near the walls reaches 41.2 m/s, and the average velocity in the narrowest section of the duct is about 31.1 m/s (Fig. 3).

Figure 4 shows the pressure field in the channels of the tested heat exchanger design. The obtained pressure distribution shows that the total pressure drop is about 3.8 kPa.

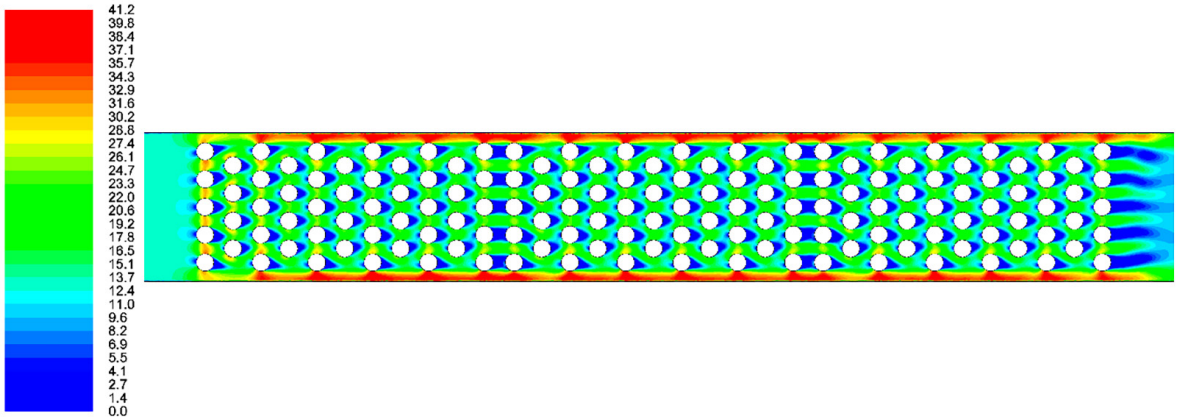

Figure 3. Velocity field in the staggered heat exchanger channel, m/s
Source: V.I. Trokhaniak (2018)

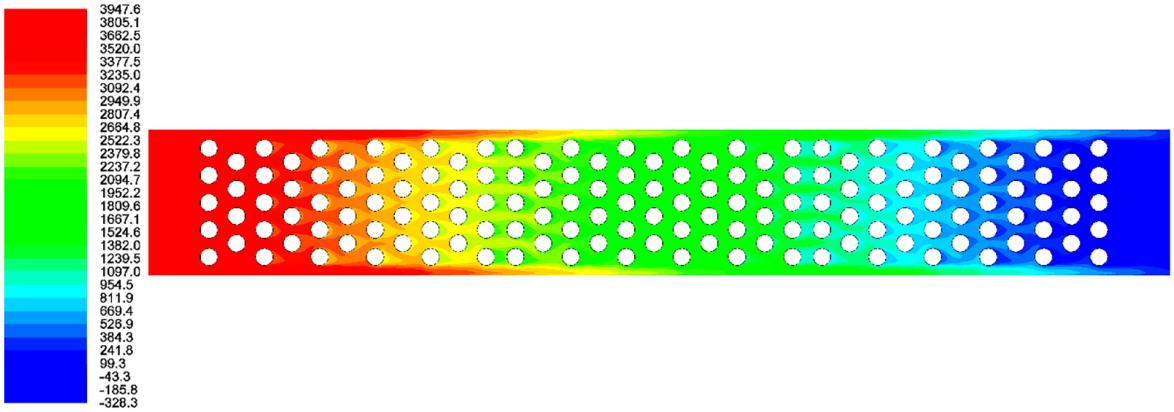

Figure 4. Pressure drop in the channel of the staggered beam, Pa
Source: V.I. Trokhaniak (2018)

As a result of the numerical modelling, the velocity field in the heat exchanger channels with a compact arrangement of the tube bundle was obtained, which is shown in Figure 5. Analysis of the results shows that the local velocity values reach their maximums and are observed in the areas adjacent to the side walls of the heat exchanger. It is characteristic that the local velocity values are twice as high as the average velocity values in the intertube channels. The analysis shows that at certain points in the channel, the air velocity can reach 85.1 m/s. At the same time, the average air velocity in the cross-section of the duct is about 41.2 m/s. Congestion zones are observed in certain sections of the duct in the pipe bundle between individual sections of the pipe bundle. Congestion zones also occur in sections of the curved duct for areas located in the aft zone of the pipes.

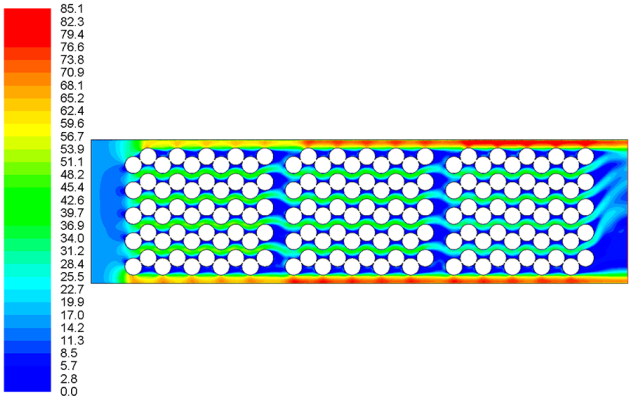

Figure 5. Air velocity in the compact beam channel, m/s
Source: compiled by the authors

Figure 6 the velocity vector distribution for a compact tube bundle. The lateral surface of an individual pipe is the first to be joined by the moulding flow and subsequently to detach the boundary layer. At the same time, congestion zones are observed in the areas of the joints of neighbouring pipes. These zones are characterised by the presence of two separation vortices. The flow velocity in these zones is significantly lower than in the main flow.

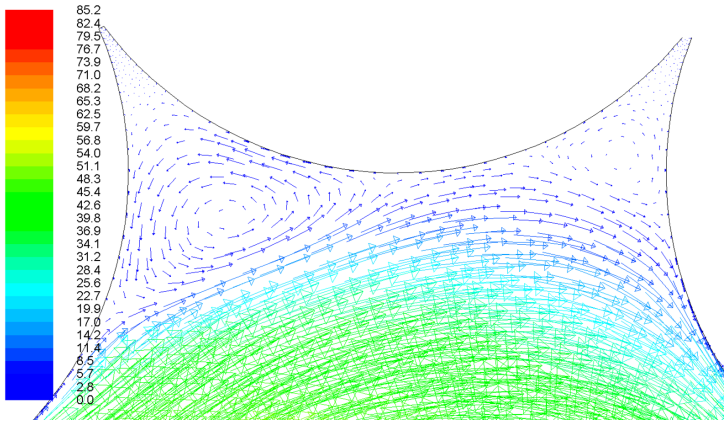

Figure 6. Velocity vector in the compact beam channel, m/s
Source: compiled by the authors

As a result of numerical modelling, the temperature field distributions in the channels of the tube bundle are shown in Figure 7. The analysis shows that the temperature of the heat carrier decreases as it approaches the outlet of the bundle channels. Assuming that the temperature at the inlet to the heat exchanger is +40°C, at the outlet of the channels its average value is +20.1°C. It is typical that near the channel walls, local temperature values are close to +30°C. Due to the high turbulence (at Re = 21420), the cold air flow at the outlet of the heat exchanger is slightly shifted upwards.

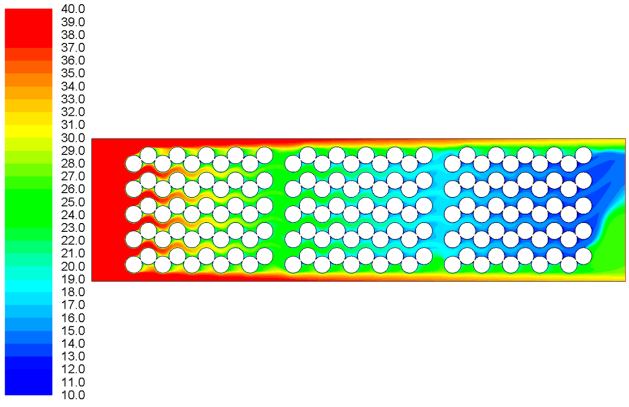

Figure 7. Temperature change in the compact beam channel, °C
Source: compiled by the authors

The pressure distributions in the channels of the compact tube bundle, acquired from numerical modelling, are shown in Figure 8.

The analysis of the found pressure fields shows that the pressure drop in this channel is about 7 kPa in total.

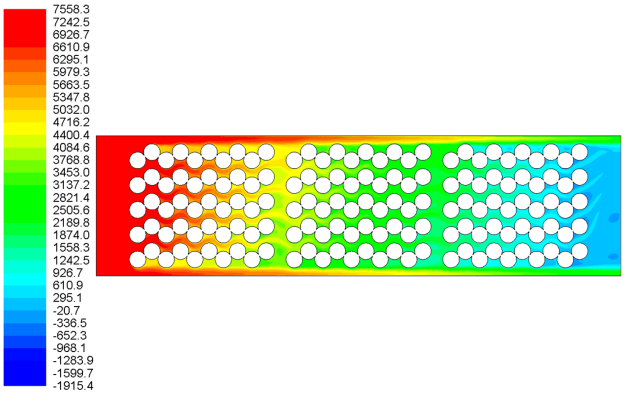

Figure 8. Pressure drop in the compact beam channel, Pa
Source: compiled by the authors

Local heat transfer results from a pipe bundle with a compact arrangement

Local distributions of the heat transfer coefficient around the circumference of the pipe reflect the main character of the influence of the heat exchange boundary layer on the pipe surface. By analysing the laws of this distribution, it is possible to determine the most ideal flow parameters, pipe arrangement in bundles and generalised relations for calculating the local heat transfer coefficient (Gorban *et al.*, 2021).

The specific heat transfer of a pipe in a bundle is the same as that of a local single pipe. The heat transfer distribution on the surface is determined by the flow properties of the pipe in the bundle, which are largely dependent on it. For a more detailed analysis of local heat transfer, Figure 9 shows the beginning and end of a pipe section. To improve the quality of the grid and obtain more detailed characteristics of the boundary layer, technical gaps were applied at the points of contact of neighbouring pipes (Fig. 9).

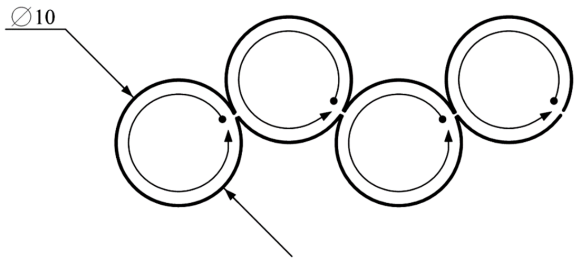

Figure 9. Start and end of the local heat distribution pipe section
Source: compiled by the authors

The peculiarities of the distribution of the local heat transfer coefficient in the first, second, and third rows were considered (Fig. 10).

Maximum values of the heat transfer coefficient, reaching up to 1335.5 W/m²·°C for the second and third rows, can be seen from the graph shown in Figure 10. As a result of the lateral influence of the flow, the process of flowing around the pipe of the second and all subsequent lines does not begin at the front point of the pipe, but at an angle of $\varphi = 151.1°$. Subsequently, as the boundary layer grows along the circumference of the pipe, heat transfer decreases. The heat transfer stabilises in the fourth row. The tubes of the second and subsequent rows are shaded by the first row in depth, so the heat transfer mode of the tubes in these rows differs from the heat transfer mode in the first row. At the front point, the first order is 1042.3 W/m²°C. The analysis of the change in local heat transfer in the tube bundle shows that the acceleration of the flow in its front part significantly affects the nature of the heat transfer distribution in all subsequent rows.

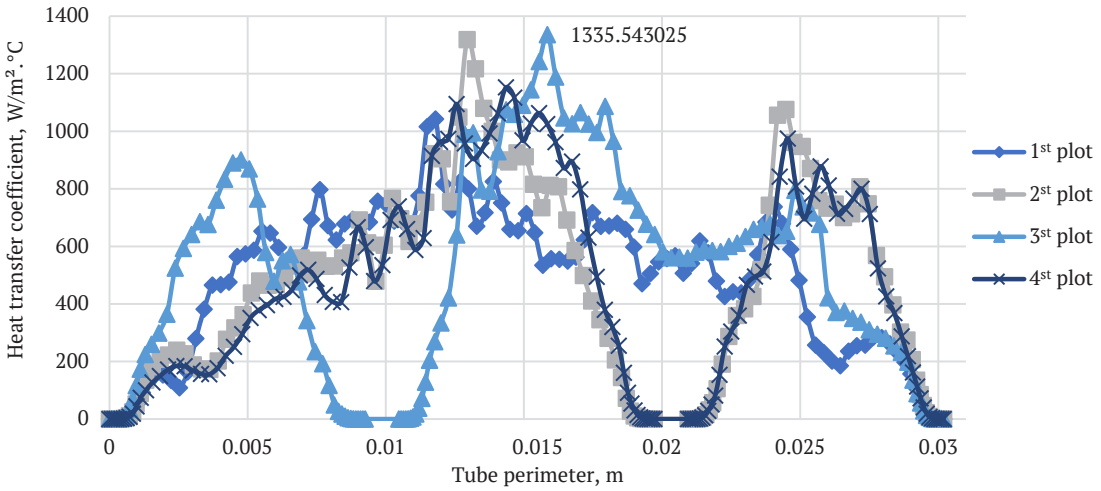

Figure 10. Local distribution of heat transfer from the pipe perimeter in a compact pipe bundle
Source: compiled by the authors

The uneven nature of the distribution of local values of heat transfer coefficients shown in Figure 10 is due to significant turbulence in the flow. Characteristically, for the first and third rows of pipes, there is a slight drop in heat transfer for an angle close to $\varphi \approx 290°$, and then a slight increase in heat transfer occurs again due to an increase in the velocity gradient in the longitudinal direction. This is due to the presence of pipes that are located directly behind the individual pipe in the bundle. The heat flux density distribution plot for the first four rows located along the length of the channel is shown in Figure 11. The maximum value of the local heat flux is about -29.44 kW/m² and is observed for the second and third rows. Figure 12 shows the local temperature distribution on the boundary layer, which reaches maximum values up to 291.1 °K. The nature of the curves is somewhat similar to that of the heat transfer coefficient.

The weight and dimensions of a shell-and-tube heat exchanger with a staggered tube bundle arrangement (1.5×1.5) were compared with a heat exchanger of a new design, which uses a tube bundle with a compact arrangement of tubes. The results of comparing the characteristics obtained in the numerical modelling are presented in Table 1.

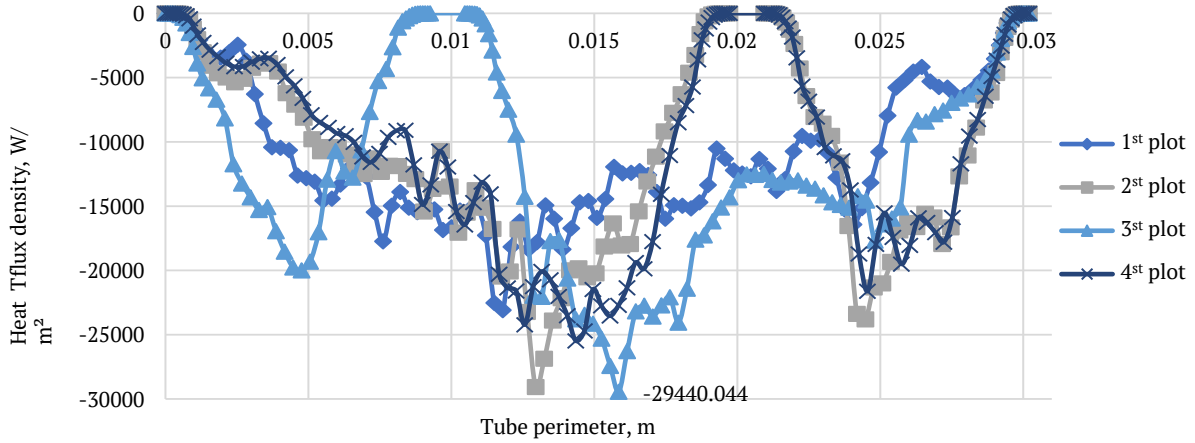

Figure 11. Local distribution of heat flux density from the pipe perimeter in a compact pipe bundle
Source: compiled by the authors

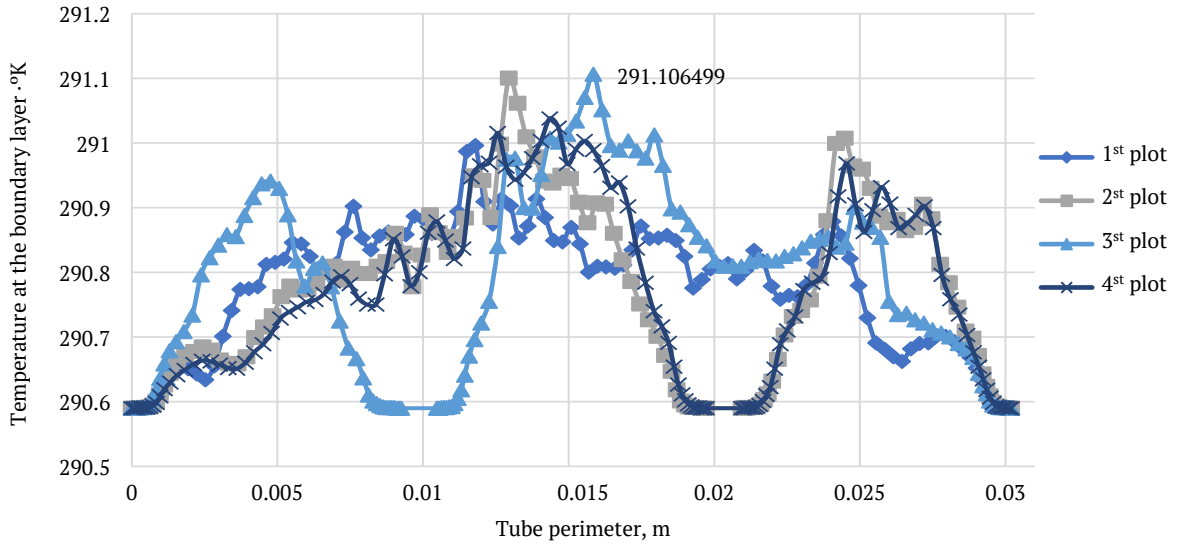

Figure 12. Local temperature distribution at the boundary layer from the pipe perimeter in a compact pipe bundle
Source: compiled by the authors

Table 1. Comparison of the weight and dimensions of a heat exchanger with a staggered (1.5x1.5) and compact tube bundle arrangement

The main parameter of the heat exchanger	Staggered tube bundle	Compact tube bundle
Heat output of the heat exchanger, W	5200	5000
Air temperature at the inlet to the heat exchanger, °C	+40	+40
Air temperature at the outlet of the heat exchanger, °C	+19.3	+20.1
Mass air flow rate, kg/s	0.25	0.25
Air heat transfer coefficient, W/m²°C	314	321
Pressure drop at the inlet and outlet of the heat exchanger, Pa	3800	7560
Length of the heat exchanger, m	0.530	0.278
Pipe height in the bundle, m	0.20	0.20
Number of pipes, pcs.	150	150
Heat exchange mass, kg	16.6	15.2

Source: compiled by the authors

The data in Table 1 shows that with the same input parameters of the heat carrier and heat exchanger capacity, the difference between the values of heat transfer coefficients averaged over the pipe surface does not exceed 3%. A comparison of the geometric dimensions of the traditional and new heat exchangers shows that the latter reduces in size by 48% and in weight by 10%.

DISCUSSION

Heat exchangers are categorised either by flow configuration (counterflow, crossflow and crossflow) or by design (concentric tube, shell, and tube and compact) (Kundu *et al.* 2008). The ultimate goal of every heat exchanger or heat transfer study is to find methods or designs that increase the heat transfer rate. One of the main features of increasing heat transfer is changing the nature of the flow from laminar to turbulent (Rahman *et al.,* 2017). The greater the turbulence, the more it facilitates heat transfer (Alexandersson *et al.,* 2002; Zotloterer, 2004). In passive methods, the rate of heat transfer is increased by modifying the surfaces of the heat transfer interface (Lanjewar *et al.,* 2011; Hasanli *et al.*, 2022). For example, N. Nagarani *et al.* (2014) used the method of artificial roughness by using low height repeating ribs on the heat transfer surface to break the laminar layer and increase turbulence during heat transfer. M.A. Elyyan *et al.* (2008), and R. Bedi *et al.* (2018) described the use of V-shaped, W-shaped, angular, and transverse ribs to create artificial roughness. A. Erdogan & C. Ozgur Colpan (2018) based the development of the problem on a shell-and-tube heat exchanger that combines a parabolic trough solar collector and an organic Rankine cycle. This allowed the total heat transfer coefficient to be reduced from 1579 to 1491 W/m^{2}K, the heat transfer surface area to be increased from 7 to 25.25 m^2, and the pumping power to be increased from 0.8723 to 0.9227 kW.

A twisted tube heat exchanger is a heat exchanger that increases the heat transfer coefficient on the tube side (Gu *et al.,* 2020). X.Z. Li *et al.* (2019) conducted a numerical study of the crossflow of twisted oval tube bundles with a linear arrangement and presented empirical correlations for the Nusselt number and Euler number. In addition, it was found that the velocity and temperature fields are periodically repeated every S/2 along the twisted oval tube. Z. Yang *et al.* (2020), N. Biçer *et al.* (2021), and A.C. Caputo *et al.* (2022) considered shell-and-tube heat exchangers with a modified design, which differ significantly from the traditional type.

It should be noted that the analysis of the numerical modelling of heat exchangers with a traditional staggered and compact arrangement of tubes in a bundle makes it possible to improve the weight and dimensions of shell-and-tube heat exchangers. The main difference between the new design of the heat exchanger and the traditional one is that it uses rows of small diameter tubes that are arranged without a gap between the tubes in the flow direction (Kundu *et al.* 2008; Lanjewar *et al.,* 2011). In addition, the neighbouring pipes are offset by a certain distance, which can vary from minimal values to a value of half the pipe diameter. This makes it possible to reduce the longitudinal dimensions of the heat exchanger by 1.5-2 times while reducing the mass of the heat exchanger by 10-15% compared to the work of M.A. Jamil *et al.* (2020). The use of continuous rows of pipes with an offset creates channels of a curved configuration in the heat exchanger, which leads to the intensification of heat transfer in the channels with a moderate increase in hydraulic losses when pumping the coolant (air) in the intertube channels.

Another important aspect of numerical modelling is the analysis of local distributions of temperatures, velocities, and pressures in curved channels. The local distributions of heat transfer coefficients, heat flux density and temperatures on the pipe surface indicate the surface areas where the local values of these parameters will be maximum. Such local extremes occur at the points where the connected flow enters after the breakaway zones formed in the recesses of curved channels, where the coolant velocity is significantly lower than in the main flow. At the points of connection of the external flow to the pipe surface, the beginning of the boundary flow is formed, where its thickness will be minimal, and the heat transfer coefficients and density of the diverted heat flow will be maximum.

The next conclusion that can be drawn from the analysis of the numerical calculation results is as follows. As follows from the local velocity distributions in the channels of the new design heat exchanger, the flow velocity near the side walls of the shell is 1.5-2 times higher than the coolant velocity in the curved channels. This leads to a redistribution of the coolant flow rate near the shell walls, which is not accompanied by an intensification of heat transfer for the extreme pipe bundles (Yang *et al.*, 2020; Biçer *et al.*, 2021; Caputo *et al.*, 2022). Therefore, to improve heat transfer for the entire bundle, it is necessary to minimise the width of the channels near the shell walls, which is due to the production technology of shell-and-tube heat exchangers, namely, the minimum distance between the pipes and the shell body when welding the pipes to the tube board and the heat exchanger shell.

The limiting case of the considered heat exchanger design with a compact pipe arrangement is the case when the displacement between adjacent pipes is zero. In this case, the hydraulic losses for pumping the coolant (air) will be minimal, and the average value of the heat transfer coefficient over the pipe surface will decrease. To increase it, it is necessary to increase the flow rate of the coolant or the average velocity of the coolant in the inter-pipe channels. Such a design of the tube bundles of a shell-and-tube heat exchanger is advisable to use, for example, for heat recovery units in cogeneration plants, where pressure losses are limited by the limit values of the pressure at the exhaust of exhaust products of internal combustion engines.

Thus, it can be generally concluded that the proposed new design of the shell-and-tube heat exchanger has advantages over known designs and can be used in the design of heat exchangers for various purposes.

CONCLUSIONS

New design solutions for a compact tube bundle of a shell-and-tube heat exchanger used for heating and cooling the supply air in poultry house ventilation systems for the summer and winter seasons have been proposed. Numerical modelling of gas dynamics and heat transfer processes in the channels of the proposed and staggered (1.5×1.5) tube bundle and in heat exchangers was carried out using ANSYS Fluent software. As a result, the temperature fields, velocities, and pressures in the studied channels of the tube bundles were obtained for staggered and compact arrangements. The obtained distributions are analysed and the ways to improve the heat transfer conditions in the channels with a compact arrangement of pipes are indicated. A method of calculation on the surface of the pipe bundle is proposed for determining the average values of the heat transfer coefficient.

As a result of the analysis of the obtained distribution of local heat transfer, a maximum value of about 1335.5 W/m^2·°C is observed on the first four rows, and the heat flux density is 29.44 kW/m^2 at an angle of $\varphi = 151.1°$. At the frontal point of the first row, the heat transfer coefficient is 1042.3 W/m^2·°C. Between the tubes, when they touch each other, local heat transfer is significantly reduced due to a drop in velocity and the creation of stagnant airflow zones. To increase the local heat transfer distributions and increase the efficiency of the heat exchanger, it is necessary to reduce the stagnant zones between the tubes in the future. Based on the analysis of numerical modelling, it can also be suggested to further reduce the distance between the outermost tubes and the heat exchanger shell (body). These actions will reduce the amount of air in these areas, and in turn, the airflow and Re number will increase in the channels between the tubes. This will be accompanied by an increase in both local and average heat transfer in compact tube bundles.

The weight and size characteristics of traditional designs of a shell-and-tube heat exchanger and a heat exchanger using a new compact bundle of small-diameter pipes with the same heat output were compared. The advantages of the new design of the heat exchanger are shown, which consist of reducing the overall dimensions by 48% and reducing the weight by 10%. In the future, to increase heat transfer, the authors recommend investigating compact tube bundles with the addition of heat transfer intensifiers in the form of fins.

ACKNOWLEDGEMENTS

To the Ministry of Education and Science of Ukraine for financial support of projects of young scientists (Kyiv), No. 110/1M-pr-2022.

CONFLICT OF INTEREST

The authors declare no conflict of interest.

REFERENCES

[1] Alam, T., & Kim, M.H. (2018). A comprehensive review on single phase heat transfer enhancement techniques in heat exchanger applications. *Renewable and Sustainable Energy Reviews*, 81, 813-839. doi: 10.1016/j.rser.2017.08.060.

[2] Alexandersson, O., Zweigbergk, K., & Zweigbergk, C. (2002). *Living Water: Viktor Schauberger and the secrets of natural energy*. Dublin: Gill Books Gateway.

[3] ANSYS. Fluent theory guide. Release 18.2. (2017). Retrieved from https://www.luis.uni-hannover.de/fileadmin/software-lizenzen/Ueberlassung/ANSYS18.2_ReleaseNotes.pdf.

[4] Bedi, R., Kiran, K., Mulla, A.M., Manoj, & Hebbar, G.S. (2018). Experimental augmentation of heat transfer in a shell and tube heat exchanger using twisted tape with baffles and hitrain wire matrix inserts – a comparative study. *IOP Conference Series: Materials Science and Engineering*, 376, article number 012003. doi: 10.1088/1757-899X/376/1/012003.

[5] Biçer, N., Engin, T., Yaşar, H., Büyükkaya, E., Aydın, A., & Topuz, A. (2021). Design optimization of a shell-and-tube heat exchanger with novel three-zonal baffle by using CFD and taguchi method. *International Journal of Thermal Sciences*, 155, article number 106417. doi: 10.1016/j.ijthermalsci.2020.106417.

[6] Bichkar, P., Dandgaval, O., Dalvi, P., Godase, R., & Dey, T. (2018). Study of shell and tube heat exchanger with the effect of types of baffles. *Procedia Manufacturing*, 20, 195-200. doi: 10.1016/j.promfg.2018.02.028.

[7] Caputo, A.C., Federici, A., Pelagagge, P.M., & Salini, P. (2022). On the selection of design methodology for shell-and-tube heat exchangers optimization problems. *Thermal Science and Engineering Progress*, 34, article number 101384. doi: 10.1016/j.applthermaleng.2022.118541.

[8] Elyyan, M.A., Rozati, A., & Tafti, D.K. (2008). Investigation of dimpled fins for heat transfer enhancement in compact heat exchangers. *International Journal of Heat and Mass Transfer*, 51, 2950-2966. doi: 10.1016/j.ijheatmasstransfer.2007.09.013.

[9] Erdogan, A., & Ozgur Colpan, C. (2018). Thermal design and modeling of shell and tube heat exchangers combining PTSC and ORC systems. *Exergetic, Energetic and Environmental Dimensions*, 2018, 279-305. doi: 10.1016/B978-0-12-813734-5.00016-0.

[10] Feizabadi, A., Khoshvaght-Aliabadi, M., & Rahimi, A.B. (2019). Experimental evaluation of thermal performance and entropy generation inside a twisted U-tube equipped with twisted-tape inserts. *International Journal of Thermal Sciences*, 145, article number 106051. doi: 10.1016/j.ijthermalsci.2019.106051.

[11] Gorban, V.F., Andreev, A.O., Stolbovy, V.O., Firstov, S.O., & Karpets, M.V. (2021). Influence of the lattice parameter on physical properties of high-entropy coatings. *Scientific Herald of Uzhhorod University. Series "Physics"*, 49, 61-65.
[12] Gorobets, V., Trokhaniak, V., Bohdan, Y., & Antypov, I. (2021). Numerical modeling of heat transfer and hydrodynamics in compact shifted arrangement small diameter tube bundles. *Journal of Applied and Computational Mechanics*, 7(1), 292-301. doi: 10.22055/JACM.2020.31007.1855.
[13] Gu, H., Chen, Y., Sund'en, B., Wu, J., Song, N., & Su, J. (2020). Influence of alternating V- rows tube layout on thermal-hydraulic characteristics of twisted elliptical tube heat exchangers. *International Journal of Heat and Mass Transfer*, 159, article number 120070. doi: 10.1016/j.ijheatmasstransfer.2020.120070.
[14] Hasanli, R., Aliyev, I., Poladov, N., Azimova, L., & Tagiyev, T. (2022). Isothermal transformations in high-strength cast iron. *Scientific Herald of Uzhhorod University. Series "Physics"*, 51, 48-58. doi: 10.54919/2415-8038.2022.51.48-58.
[15] Hojjat, M. (2020). Nanofluids as coolant in a shell and tube heat exchanger: ANN modeling and multi-objective optimization. *Applied Mathematics and Computation*, 365, article number 124710. doi: 10.1016/j.amc.2019.124710.
[16] Jamil, M.A., Goraya, T.S., Shahzad, M.W., & Zubair, S.M. (2020). Exergoeconomic optimization of a shell-and-tube heat exchanger. *Energy Conversion and Management*, 226, article number 113462. doi: 10.1016/j.enconman.2020.113462.
[17] Khmelnik, S.I. (2010). *Navier-Stokes equations. On the existence and the search method for global solutions*. Charleston: CreateSpace Independent Publishing Platform.
[18] Kundu, P.K., Cohen, I.M., & Dowling, D.R. (2008). *Fluid mechanics* (4 Ed.). Amsterdam: Elsevier.
[19] Lanjewar, A., Bhagoria, J.L., & Sarviya, R.M. (2011). Heat transfer and friction in solar air heater duct with W-shaped rib roughness on absorber plate. *Energy*, 36, 4531-4541. doi: 10.1016/j.energy.2011.03.054.
[20] Li, X.Z., Zhu, D.S., Yin, Y.D., Tu, A., & Liu, S.J. (2019). Parametric study on heat transfer and pressure drop of twisted oval tube bundle with in line layout. *International Journal of Heat and Mass Transfer,* 135, 860-872. doi: 10.1016/j.ijheatmasstransfer.2019.02.031.
[21] Lim, T.-W., & Choi, Y.-S. (2020). Thermal design and performance evaluation of a shell-and-tube heat exchanger using LNG cold energy in LNG fuelled ship. *Applied Thermal Engineering*, 171, article number 115120. doi: 10.1016/j.applthermaleng.2020.115120.
[22] Marzouk, S.A., Abou Al-Sood, M.M., El-Fakharany, M.K., & El-Said, E.M.S. (2022). A comparative numerical study of shell and multi-tube heat exchanger performance with different baffles configurations. *International Journal of Thermal Sciences*, 179, article number 107655. doi: 10.1016/j.ijthermalsci.2022.107655.
[23] Nagarani, N., Mayilsamy, K., Murugesan, A., & Kumar, G.S. (2014). Review of utilization of extended surfaces in heat transfer problems. *Renewable and Sustainable Energy Reviews*, 29, article number 604613. doi: 10.1016/j.rser.2013.08.068.
[24] Rahman, M.M., Tan, J.H., Fadzlita, M.T., & Muzammil, A.W.K. (2017). A review on the development of gravitational water vortex power plant as alternative renewable energy resources. *IOP Conference Series: Materials Science and Engineering*, 217, article number 012007. doi: 10.1088/1757-899X/217/1/012007.
[25] Riaz, M.T., Cheema, T.A., Tayyab, M., Khan, A.U.A., Amber, K.P., Sajid, M.B., Park, C.W. (2022). Investigation of free and forced vortex induced thermal energy exchange potential. *Sustainable Energy Technologies and Assessments*, 52, article number 102107. doi: 10.1016/j.seta.2022.102107.
[26] Talebi, M., & Lalgani, F. (2021). Assessment of thermal behavior of variable step twist in the elliptical spiral. *International Journal of Thermal Sciences*, 170, article number 107126. doi: 10.1016/j.ijthermalsci.2021.107126.
[27] Tayyab, M., Cheema, T.A., Malik, M.S., Muzaffar, A., Sajid, M.B., & Park, C.W. (2020). Investigation of thermal energy exchange potential of a gravitational water vortex. *Renewable Energy*, 162, 1380-1398. doi: 10.1016/j.renene.2020.08.097.
[28] Trokhaniak, V., Gorobets, V., Shelimanova, O., & Balitsky, A. (2023). Research of thermal and hydrodynamic flows of heat exchangers for different air cooling systems in poultry houses. *Machinery & Energetics*, 14(1), 68-78. doi: 10.31548/machinery/1.2023.68.
[29] Trokhaniak, V.I. (2018). *Power saving system in poultry-houses with usage of soil low-potential energy*. Kyiv: Komprint.
[30] Wang, C., Cui, Z., Yu, H., Chen, K., & Wang, J. (2020). Intelligent optimization design of shell and helically coiled tube heat exchanger based on genetic algorithm. *International Journal of Heat and Mass Transfer*, 159, article number 120140. doi: 10.1016/j. ijheatmasstransfer.2020.120140.
[31] Yang, Z., Ma, Y., Zhang, N., & Smith, R. (2020). Design optimization of shell and tube heat exchangers sizing with heat transfer enhancement. *Computers & Chemical Engineering*, 137, article number 106821. doi: 10.1016/j.compchemeng.2020.106821.
[32] Zotloterer, F. (2004). Hydroelectric power station. Austria Patent AU2003294512. Retrieved from https://patents.google.com/patent/AU2003294512A1/en.

Віктор Іванович Троханяк
Кандидат технічних наук, доцент
Національний університет біоресурсів і природокористування України
03041, вул. Героїв Оборони, 15, м. Київ, Україна
https://orcid.org/0000-0002-8084-1568
Валерій Григорович Горобець
Доктор технічних наук, професор
Національний університет біоресурсів і природокористування України
03041, вул. Героїв Оборони, 15, м. Київ, Україна
https://orcid.org/0000-0003-1180-4509

Чисельне моделювання теплообміну та газодинаміки компактних пучків труб нової конструкції

Анотація. При розробці нових типів конструкцій теплообмінних апаратів важливу роль відіграють такі фактори, як їх масогабаритні характеристики, ефективність теплопереносу через поверхню, що розділяє теплоносії, втрати тиску в трактах для кожного з теплоносіїв та інші параметри, які характеризують теплообмінний апарат. Таким чином, наукові дослідження у даній сфері є актуальними і вимагають свого рішення. Мета роботи полягала у розробці та впровадженні принципово нових підходів конструкційних параметрів кожухотрубних теплообмінників, у яких гладкотрубні пучки розміщенні якомога компактно при їх поперечному обтіканні. Для цього було проведене чисельного моделювання в каналах теплообмінників і дослідження процесів теплообміну та газодинаміки. Для розрахунку гідродинаміки і теплопереносу в каналах трубного пучка використовували пакет прикладних програм ANSYS Fluent. Проведено чисельне моделювання процесів гідродинаміки і теплопереносу при обтіканні компактного пучка труб малого діаметра. Математична модель включає рівняння Нав'є-Стокса, рівняння енергії і рівняння, які описують турбулентність зовнішнього потоку. В якості моделі турбулентності вибрана k-ε модель, яка добре описує турбулентність в каналах. Результати чисельного моделювання показали на виході з каналів компактного пучка труб, усереднене значення якого складає +20.1°С. Характерно, що поблизу стінок каналу локальні значення температур мають значення близькі до +30°С. Швидкість повітря в окремих точках каналу досягає 85,1 м/с. При цьому середня швидкість повітря в поперечному перерізу каналу має значення близько 41,2 м/с при Re = 21420. Продемонстровано, що максимальні значення локальних коефіцієнтів тепловіддачі для труб в компактному пучку спостерігаються в областях приєднання потоку до поверхні труб і на початку формування межового шару. Максимальні значення коефіцієнта тепловіддачі, що досягає до 1335,5 Вт/м^2°С для другого та третього рядів, а у передній точці першого порядку становить 1042,3 Вт/м^2°С. Отримані результати дадуть змогу покращити масогабаритні показники кожухотрубних теплообмінників та знизити їх собівартість

Ключові слова: рівняння Нав'є-Стокса; Computational Fluid Dynamics; тепломасообмін; міжтрубні канали; масогабаритні показники

ТЕХНІКА ТА ЕНЕРГЕТИКА

Науковий журнал

Том 14, № 3. 2023

Заснований у 2010 р. Виходить чотири рази на рік

Оригінал-макет видання виготовлено у відділі науково-технічної інформації
Національного університету біоресурсів і природокористування України

Відповідальний редактор:
Г. Івченко

Редагування англомовних текстів:
С. Воровський, К. Касьянов

Комп'ютерна верстка:
О. Глінченко

Підписано до друку 11 серпня 2023 р. Формат 60*84/8
Умов. друк. арк. 10,6
Наклад 50 прим.

Адреса видавництва:
Національний університет біоресурсів і природокористування України
03041, вул. Героїв Оборони, 15, м. Київ, Україна
E-mail: info@technicalscience.com.ua
www: https://technicalscience.com.ua/uk

MACHINERY & ENERGETICS

Scientific Journal

Volume 14, No. 3. 2023

Founded in 2010. Published four times per year

The original layout of the publication is made in the Department of Scientific and Technical Information of National University of Life and Environmental Sciences of Ukraine

Managing editor:
H. Ivchenko

Editing English-language texts:
S. Vorovsky, K. Kasianov

Desktop publishing:
O. Glinchenko

Signed for print of August 11, 2023. Format 60*84/8
Conventional printed pages 10.6
Circulation 50 copies

Editors Office Address:
National University of Life and Environmental Sciences of Ukraine
03041, 15 Heroiv Oborony Str., Kyiv, Ukraine
E-mail: info@technicalscience.com.ua
www: https://technicalscience.com.ua/en